UNIVERSITY OF ALBERTA

ASPECTS OF THE GEOCHEMISTRY AND MINERALOGY OF THE ICE RIVER ALKALINE INTRUSIVE COMPLEX, YOHO NATIONAL PARK, BRITISH COLUMBIA

BY

ANDREW JOHN LOCOCK

©

A thesis submitted to the Faculty of Graduate Studies and Research in partial fulfillment of the requirements for the degree of Master of Science.

DEPARTMENT OF GEOLOGY

Edmonton, Alberta

FALL 1994

National Library of Canada
Bibliothèque nationale du Canada

Acquisitions and Bibliographic Services Branch
Direction des acquisitions et des services bibliographiques

395 Wellington Street
Ottawa, Ontario
K1A 0N4

395, rue Wellington
Ottawa (Ontario)
K1A 0N4

Your file *Votre référence*

Our file *Notre référence*

The author has granted an irrevocable non-exclusive licence allowing the National Library of Canada to reproduce, loan, distribute or sell copies of his/her thesis by any means and in any form or format, making this thesis available to interested persons.

L'auteur a accordé une licence irrévocable et non exclusive permettant à la Bibliothèque nationale du Canada de reproduire, prêter, distribuer ou vendre des copies de sa thèse de quelque manière et sous quelque forme que ce soit pour mettre des exemplaires de cette thèse à la disposition des personnes intéressées.

The author retains ownership of the copyright in his/her thesis. Neither the thesis nor substantial extracts from it may be printed or otherwise reproduced without his/her permission.

L'auteur conserve la propriété du droit d'auteur qui protège sa thèse. Ni la thèse ni des extraits substantiels de celle-ci ne doivent être imprimés ou autrement reproduits sans son autorisation.

ISBN 0-315-95070-6

Canada

UNIVERSITY OF ALBERTA

RELEASE FORM

NAME OF AUTHOR: Andrew John Locock

TITLE OF THESIS: Aspects of the geochemistry and mineralogy of the Ice River Alkaline Intrusive Complex, Yoho National Park, British Columbia

DEGREE: Master of Science

YEAR THIS DEGREE GRANTED: 1994

Permission is hereby granted to the University of Alberta Library to reproduce single copies of this thesis and to lend or sell such copies for private, scholarly or scientific research purposes only.

The author reserves all other publication and other rights in association with the copyright in the thesis, and except as hereinbefore provided neither the thesis nor any substantial portion thereof may be printed or otherwise reproduced in any material form whatever without the author's prior written permission.

Andrew Locock

13943-107A Avenue
Edmonton, Alberta
Canada T5M 2A8

Date August 30, 1994

UNIVERSITY OF ALBERTA

FACULTY OF GRADUATE STUDIES AND RESEARCH

The undersigned certify that they have read, and recommend to the Faculty of Graduate Studies and Research for acceptance, a thesis entitled "Aspects of the geochemistry and mineralogy of the Ice River Alkaline Intrusive Complex, Yoho National Park, British Columbia" submitted by Andrew John Locock in partial fulfillment of the requirements for the degree of Master of Science.

Dr. D.G.W. Smith (Supervisor)

Dr. H. Baadsgaard

Dr. R.W. Luth

Dr. T. Chacko

Dr. R.F. Egerton

Date June 21, 1994

To my parents.

ABSTRACT

The Ice River complex is a large (29 km^2) alkaline pluton situated mainly in Yoho National Park, British Columbia. The intrusion consists of pyroxenite-melteigite-ijolite-urtite cumulates, miaskitic nepheline and sodalite syenites, peralkaline pegmatites, and calcite-carbonatite.

The complex intruded limestones and shales of Cambrian and Cambro-Ordovician age. The age of the intrusion has been determined, using the U-Pb isotopic system, to be 356 $\pm$ 6 Ma (2σ). The Rb-Sr, Sm-Nd, and Pb-Pb isotopic systems yielded scatterchrons (369 $\pm$ 17, 359 $\pm$ 197, and 346 $\pm$ 52 Ma respectively, uncertainties 2σ * $MSWD^{1/2}$) whose slope ages overlap, within error, the age determined using U-Pb methods. The complex was transported (during the Laramide orogeny) roughly 200 km eastwards from its original site of emplacement. The prehnite-pumpellyite facies metamorphism that accompanied orogenesis is considered to have disturbed the Rb-Sr system, through both thermal effects, and minor fluid alteration of the feldspars and feldspathoids. The Sm-Nd and Pb-Pb systems may have been disturbed by slight crustal contamination during ascent and emplacement. Despite the disturbance of the isotope systems, the Sr and Nd initial ratios and the least radiogenic Pb data are consistent with the derivation of the complex from a depleted portion of the mantle.

Investigations of the whole-rock and trace element chemical relations and the chemical compositions of the mafic minerals resulted in the following account of the evolution of the complex. The intrusion is considered to have crystallized from a single carbonate-bearing silicate magma. The feldspar-free, mafic-ultramafic cumulates crystallized first. The remaining magma split, as a result of liquid immiscibility, into a carbonatite magma and a syenitic magma. These magmas evolved and crystallized almost simultaneously, producing the calcite-carbonatite, and a zoned syenite complex of miaskitic nepheline and sodalite syenites respectively.

Titanian andradite and schorlomite are locally abundant minerals in the

rocks of the Ice River complex. A specimen of the latter yielded a concordant U-Pb age, and was also investigated to characterize its crystal chemistry. The results of chemical analysis, X-ray absorption near-edge spectroscopy, and Mössbauer spectroscopy are consistent with the following generalized structural formula for schorlomite: $\{Ca\}_3[Ti,Fe^{3+},Fe^{2+}]_2(Si,Fe^{3+},Fe^{2+})_3O_{12}$

ACKNOWLEDGEMENTS

Firstly, I would like to recognize the late Dr. Richard St. J. Lambert, who sparked my interest in the Ice River complex, and without whose support this work would not have come to pass.

I would also like to thank my parents, for their work, patience, and understanding.

Special thanks to Dr. D.G.W. Smith for his tutelage and support in this project and mineralogy in general.

The interest and assistance of Dr. H. Baadsgaard in the continuance of this thesis are greatly appreciated.

Material for this work was collected mainly in Yoho National Park. I would like to thank the staff of the Parks Service for their assistance, especially Gordon Rutherford, Cal Sime, Helen Elder, Kevin Astridge, and Brenda Gabriel-Lane.

My field collecting was facilitated by the able assistance of Rob Hardy, and also Dr. D.G.W. Smith.

This work was carried out with the assistance of an NSERC miscellaneous grant for which I thank Dr. B.D.E. Chatterton, and Dr. R. Bustard.

The loan, by Dr. R. Herd, of the Geological Survey of Canada's collection of Ice River samples is acknowledged.

I am grateful to Dr. H. Baadsgaard for his assistance in the geochronology work and the use of his laboratory facilities. Thanks are also tendered to Wayne Day, Dr. M.J.M. Duke, and Agnes Koffyberg for their assistance, and especially to Dr. P.A. Cavell for her unflagging help and many insightful discussions regarding alkaline rocks.

The XRF and INAA analyses provided by Dr. P. Hooper and Dr. M.J.M. Duke are appreciated, as is the technical assistance of Alex Stelmach, Don Resultay, Diane Caird, and Paul Wagner.

I would like to thank Drs. R.W. Luth, R.G. Cavell, D.G.W. Smith, and

M.J.M. Duke for their very hard work and assistance in the preparation of the chapter on schorlomite. Dr. D. Canil is acknowledged for the low-temperature Mössbauer spectrum. The help of Mr. Swindlehurst in obtaining optical and infrared spectra is appreciated. Thanks go to Roman Wasarab for his valuable assistance with the error-propagation calculations. Drs. G. George, I. Pickering, and B. Hedman are acknowledged for their role in the XANES study.

The figures and plates in this work could not have been produced without the invaluable help of Paul Blanchon, and also Eugene Dembicki and Peter Kleespies.

Discussions with Dr. T. Chacko are especially appreciated.

Careful editing by Peter Kleespies and James Farquhar, as well as Drs. R.W. Luth, M.J.M. Duke, P.A. Cavell, R.G. Cavell, D.G.W. Smith, and R. Creaser, greatly improved parts of this thesis.

Finally, I would like to thank some of my fellow graduate students and other friends for their support and understanding throughout the past four years: Peter K., James, Kenton, Ian, Paul, Peter L., Bjarni, Rob H., Jody, Eugene, Agnes, Marilyn, Ron M., Helen and Rod.

TABLE OF CONTENTS

1. GENERAL INTRODUCTION 1
1.1 LOCATION 1
1.2 GEOLOGIC SETTING 1
1.3 HISTORY OF GEOLOGICAL INVESTIGATIONS 3
1.4 RATIONALE FOR PRESENT STUDY 9
1.5 GEOLOGY OF THE COMPLEX 9
1.6 REFERENCES CITED 11

2. RADIOISOTOPIC SYSTEMATICS OF THE ICE RIVER COMPLEX . 16
2.1 INTRODUCTION 16
2.1.1 Geology 16
2.1.2 Geochronology 20
2.2 MATERIAL AND METHODS 20
2.3 ISOTOPIC RESULTS 24
2.3.1 U-Pb 24
2.3.2 Rb-Sr 28
2.3.3 Sm-Nd 34
2.3.4 Pb-Pb 39
2.4 DISCUSSION 46
2.4.1 Age 46
2.4.2 Disturbance of isotope systems 46
2.4.3 Origin 51
2.5 CONCLUSIONS 53
2.6 REFERENCES CITED 53

3. CHEMICAL RELATIONS OF THE ROCKS AND MINERALS OF THE ICE RIVER COMPLEX 59
3.1 INTRODUCTION 59
3.1.1 Geological units of the complex 60

3.1.2 Petrographic features 63
3.2 MATERIALS AND METHODS 64
3.2.1 X-ray fluorescence analysis (XRF) 65
3.2.2 Instrumental neutron activation analysis (INAA) 66
3.2.3 Electron microprobe analysis 66
3.3 RESULTS 67
3.3.1 Whole-rock compositions 67
3.3.2 Mineral compositions 79
3.4 DISCUSSION 98
3.5 CONCLUSIONS 100
3.6 REFERENCES CITED 101

4. SPECTROSCOPY OF THE CATION DISTRIBUTION IN THE SCHORLOMITE SPECIES OF GARNET 105
4.1 INTRODUCTION 105
4.2 MATERIAL AND METHODS 107
4.2.1 X-ray powder diffraction 108
4.2.2 Electron microprobe analyses 108
4.2.3 Instrumental neutron activation analysis (INAA) 109
4.2.4 X-ray absorption near-edge spectroscopy 110
4.2.5 Ferrous iron determination 111
4.2.6 Hydroxyl content 111
4.2.7 Mössbauer spectroscopy 111
4.2.8 Infrared and optical spectroscopy 112
4.3 RESULTS 112
4.3.1 Chemical composition 113
4.3.2 X-ray absorption near-edge spectroscopy 119
4.3.3 Infrared spectroscopy 122
4.3.4 Mössbauer spectroscopy 125
4.3.5 Optical spectroscopy 125

4.4 DISCUSSION 131
4.4.1 Tetrahedral ferrous iron 131
4.4.2 Site occupancies 133
4.4.3 Intervalence charge transfer 135
4.5 CONCLUSIONS 137
4.6 REFERENCES CITED 138
4.7 MANUSCRIPT RELEASE 144

5. SUMMARY 145
5.1 REFERENCES CITED 147

APPENDIX 1: FERROUS IRON DETERMINATION 149

APPENDIX 2: SAMPLE ROCK-TYPES AND LOCATIONS 152

APPENDIX 3: INFORMATION FOR PARKS SERVICES 154
REFERENCES CITED 156

APPENDIX 4: PETROGRAPHIC DESCRIPTIONS 158

LIST OF TABLES

Table 2.1 Previous radioisotopic age determinations for the Ice River Complex 21

Table 2.2 Modal analyses of the samples from which minerals were separated 23

Table 2.3 U-Pb data, Ice River complex 25

Table 2.4 Rb-Sr data, Ice River complex 30

Table 2.5 Sm-Nd data, Ice River complex 36

Table 2.6 Sm-Nd data, feldspar-free and carbonatite series 40

Table 2.7 Pb-Pb data, Ice River complex 42

Table 3.1 Whole-rock major, minor and trace element compositions 68

Table 3.2 Chemical compositions of clinopyroxene from the Ice River complex 80

Table 3.3 Chemical compositions of amphibole from the Ice River complex 84

Table 3.4 Chemical compositions of garnet from the Ice River complex .. 86

Table 3.5 Chemical compositions of olivine, wollastonite, pectolite and zoisite 95

Table 4.1 Mineral standards used for synchrotron study 110

Table 4.2 Physical parameters of Ice River schorlomite 113

Table 4.3 Electron microprobe analyses of Ice River schorlomite 114

Table 4.4 Chemical analysis and cation proportions of schorlomite 117

Table 4.5 Energies (eV) of Ti and V X-ray absorption features 121

Table 4.6 Mössbauer parameters of ^{57}Fe in schorlomite 129

Table 4.7 Cation distribution of Ice River schorlomite 134

LIST OF FIGURES

Figure 1.1 Geological map of the Ice River alkaline intrusive complex showing the national park boundaries (after Currie, 1975). . . 2

Figure 2.1 Geological map of the Ice River complex (after Currie, 1975). 17

Figure 2.2 U-Pb concordia diagram for the nine sample aliquots 27

Figure 2.3 Expanded U-Pb concordia diagram in the region 320-365 Ma, displaying the concordant nature of the schorlomite at 356 Ma. 29

Figure 2.4 Rb-Sr isochron diagram showing the scatter of the data. The best fit line yields an age of 369 $\pm$ 17 Ma (2σ *$MSWD^{1/2}$). 33

Figure 2.5 Sm-Nd isochron diagram showing the scatter of the data. The best fit line yields an age of 359 $\pm$ 197 Ma (2σ *$MSWD^{1/2}$). 38

Figure 2.6 Sm-Nd isochron diagram depicting the subset of the feldspar-free and carbonatite series of rocks and minerals. These data yield an isochron with an age of 363 $\pm$ 34 Ma, MSWD = 0.46. 41

Figure 2.7 Pb-Pb diagram showing a reference line with a slope age of 356 Ma constrained to pass through the schorlomite. 44

Figure 2.8 Expanded Pb-Pb diagram displaying the scatter of the data. The dashed line is the model curve of Stacey and Kramers (1975). 45

Figure 2.9 Epsilon Nd-Sr anti-correlation plot at 356 Ma. The solid line is the mantle array. 49

Figure 3.1 Geological map of the Ice River complex (after Currie, 1975). 61

Figure 3.2 Oxide variation diagrams for the Ice River complex. 74

Figure 3.3 Oxide and halogen variation diagrams for the Ice River complex. 75

Figure 3.4 Rare earth element diagrams for the cumulate rocks. 77

Figure 3.5 Rare earth element plots for the syenitic and carbonatite series. 78

Figure 3.6 Pyroxene classification diagram (after Morimoto, 1989). 88

Figure 3.7 Compositional variation trends of the clinopyroxenes. 89

Figure 3.8 Electron microprobe analyses of clinopyroxenes from the Ice River complex plotted in the system Na-Mg-(Fe^{2+}+Mn) 91

Figure 3.9 Compositional variation of the amphiboles of the complex. . . 92

Figure 3.10 Amphibole evolution diagram (after Platt and Woolley, 1986). 93

Figure 4.1 Unpolarized infrared absorption spectrum of hydroxyl in Ice River schorlomite, 85 μm thick, with strongest peak at 3564 cm^{-1}. 118

Figure 4.2 Background-subtracted Ti K-edge spectra for schorlomite, and the model compounds titanite ($^{[6]}Ti^{4+}$), and rutile ($^{[6]}Ti^{4+}$). 120

Figure 4.3 Background-subtracted V K-edge spectra for schorlomite, and the model compounds vanadinite ($^{[4]}V^{5+}$), descloizite ($^{[4]}V^{5+}$), and cavansite ($^{[5]}V^{4+}$). 123

Figure 4.4 Unpolarized near-infrared absorption spectra of schorlomite, 30 μm thick, and heated schorlomite, 50 μm thick. 124

Figure 4.5 Mössbauer spectrum of ^{57}Fe in schorlomite, acquired at 295 K. 126

Figure 4.6 Mössbauer spectrum of ^{57}Fe in schorlomite, taken at 80 K. . . 127

Figure 4.7 Mössbauer spectrum of ^{57}Fe in heated schorlomite, acquired at 295 K. 128

Figure 4.8 Unpolarized optical absorption spectra of schorlomite, 10 μm thick, and heated schorlomite, 50 μm thick. 130

Figure A2.1 Geological map of the Ice River complex (after Currie, 1975). 153

Figure A3.1 Geological map of the Ice River complex (after Currie, 1975), showing the boundaries of the national parks. 155

LIST OF PLATES

Plate 2.1 Photomicrographs of the eudialyte syenite 35
Plate 3.1 Photomicrographs of zoisite microlites in nepheline 97

LIST OF ABBREVIATIONS

a	year
Å	angstrom
Ae	aegirine
Ae-Aug	aegirine-augite
Al iv	tetrahedrally coordinated aluminum
(aq)	aqueous
CHUR	chondritic uniform ratio
Di	diopside
dod	dodecahedral coordination
eud	eudialyte
eV	electron volts
Fo_{76}	76 molar percent forsterite
FTIR	Fourier transform infrared spectroscopy
FWHM	full peak width at half maximum peak height
GBq	gigabecquerel
hblndite	hornblendite
Hd	hedenbergite
HF	hydrofluoric acid
INAA	instrumental neutron activation analysis
IVCT	intervalence charge transfer
K	kelvin
kbar	kilobar
keV	kilo-electron volts
Ma	million years
mCi	millicurie
mel	melanite
MSWD	mean squared weighted deviation
n =	number of ...
n	index of refraction

n	neutrons
NAA	neutron activation analysis
ne	nepheline
oct	octahedral coordination
ol	olivine
parg	pargasite
ppm	parts per million
pv	perovskite
R	linear correlation coefficient
REE	rare earth element
SK	Stacey and Kramers (1975)
sod	sodalite
T	Tesla
tet	tetrahedral coordination
woll	wollastonite
wt%	weight percent
XANES	X-ray absorption near-edge spectroscopy
XRD	X-ray diffraction
XRF	X-ray fluorescence analysis
$^{[4]}X$	fourfold or tetrahedral coordination of X
$^{[6]}X$	sixfold or octahedral coordination of X
$^{[8]}X$	eightfold or triangular dodecahedral coordination of X
ZAF	atomic number, absorption, and fluorescence
ϵ^{356}_{CHUR}	epsilon neodymium at 356 million years
ϵ^{356}_{UR}	epsilon strontium at 356 million years
σ	one standard deviation

Note - the following were not included in this list: common units of mass, length, time, and temperature; elemental or isotopic symbols; acronymns of institutions or tradenames.

1. GENERAL INTRODUCTION

The Ice River complex is the largest plutonic body (and one of only two carbonatite-bearing alkaline intrusions) in the Canadian Rocky Mountains (Pell and Höy, 1989). It is an arcuate body, covering some 29 km^2, that consists of layered pyroxenite-melteigite-ijolite-urtite cumulates, miaskitic nepheline and sodalite syenites, peralkaline pegmatites, and calcite-carbonatite (Currie, 1975). This thesis, which is in paper-format, focuses on the age, origin, and evolution of the Ice River complex, as well as the crystal chemistry of some of the unusual minerals of the intrusion.

1.1 LOCATION

The Ice River complex is centered at 51°10' N latitude and 116°25' W longitude in the western Main Ranges of the Canadian Rocky Mountains, in the Foreland Belt of the Canadian Cordillera (Currie, 1975). The intrusion is situated roughly 23 km south of the town of Field and 40 km east-southeast of Golden, British Columbia. Most of the complex outcrops in the valley of the Ice River in Yoho National Park. The remainder is exposed in the valley of Moose Creek, mainly in Kootenay National Park, but also in the region of the valley between the parks (Figure 1.1). Permission must be obtained from the Parks Service to conduct geological field-work in the national parks.

1.2 GEOLOGIC SETTING

The Ice River complex is hosted by folded and faulted sedimentary rocks of Cambrian and lower-Ordovician age (Currie, 1975). These miogeoclinal strata are interpreted to have been deposited onto the shallow-water platforms, and to have accumulated in the deep-water environments, along the passive western margin of Ancestral North America (Fritz *et al.*, 1991). The Cambrian shales of the Chancellor Formation, the Cambrian

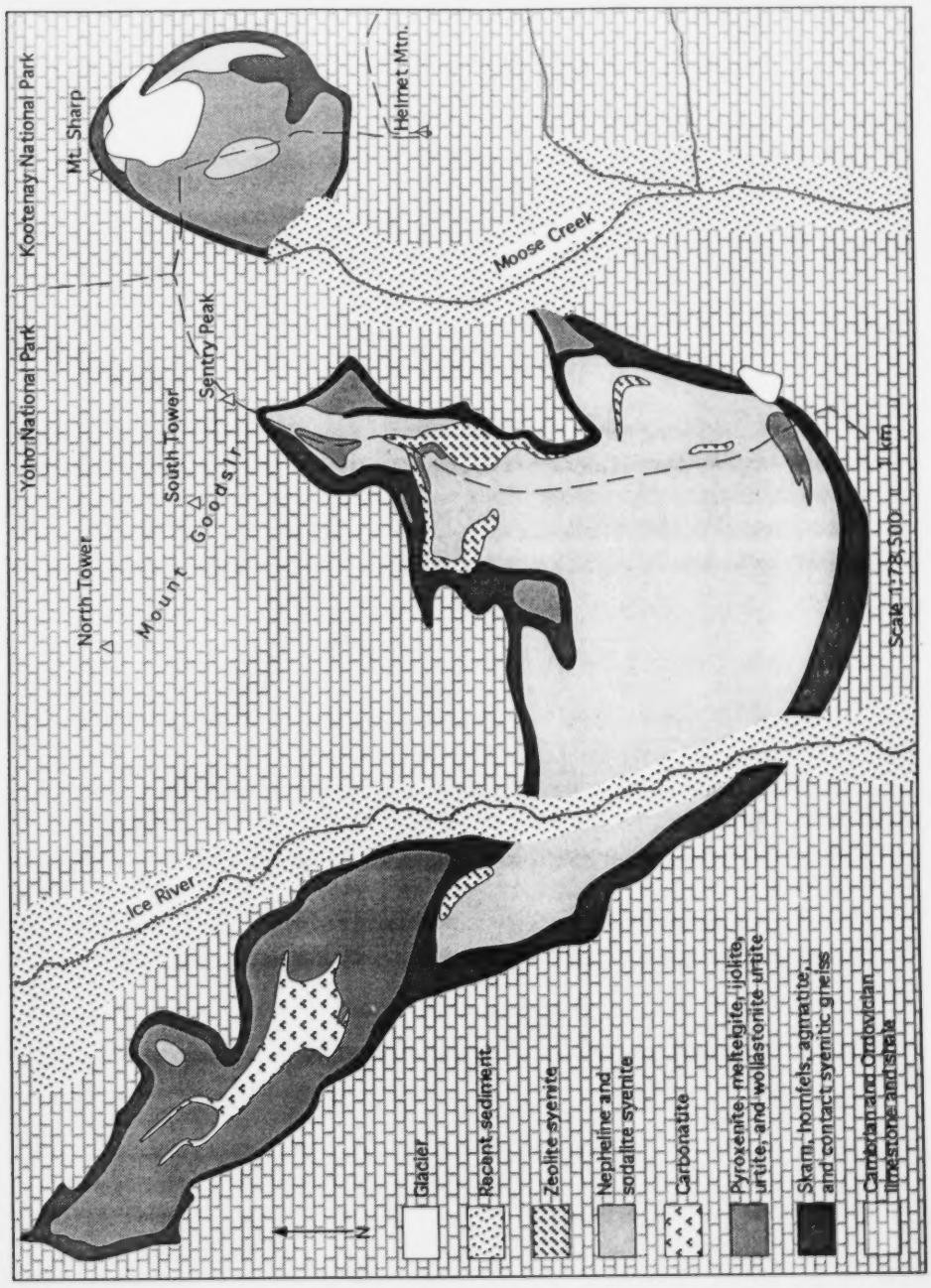

Figure 1.1 Geological map of the Ice River alkaline intrusive complex showing the national park boundaries (after Currie, 1975).

limestones and shales of the Ottertail Formation, and the Cambrian-Ordovician shales of the McKay Group comprise the host rocks of the complex (Currie, 1975). The sedimentary rocks in the immediate area are virtually free of fossils (Currie, 1975).

The host strata of the complex are mildly to severely sheared, and have been regionally metamorphosed (along with the complex) to prehnite-pumpellyite facies (Currie, 1975; Pell and Höy, 1989; Greenwood *et al.*, 1991). The complex is relatively undisturbed in comparison to the sedimentary rocks, and is considered to have behaved as a rigid, competent mass during deformation (Currie, 1975). This metamorphic activity is considered to have occurred during Cretaceous-Paleocene (Laramide) orogenesis, when the complex and its host strata were thrust approximately 200 km to the east, along a west-dipping décollement surface (Gabrielse, 1991). Therefore, the Ice River complex is no longer at the original geographic location where it was emplaced.

1.3 HISTORY OF GEOLOGICAL INVESTIGATIONS

The Ice River complex has been a focus of geological investigations for over a century. This section follows (chronologically) the evolution of geological opinion about the complex through summaries of the material published.

The history of geological investigations into the Ice River complex began with the observations of James Hector (later Sir), a member of the Palliser expedition (to explore western British North America). In 1858, he observed "...masses of true gneiss...[and] greenstone dykes", in the valley of the Beaverfoot River (Hector, 1863), into which the Ice River drains. Later authors considered this material to have been derived from the complex (Dawson, 1886).

Dawson (1886) made the first geological description of the Ice River complex proper, identifying it as a post-Cambrian, pre-orogenic, intrusive mass

of nepheline syenite and related rocks. Dawson commented on the disturbed nature of the complex, the contact metamorphism of the surrounding sedimentary rocks, and the presence of sodalite and ilmenite in the veins of the complex. Dawson also presented a rough quantitative analysis of the ilmenite.

Harrington (1886) reported an analysis of Ice River sodalite (collected by Dawson), and compared it to sodalite from the Montreal area. He also suggested that the sodalite from the Rocky Mountains could be used for jewellery.

Barlow (1900) suggested (in an abstract), that on the basis of the silica contents of specimens collected by Dawson in 1884, the rocks of the Ice River complex represented a complete magmatic differentiation sequence from ijolite to nepheline and sodalite syenite.

Analyses of schorlomite, and "hydronephelite" (natrolite) spherules separated by Barlow from the samples of Dawson, were reported by Hoffmann (1902). Hoffmann considered that the results of the analysis of schorlomite did not yield a rational formula, and therefore recalculated the analysis, assuming that all of the iron was Fe^{3+}, and that some of the titanium was in reduced form. (The crystal chemistry of schorlomite is examined in Chapter 4 of this thesis).

Bonney (1902) presented a petrographic description of sodalite syenite, and concluded that in the Ice River complex, sodalite was a secondary phase, "deposited from a state of solution".

Apparently spurred on by the prior publication by Bonney, Barlow (1902) discussed the petrography and whole-rock chemistry of samples of the complex in greater detail than in his turn-of-the-century abstract. Barlow recognized in his samples six distinct types of rock: ijolite, transition ijolite, biotite-aegirine-ijolite, nepheline syenite, sodalite syenite, and cancrinite syenite. He suggested that the ijolite, which contained abundant amphibole, was therefore a new variety, hornblende ijolite. Barlow also tentatively identified rosenbuschite, secondary calcite, analcime, and perovskite/pyrochlore

as occurring in nepheline syenite pegmatites.

Allan (1912a) first published, in the form of a summary report, the results of his investigations into the Ice River complex (his Ph.D. thesis topic at the Massachusetts Institute of Technology). This paper divided the Ice River complex into two major rock-types, an early mafic type that formed sill-like extensions in the intrusion, and a later felsic type that brecciated and enclosed fragments of the mafic type. Allan considered that the two types were transitional into one another and represented a single period of intrusion, although the types might represent immiscible portions of the magma. He also suggested that the intrusion post-dated the main period of mountain-building (orogenesis) and itself caused a later period of folding.

Later in the same year, Allan (1912b) had revised his views about the age of the complex in the circulated abstract of his Ph.D. thesis. He considered that the intrusion was older than the main period of deformation during the Laramide orogeny, but younger than an earlier period of folding. Allan described the complex as a laccolith formed by a single magma that separated into diverse rock-types by various processes of differentiation.

Allan (1914) published his work on the Ice River complex in the form of a memoir with the Geological Survey of Canada. This landmark study (considered by many subsequent authors to be "monumental") described the Ice River complex in great detail: its extent, petrology, mineralogy, structural relationships, contact and regional metamorphism, and postulated mechanisms for its formation and evolution. Allan expanded upon his previous work, differing only in the interpretation of the age of the complex, which he considered now to be contemporaneous with mountain-building.

Phillips (1916) described the crystallographic forms and chemical composition of natrolite crystals from the Ice River complex.

Warren and Allan (1917) presented the description and chemical analysis of a titaniferous augite (titanian diopside) from a pyroxenite of the Ice River complex.

Ellsworth and Walker (1925) reported the occurrence and chemical analyses of cerium-bearing perovskite ("knopite") and titanian magnetite. Both minerals had been noted in passing by Allan (1914), but had not been analyzed at that time.

Jones (1955) described in his M.Sc. thesis the geology of the Garnet Mountain - Aquila Ridge area, and concentrated especially on the petrology and mineralogy of the large inclusion of "metasomatized limestone" that outcrops there.

Mutch (1957) in his M.Sc. thesis, briefly redescribed the petrology of the complex, and cast doubt on whether differentiation was an important process in its formation.

In perhaps the most surprising paper on the Ice River complex, Gussow and Hunt (1959) stated that they had identified a fossil soil derived from the underlying igneous rocks. The sedimentary rocks in the vicinity of the Ice River complex therefore overlay this fossil soil and also therefore the plutonic rocks, implying a Precambrian age for the complex.

Lowdon (1960) obtained K-Ar ages of 340 and 330 Ma ($\pm$ 23 Ma) on biotite from rocks of the complex, and suggested a mid-Paleozoic crystallization age.

Campbell (1961) using samples collected by Allan, studied the chemical variation of the rocks in the complex, and concluded the intrusion formed by magmatic differentiation in the order: pyroxenite, ijolite, nepheline syenite, with sodalite syenite as pneumatolytic hybrid.

Further K-Ar ages (355 $\pm$ 18, 360 $\pm$ 18, and 304 $\pm$ 15 Ma) for biotite from rocks of the complex were obtained by Baadsgaard *et al.* (1961). The youngest of the three dates was discounted; this biotite sample was thought to have been slightly altered.

Rapson (1963) also reported K-Ar age determinations (327 $\pm$ 5, 336 $\pm$ 5, and 392 $\pm$ 10 Ma) on altered biotite from a minette sill, and from two hypersthene and plagioclase-bearing rocks (technically norites from the

description, a rock-type not observed by any other author, and not mentioned by Rapson in her subsequent papers). Rb-Sr ages were also determined on the same biotite separates, but the radiogenic strontium content was apparently too low for satisfactory results to be obtained.

Rapson (1964) was the first to recognize the presence of carbonatite in the Ice River complex. Previous authors had noted the outcrop but interpreted it to be altered and metasomatized limestone (Allan, 1914; Jones, 1955).

The carbonatite was more fully described by Rapson (1966) who suggested the following order of emplacement: basic and ultrabasic differentiates, followed by carbonatite, then nepheline syenite, and finally various minor lamprophyre dykes.

Deans *et al.* (1966) reported (for samples collected by Rapson) Sr isotopic compositions and trace element (Nb, La, Sr, Ba, Zr) contents of the carbonatite and host limestones. They concluded that the carbonatite was substantially different from the host limestones and could not have been produced by simple metamorphism.

The most recent work dealing with the petrology and evolution of the Ice River complex is that of Currie (1975). He re-mapped the complex, and studied it using whole-rock major element chemical relations, mass-balance calculations, and mineral chemical compositions (determined by electron microprobe). Currie divided the complex into two portions. The older part consisted of a feldspar-free intrusion ranging from pyroxenite through ijolite to urtite with a carbonatite plug. The younger, cross-cutting portion was a zoned pipe of nepheline and sodalite syenites. He postulated that an originally nephelinitic magma was emplaced at about 1000°C, 2.5 kbar total pressure, with a partial pressure of carbon dioxide of 0.75 to 1.25 kbar, and an oxygen fugacity near the quartz-fayalite-magnetite buffer. This magma split into the two portions by silicate-silicate liquid immiscibility, with the syenitic fraction becoming rich in alkaline aqueous fluids. Currie observed that parts of the complex were metasomatized, while in contrast the country rocks, although

thermally metamorphosed, were not significantly metasomatized. The fluids generated by the syenitic rocks were interpreted to have remained inside the complex, resulting in the development of late peralkaline rocks, and the lack of fenitization around the complex. Currie also obtained K-Ar dates on biotite (220 $\pm$ 8 and 233 $\pm$ 11 Ma) but interpreted the age of the complex to be roughly 245 Ma.

Gussow responded to Currie's work in both a paper (Gussow, 1977a) reiterating his own views (based on Gussow and Hunt (1959), and presenting no new data), and in a vitriolic review of Currie's bulletin (1977b).

Grice and Gault (1981) reported the occurrence of edingtonite and natrolite in late-stage pockets in the nepheline syenite.

Stevens *et al.* (1982) obtained a K-Ar date on "hornblende" (most probably hastingsite, see Chapter 3) from syenite of 421 $\pm$ 11 Ma.

Grice *et al.* (1984) expanded on their description of edingtonite from the Ice River complex and compared it to edingtonite from the Brunswick No. 12 mine in New Brunswick, the only other known locality in Canada.

Hunt and Roddick (1987) re-analyzed (K-Ar) an improved mineral separate of the amphibole of Stevens *et al.* (1982) and published an identical result (421 $\pm$ 11 Ma).

Parrish *et al.* (1987) tried to determine the age of the complex by using the U-Pb, Rb-Sr and Ar-Ar isotopic analysis of minerals separated from a single sample of nepheline syenite. They concluded that all isotopic systems were somewhat disturbed, but despite these complications, they estimated an age of 368 $\pm$ 4 Ma.

Hunt and Roddick (1988) in the last published paper on the Ice River complex, re-analyzed (again) an aliquot of the amphibole first examined by Stevens *et al.* (1982). Hunt and Roddick obtained a K-Ar age of 459 $\pm$ 17 Ma, and proposed the presence of large amounts of excess argon in the sample.

1.4 RATIONALE FOR PRESENT STUDY

As may be observed from the above history, despite more than a century of geological investigations of the complex, the age of emplacement, and origin of the magma(s) that formed the intrusion, are still matters of debate and uncertainty. This thesis was undertaken in an attempt to resolve some of the uncertainty regarding these matters. Chapter 2 deals with the radioisotopic systematics of the Ice River complex - specifically the determination of its age, origin of its parental magma, and reasons for disturbance of the isotope systems. Chapter 3 investigates the evolution of the complex through examination of whole-rock chemical relations and the chemical compositions of some of the minerals. Chapter 4 examines the crystal chemistry of schorlomite, concentrating on the roles of iron and titanium in the garnet structure.

1.5 GEOLOGY OF THE COMPLEX

The geology of the Ice River complex is described thoroughly in the work of Allan (1914) and Currie (1975), a summary of which can be found in Pell (1987). A synopsis of the geology from these sources and the present author's observations follows. The rocks of the Ice River complex comprise three major series: a feldspar-free ultramafic-mafic series, a carbonatite series, and a syenitic series (Figure 1.1). In addition, several types of dykes (lamprophyres, carbonatite, nepheline syenite) and sodalite-bearing veins cross-cut units of the complex and its host strata (Allan, 1914; Currie, 1975; Pell, 1987).

The feldspar-free series of rocks consists of repetitive layers of sequences of graded cumulates (clinopyroxenite, melteigite, olivine hornblendite, ijolite, pargasite ijolite, melanite ijolite, urtite, and wollastonite urtite) (Currie, 1975). Ijolite is the major unit in this series; the other rock-units are subordinate in their abundance. The rock units are mesocratic to melanocratic, and are characterized by a general lack of feldspar, and the presence of primary calcite as an accessory phase. The layers range in thickness from roughly 10 to 200

m, and increase in nepheline content towards the top of each layer (Currie, 1975). The occurrence of a rock-unit is variable from layer to layer, as is its grain size. Pegmatitic patches, schlieren and veins are common; modal and grain size heterogeneities are sometimes as great intra-unit as inter-unit. In general, boundaries between the units are completely gradational (with some exceptions). Contacts between the layers are sharp and display sedimentary-type structures (channel scouring, disconformable layering) (Currie, 1975). The stratigraphically lowest layers start with clinopyroxenite; higher in the complex the base of successive layers is rarely more mafic than ijolite (Currie, 1975). The cumulates vary mainly in their clinopyroxene:nepheline ratios. The clinopyroxene ranges in composition from titanian diopside to sodian hedenbergite. Other locally important minerals include: olivine (chrysolite), garnet (schorlomite-melanite), amphibole (kaersutite-pargasite-hastingsite), mica (phlogopite-biotite) and wollastonite-1*A*. Accessory minerals include: apatite, perovskite, calcite, magnetite, pyrrhotite, titanite, zoisite, pectolite, natrolite and cancrinite (Allan, 1914; Ellsworth and Walker, 1925; Currie, 1975; Pell, 1987).

There are three major types of carbonatite in the Ice River complex: a main body of buff-weathering calcite-carbonatite, a black-weathering iron-rich variety that occurs as siderite-rich carbonatite dykes associated with the main body, and a red-weathering variety that cross-cuts the buff carbonatite (Pell, 1987). The main body of carbonatite is a lenticular mass (400 m by 1500 m in dimensions) that is roughly concordant with the ijolitic rocks, but transects them in detail (Currie, 1975). This carbonatite consists mainly of ferroan calcite, with minor aegirine-augite, phlogopite and apatite, and accessory pyrite, strontianite, pyrochlore, and ilmenite. Carbonatite dykes occur most frequently in the layered feldspar-free series, but are found throughout the complex. The dykes are more abundant toward the margin of the main carbonatite body (Currie, 1975). The physical relationships of the carbonatites with the syenitic series preclude determination of an unambiguous order of emplacement. Some carbonatite dykes are reported to contain syenitic xenoliths and to cross-

cut the syenitic rocks, but nepheline syenite is described as having intruded the main carbonatite mass (Currie, 1975; Pell, 1987).

The syenitic series of rocks consists chiefly of melanocratic to leucocratic miaskitic nepheline syenite, with subordinate sodalite syenite, and rare peralkaline nepheline syenite pegmatites, zeolite syenite and eudialyte syenite (Currie, 1975; Pell, 1987). The syenites form an elliptical mass, zoned from a pale green sodalite syenite core through leucocratic nepheline syenite to melanocratic nepheline syenite at the margin. Nepheline syenite dykes were observed to cross-cut the ijolitic rocks of the feldspar-free series. The sodalite and nepheline syenites are composed dominantly of orthoclase microperthite, nepheline, amphibole (hastingsite, minor kaersutite), clinopyroxene (sodian hedenbergite-aegirine) and sodalite. Accessory minerals include biotite, titanite, cancrinite, calcite, apatite, zircon, melanite and occasionally fluorite, lavenite, lamprophyllite, lorenzenite and ilmenite (Currie, 1975). Rare late-stage pneumatolytic pockets and seams occur in the nepheline syenite, often bearing a low-temperature, agpaitic mineral assemblage which may include calcite, natrolite, edingtonite, ancylite, catapleiite, aegirine, zircon, magnetite, ilmenite, pyrite, and galena (Phillips, 1916; Currie, 1975; Grice and Gault, 1981; Grice *et al.*, 1984). The peralkaline nepheline syenite pegmatites are located near the stratigraphic top of the complex. Sodalite veins are common throughout the complex. Occasionally the nepheline syenites are hydrothermally altered (the zeolite syenite) to a mixture of orthoclase microperthite, natrolite, cancrinite, analcime, aegirine, calcite, hematite and sericite. The eudialyte syenite consists of eudialyte, nepheline, albite, aegirine, chlorite and calcite (Allan, 1914; Currie, 1975; Pell, 1987).

1.6 REFERENCES CITED

Allan, J.A. (1914) Geology of Field Map-area, B.C. and Alberta. Memoir 55, 312 p. Geological Survey of Canada, Ottawa.

———————— (1912a) Ice River District, British Columbia. Geological Survey of Canada Summary Report, Sessional Paper No. 26, 135-144.

———————— (1912b) Geology of the Ice River District, British Columbia. Abstract of thesis, 12 p. Massachusetts Institute of Technology.

Baadsgaard, H., Folinsbee, R.E., and Lipson, J. (1961) Potassium-argon dates of biotites from Cordilleran granites. Geological Society of America Bulletin, 72, 689-702.

Barlow, A.E. (1900) The nepheline rocks of Ice River, B.C. (abs.). Science, 11, 1022.

———————— (1902) On the nepheline rocks of Ice River, British Columbia. The Ottawa Naturalist, June, 70-76.

Bonney, T.G. (1902) On a sodalite syenite (ditroite) from Ice River Valley, Canadian Rocky Mountains. The Geological Magazine, 9, 199-206.

Campbell, F.A. (1961) Differentiation trends in the Ice River Complex, British Columbia. American Journal of Science, 259, 173-180.

Currie, K.L. (1975) The Geology and Petrology of the Ice River Alkaline Complex, British Columbia. Bulletin 245, 68 p. Geological Survey of Canada, Ottawa.

Dawson, G.M. (1886) Geological and Natural History Survey of Canada Annual Report, Volume 1, 122B-124B.

Deans, T., Snelling, N. J., and Rapson, J.E. (1966) Strontium isotopes and trace elements in carbonatites and limestones from Ice River, British Columbia. Nature, 210, 290-291.

Ellsworth, H.V. and Walker, J.F. (1925) Knopite and magnetite occurrence, Moose Creek, southeastern British Columbia. Geological Survey of Canada, Summary Report, 1925, Part A, 230A-232A.

Fritz, W.H., Cecile, M.P., Norford, B.S., Morrow, D., and Geldsetzer, H.H.J. (1991) Cambrian to Middle Devonian assemblages. In Geology of the Cordilleran Orogen in Canada, H. Gabrielse and C.J. Yorath (ed.). Geological Survey of Canada, Geology of Canada, No.4, 151-218.

Gabrielse, H. (Compiler) (1991) Structural styles, Chapter 17. In Geology of the Cordilleran Orogen in Canada, H. Gabrielse and C.J. Yorath (ed.). Geological Survey of Canada, Geology of Canada, No.4, 571-675.

Greenwood, H.J., Woodsworth, G.J., Read, P.B., Ghent, E.D., and Evenchick, C.A. (1991) Metamorphism, Chapter 16. In Geology of the Cordilleran Orogen in Canada, H.Gabrielse and C.J. Yorath (ed.). Geological Survey of Canada, Geology of Canada, No.4, 533-570.

Grice, J.D., and Gault, R.A. (1981) Edingtonite and natrolite from Ice River, British Columbia. Mineralogical Record, July-August, 221-226.

Grice, J.D., Gault, R.A. and Ansell, H.G. (1984) Edingtonite: the first two Canadian occurrences. Canadian Mineralogist, 22, 253-258.

Gussow, W.C., and Hunt, C.W. (1959) Age of the Ice River Complex, Yoho National Park, British Columbia. Journal of the Alberta Society of Petroleum Geologists, 7, 62.

Gussow, W.C. (1977a) The Ice River Complex, British Columbia, *is* Precambrian basement. Bulletin of Canadian Petroleum Geology, 25, 505-517.

———— (1977b) Review of: Geology and Petrology of the Ice River Alkaline Complex, British Columbia, by K. L. Currie. Bulletin of Canadian Petroleum Geology, 25, 707-709.

Harrington, B.J. (1886) On some Canadian minerals. Proceedings and Transactions of the Royal Society of Canada, 4, 81-83.

Hector, J. (1863) No. 5, Hector's Branch Expeditions, 1858. In The Journals, Detailed Reports, and Observations Relative to The Exploration, by Captain Palliser, of That Portion of British North America, which, in Latitude lies between the British Boundary Line and the Height of Land of Watershed of the Northern or Frozen Ocean Respectively, and in Longitude between the Western Shore of Lake Superior and the Pacific Ocean. During the Years 1857, 1858, 1859 and 1860. G.E. Eyre and W. Spottiswoode, London.

Hoffmann, G.C. (1902) Report of the Section of Chemistry and Mineralogy. Geological Survey of Canada Annual Report, Volume 12, 12R-13R.

Hunt, P.A., and Roddick, J.C. (1987) A compilation of K-Ar ages, Report 17. In Radiogenic Age and Isotopic Studies: Report 1, Geological Survey of Canada, Paper 87-2, 143-210.

———— (1988) A compilation of K-Ar ages, Report 18. In Radiogenic Age and Isotopic Studies: Report 2, Geological Survey of Canada, Paper 88-2, 127-153.

Jones, W.C. (1955) Geology of the Garnet Mountain-Aquila Ridge area, Ice River, British Columbia. M.Sc. thesis, University of British Columbia, Vancouver, British Columbia.

Lowdon, J.A. (1960) Age determinations by the Geological Survey of Canada. Geological Survey of Canada, Paper 60-17, 6-7.

Mutch, T.A. (1957) The Petrology of a portion of the Ice River, British Columbia, Igneous Complex. M.Sc. thesis, Rutgers University, New Brunswick, New Jersey.

Parrish, R.R., Heinrich, S., and Archibald, D. (1987) Age of the Ice River complex, southeastern British Columbia. In Radiogenic Age and Isotopic Studies: Report 1, Geological Survey of Canada, Paper 87-2, 33-37.

Pell, J.A. (1987) Open File 1987-17 Alkaline ultrabasic rocks in British Columbia. Province of British Columbia, Ministry of Energy, Mines and Petroleum Resources, Mineral Resources Division, Geological Survey Branch.

Pell, J.A., and Höy, T. (1989) Carbonatites in a continental margin environment - the Canadian Cordillera. In K. Bell, Ed., Carbonatites, Genesis and Evolution, p. 200-220. Unwin Hyman, London.

Phillips, A.H. (1916) Some new forms of natrolite. American Journal of Science, 42 (whole number 192), 472-474.

Rapson, J.E. (1963) Age and aspects of metamorphism associated with the Ice River Complex, British Columbia. Bulletin of Canadian Petroleum Geology, 11, 116-124.

———— (1964) Intrusive carbonate in the Ice River Complex, British Columbia. Bulletin of the American Association of Petroleum Geologists, 48, 543.

———— (1966) Carbonatite in the Alkaline Complex of the Ice River area, southern Canadian Rocky Mountains. Mineralogical Society of India, IMA volume, 9-22.

Stevens, R.D., Delabio, R.N., and Lachance, G.R. (1982) Age determinations and geological studies. K-Ar isotopic ages, Report 16, Geological Survey of Canada, Paper 82-2, 1-14.

Warren, C.H., and Allan, J.A. (1917) A titaniferous augite from Ice River, British Columbia. American Journal of Science, 43, 75-78.

2. RADIOISOTOPIC SYSTEMATICS OF THE ICE RIVER COMPLEX

2.1 INTRODUCTION

The first alkaline intrusion to be recognized in British Columbia was the Ice River complex (Dawson, 1886). It is not only the largest intrusion in the Canadian Rocky Mountains, but is perhaps the most contentious in terms of age of emplacement. This study re-examines the age and genesis of the Ice River complex using the Rb-Sr, Sm-Nd, Pb-Pb, and U-Pb isotopic systems.

2.1.1 Geology

The geology of the Ice River complex is thoroughly described in the work of Allan (1914) and Currie (1975), a summary of which can be found in Pell (1987a). A synopsis of the geology (from these sources and the present author's observations) follows. The Ice River complex is situated in the western Main Ranges of the Rocky Mountains, 23 km south of Field and 40 km east-southeast of Golden, B.C. The majority of the complex outcrops in Yoho and Kootenay National Parks with the remainder in the Moose Creek valley between the parks. The complex is exposed as an arcuate body approximately 19 km in length, with a maximum width of 4 km, covering about 29 km^2. It intruded Cambrian shales and limestones of the Chancellor and Ottertail Formations as well as the Cambrian-Ordovician shales of the McKay Group. Skarn and widespread hornfels resulted from the contact metamorphism of these host rocks. Metasomatized and deformed-brecciated rocks (agmatite and aegirine-feldspar fenite, often with a strong gneissic texture) are also found close to the border of the intrusion (Currie, 1975; Pell, 1987a).

The rocks of the Ice River complex comprise three major series: a feldspar-free ultramafic-mafic series, a carbonatite series, and a syenitic series (Figure 2.1). This division neglects the minor dyke rocks associated with the complex (lamprophyres, carbonatites, and sodalite veins). The layered feldspar-free series formed before the carbonatite or syenitic series, as the latter two

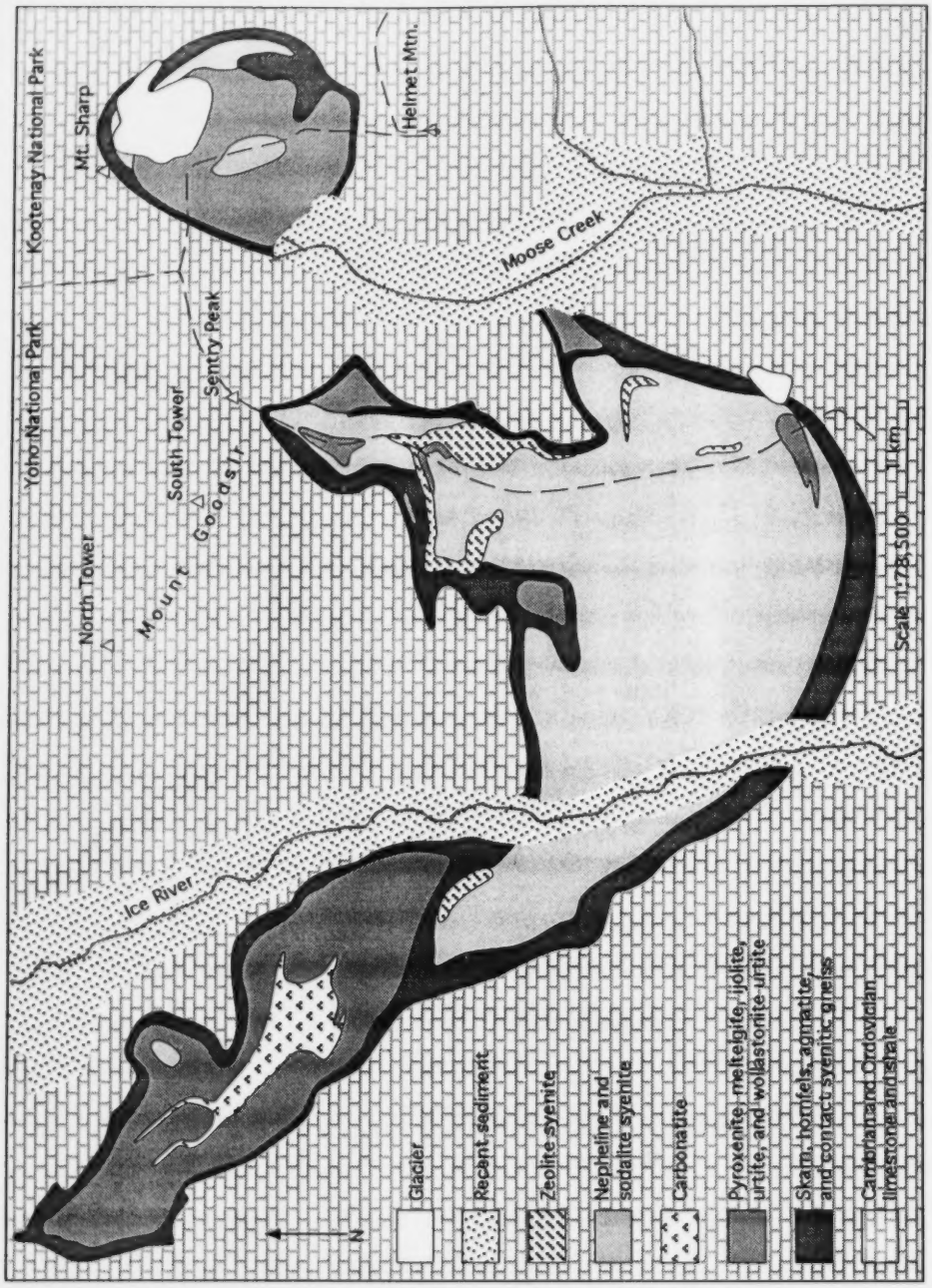

Figure 2.1 Geological map of the Ice River complex (after Currie, 1975).

series form dykes that cross-cut the former, and ultramafic-mafic xenoliths (up to several metres in length) are found in the syenitic rocks. The relationships of the carbonatites with the syenitic series preclude determination of an order of emplacement. Some carbonatite dykes are reported to contain syenitic xenoliths and to cross-cut the syenitic rocks, but nepheline syenite is described as having intruded the main carbonatite body (Currie, 1975; Pell, 1987a).

The feldspar-free rock series consists of repetitive layers of a sequence of graded cumulates (clinopyroxenite, melteigite, olivine hornblendite, ijolite, pargasite ijolite, melanite ijolite, urtite, and wollastonite urtite). The layers range in thickness from roughly 10 to 200 m, and increase in nepheline content toward the top of each layer (Currie, 1975). Cumulate pegmatitic patches, veins and schlieren are common. Ijolite is the most abundant rock type; the other cumulates are subordinate in occurrence. The cumulate units vary mainly in their clinopyroxene : nepheline ratios. The clinopyroxene ranges in composition from titanian diopside to sodian hedenbergite. Other locally important minerals include: olivine (chrysolite), garnet (schorlomite-melanite), amphibole (kaersutite-pargasite-hastingsite), mica (phlogopite-biotite), and wollastonite-1*A*. Accessory minerals include: apatite, perovskite, calcite, magnetite, pyrrhotite, titanite, zoisite, pectolite, natrolite, and cancrinite (Allan, 1914; Ellsworth and Walker, 1925; Currie, 1975; Pell, 1987a).

Carbonatite in the Ice River complex occurs in a number of localities and displays considerable lithologic variation. The major body of carbonatite in the complex is a roughly concordant lenticular mass of calcite-carbonatite 400 m wide and 1500 m long that cuts the enclosing ijolite. This carbonatite consists mainly of ferroan calcite, with accessory aegirine-augite, phlogopite, apatite, pyrite, strontianite, pyrochlore, and ilmenite. Much of the main body of carbonatite appears to have been heavily weathered, with large amounts of 'limonite' (undifferentiated hydrous iron oxides) and voids giving rise to a sparry appearance. A second, more silicate (phlogopite)-rich variety of carbonatite tends to have a marked banding. Carbonatite dykes and sills occur

throughout the complex, and are particularly abundant in the feldspar-free series of rocks (Rapson, 1966; Currie, 1975; Pell, 1987a).

The syenitic series of rocks consists chiefly of melanocratic to leucocratic nepheline syenite, with subordinate sodalite syenite, and rare eudialyte syenite. The syenites form an elliptical mass, zoned from a pale green sodalite syenite core through leucocratic nepheline syenite to melanocratic syenite at the margin. The sodalite and nepheline syenites are composed dominantly of nepheline, K-feldspar (orthoclase) microperthite, amphibole (hastingsite, minor kaersutite), clinopyroxene (sodian hedenbergite-aegirine), and sodalite. Accessory phases include biotite, titanite, cancrinite, calcite, apatite, zircon, melanite, and occasionally fluorite, lavenite, lamprophyllite, lorenzenite and ilmenite. Rare late-stage pockets and seams occur in the nepheline syenite. The major constituents of these pockets are calcite, natrolite, and edingtonite; more rarely, ancylite, catapleiite, aegirine, zircon, magnetite, phlogopite, pyrite, and galena are present (Phillips, 1916; Currie, 1975; Grice and Gault, 1981; Grice *et al.*, 1984). Occasionally the syenites are hydrothermally altered to a mixture of orthoclase microperthite, natrolite, cancrinite, analcime, aegirine, calcite, hematite and sericite. The eudialyte syenite consists of eudialyte, nepheline, albite, aegirine, chlorite and calcite (Allan, 1914; Currie, 1975; Pell, 1987a).

The magma that emplaced the Ice River complex was not intruded at its present geographic location. During Cretaceous-Paleocene (Laramide) orogenesis, the complex and its host Paleozoic strata were thrust eastwards, along a west-dipping décollement surface, approximately 200 km (Gabrielse, 1991). The sedimentary rocks and the complex were regionally metamorphosed to prehnite-pumpellyite facies during this activity (Currie, 1975; Pell and Höy, 1989; Greenwood *et al.*, 1991). The rigid mass of the complex must have behaved more competently during deformation than the host sedimentary rocks because the igneous rocks are relatively undisturbed in comparison to the surrounding penetratively deformed strata (Currie, 1975).

2.1.2 Geochronology

The age of crystallization of the Ice River complex has been a matter of discussion for over a century. Dawson (1886), in the first published geological investigation of the area, considered the complex to be younger than the surrounding sedimentary rocks, "...but older in date than ...the main period of mountain upheaval." However, Allan (1914) concluded, based on structural arguments, that the intrusion of the Ice River complex was contemporaneous with orogenesis. The most novel interpretation of the age of the complex was that of Gussow and Hunt (1959); based on the probably erroneous identification of a paleosol (fossil soil) at the boundary of the nepheline syenite, they concluded that the complex was Precambrian basement overlain by Paleozoic sedimentary rocks. This opinion was reiterated by Gussow (1977a) and Gussow (1977b) on the basis of the same observation.

Radioisotopic dating was first applied to the Ice River Complex by Lowdon (1960). A summary of his data and subsequently determined radioisotopic ages for the Ice River complex is shown in Table 2.1. Most of the dates cluster around the Devonian and Mississippian periods (409 - 323 Ma, Harland *et al.*, 1990). As can be observed on Table 2.1, consensus regarding the age of emplacement of the Ice River complex is lacking.

2.2 MATERIAL AND METHODS

Specimens, judged to be representative, were collected during reconnaissance sampling from all the major phases of the complex for radioisotopic analysis. Whole-rock powders were prepared for all samples following the methods of Duke (1993; p. 212). Four samples were chosen for mineral separation: a perovskite melteigite, a wollastonite urtite, a calcite carbonatite, and a nepheline syenite. Minerals were separated from the 120 - 170 U.S. mesh size fraction. Strongly magnetic material was removed using a hand magnet. Mineral separates were then produced with the use of tetrabromoethane, diiodomethane, and a Frantz Isodynamic Magnetic

Table 2.1 Previous radioisotopic age determinations for the Ice River Complex

Reference	Age Ma (2σ)	Method	Comments by references
Lowdon (1960)	340±23	K-Ar biotite	syenite dyke
	330±23	K-Ar biotite	pyroxenite
Baadsgaard *et al.* (1961)	355±18	K-Ar biotite	jacupirangite
	360±18	K-Ar biotite	minette
	304±15	K-Ar biotite	slightly altered?, pegmatitic phase
Rapson (1963)	392±10	K-Ar biotite pyroxenite	whole rock determination
	336±5	K-Ar biotite	altered biotite pegmatite
	280±30	Rb-Sr biotite	altered biotite pegmatite, $^{87}Sr/^{86}Sr$ too low for reliable age
	327±5	K-Ar biotite	highly altered minette
	244±45	Rb-Sr biotite	highly altered minette, $^{87}Sr/^{86}Sr$ too low for reliable age
Currie (1975)	233±11	K-Ar biotite	mela-ijolite
	220±8	K-Ar biotite	nepheline syenite
Stevens *et al.* (1982)	421±11	K-Ar 'hornblende'	excess argon?, nepheline syenite
Hunt and Roddick (1987)	421±11	K-Ar 'hornblende'	excess argon?, nepheline syenite
Parrish *et al.* (1987)	368±4	U-Pb zircon, titanite	all isotope systems somewhat
	372±4	Ar-Ar 895°C 'hornblende'	disturbed, nepheline syenite
Hunt and Roddick (1988)	459±17	K-Ar 'hornblende'	excess argon?, nepheline syenite
Heaman, pers. comm. (1994)	357	U-Pb perovskite	reliable age of crystallization

Separator®, followed by hand-picking. The constituent phases of the four rocks are listed in Table 2.2.

Mineral samples for U-Pb analysis were: perovskite (from melteigite), titanite (from wollastonite urtite), titanite (from nepheline syenite), pyrochlore (from calcite carbonatite), and schorlomite (a megacryst from ijolite).
The U-Pb analytical procedure used followed that outlined in Baadsgaard and Lerbekmo (1983) for all of the minerals, except the pyrochlore, for which the techniques of Romer and Wright (1992) were used. Uncertainties in the U-Pb data were calculated using in-house programs of Dr. H. Baadsgaard and the results used in the Isoplot program of Ludwig (1990). These, and all further uncertainties, except where noted, are quoted at the 2σ level of significance. The constants used were $\lambda_{U238} = 1.55125 \times 10^{-10}\ a^{-1}$, $\lambda_{U235} = 9.845 \times 10^{-10}\ a^{-1}$, and $^{238}U/^{235}U = 137.88$ (Steiger and Jäger, 1977). The Pb blank was determined to be 0.86 ng by isotope dilution analysis using a ^{206}Pb spike.

All of the whole-rock samples and some of the minerals were analyzed isotopically for Rb-Sr, Sm-Nd, and Pb. Following sample dissolution, Rb, Sr, Sm and Nd were separated by standard cation-exchange chromatography (Duke, 1993; pp. 235-236), and Pb was separated by barium nitrate coprecipitation followed by anion-exchange chromatography (Cavell, 1986; pp. 386-387). Two aliquots of each sample were used, one to determine the isotopic composition of Nd and Pb, and the other to determine by isotope dilution the concentrations of Sm, Nd, Rb and Sr, as well as the $^{87}Sr/^{86}Sr$ isotope ratio, using $^{145}Nd+^{147}Sm$ and $^{87}Rb+^{84}Sr$ mixed spikes. Mass spectrometric analyses of Rb, Sr, Sm, Nd and Pb were made following the procedures of Duke (1993; pp. 237-238). A single-load method was used for Sm and Nd (Duke, 1993; p. 238). The NBS 987 standard yielded an $^{87}Sr/^{86}Sr$ value of 0.71025 ± 10 ($n = 15$), and the La Jolla standard solution was measured at $^{143}Nd/^{144}Nd = 0.511816 \pm 20$ ($n = 33$); a correction factor of 1.000062 was applied to the $^{143}Nd/^{144}Nd$ measured ratios to correct for deviation from the accepted La Jolla value of 0.511858. Reported $^{87}Sr/^{86}Sr$ ratios were

Table 2.2 Modal analyses of the samples from which minerals were separated

Ice 38 wollastonite urtite		I90.3 perovskite melteigite		I92.35 nepheline syenite		I90.13 carbonatite	
mineral	modal %	mineral	modal %	mineral	modal %	mineral	modal %
nepheline	68	diopside	38	orthoclase perthite	48	calcite	88.5
hedenbergite	15	nepheline	31	nepheline	30	aegirine-augite	7
wollastonite	10	perovskite	6.5	hastingsite	9.5	biotite	3
titanite	2.5	apatite	6	hedenbergite	4	apatite	1.5
calcite	2	biotite	5	sodalite	3.5	pyrochlore	<1
sodalite	1	cancrinite	3.5	titanite	2.5	hematite	<1
cancrinite	1	magnetite	3	cancrinite	1.5	ilmenite	<1
biotite	<1	pyrrhotite	3	apatite	1	strontianite	<1
pyrite	<1	calcite	2.5				
apatite	<1	titanite	1.5				
pectolite	<1						

Modes were determined by point-counting of thin sections, or a rock slab in the case of the carbonatite.

normalized to $^{86}Sr/^{88}Sr$ = 0.1194, and $^{143}Nd/^{144}Nd$ isotopic ratios were normalized to $^{146}Nd/^{144}Nd$ = 0.7219 (Lugmair and Marti, 1978). Mass fractionation correction factors used for Pb were 1.2, 1.3, and 1.4 per mil/amu for $^{206}Pb/^{204}Pb$, $^{207}Pb/^{204}Pb$, and $^{208}Pb/^{204}Pb$, respectively (Duke, 1993; p. 237). The constants used were $\lambda_{Rb87} = 1.42 \times 10^{-11}$ a^{-1}, and $\lambda_{Sm147} = 6.54 \times 10^{-12}$ a^{-1} (Steiger and Jäger, 1977; Lugmair and Marti, 1978). Procedural blanks were assumed to be 0.06 ng Sm, 0.95 ng Nd, 0.1 ng Rb, 0.3 ng Sr, and 1.2 ng Pb (Duke, 1993; p. 234, 236-237).

2.3 ISOTOPIC RESULTS

2.3.1 U-Pb

The results of the U-Pb isotopic analyses are listed in Table 2.3. In several instances a second aliquot of a sample was analyzed, after further hand-picking, in an attempt to decrease the discordancy of the sample. In the case of the pyrochlore, one aliquot was also leached for ten minutes in 10% $HF_{(aq)}$, the leached shell removed, and the unleached core analyzed (Romer and Wright, 1992); this procedure dramatically decreased the discordancy of the pyrochlore.

A conventional U-Pb concordia plot is shown in Figure 2.2 for the nine sample aliquots. By using the errors assigned in Table 2.3, and a correlation coefficient of R = 0.993, the data in Figure 2.2 lie on a discordia line with an upper concordia intercept age of 356 $\pm$ 6 Ma (calculated with Model 1 of Ludwig, 1990). The mean squared weighted deviation (MSWD) of this discordia line is 0.23, and is within the uncertainty of the expected value for n = 9 points of 0.71 $\pm$ 1.07 (Wendt and Carl, 1991). The discordant minerals have experienced lead loss to differing degrees, presumably because of differences in their grain sizes, crystal lattices, and concentrations of radioactive elements (Faure, 1986). The lower end of the discordia line intersects concordia at about 13 $\pm$ 3 Ma. In the absence of any other evidence for a geologic event at this time, this date is close enough to zero that no significance is attached to it; lead loss may have been diffusional rather than episodic. Only

Table 2.3 U-Pb data, Ice River complex

Sample	Weight mg	^{238}U ppm	^{235}U ppm	^{206}Pb ppm	^{207}Pb ppm	^{208}Pb ppm	Pb_{common} ppm
Ice 38 titanite	401.5	17.97	0.129	0.868	0.047	0.483	0.769
I90.13 pyrochlore	22.5	1.12×10^5	802.8	1412	75.014	62.681	24.515
I90.13* pyrochlore	3.0	9.10×10^4	651.8	2237	119.73	150.17	1103
I90.13** pyrochlore	0.9	6.82×10^4	488.1	2502	134.99	116.10	527.4
I92.35 titanite	1040.1	20.38	0.146	0.924	0.050	1.441	0.840
I92.35* titanite	517.5	18.73	0.134	0.866	0.047	1.349	0.786
I90.3 perovskite	303.4	142.01	1.017	6.612	0.356	53.787	1.397
I90.3* perovskite	228.0	141.94	651.8	6.613	0.356	53.753	1.274
I90.4 schorlomite	515.2	38.41	0.275	1.885	0.102	0.43	0.100

* these fractions re-cleaned by further hand-picking
** this sample was leached in 10% HF for 10 minutes, and the exterior discarded

Table 2.3 - continued

Sample	$\frac{^{206}Pb}{^{204}Pb}$	$\frac{^{206}Pb}{^{238}U}$ (1 σ %)	$\frac{^{207}Pb}{^{235}U}$ (1 σ %)	$\frac{^{207}Pb}{^{206}Pb}$ (1 σ %)	$^{207}Pb/^{206}Pb$ age (Ma 1 σ)
Ice 38 titanite	57.25	0.05580 (0.612)	0.41388 (2.178)	0.05380 (1.57)	363 (6.6)
I90.13 pyrochlore	2020.2	0.01455 (0.599)	0.10608 (0.674)	0.05287 (0.106)	323 (2.4)
I90.13* pyrochlore	88.79	0.02840 (0.747)	0.20855 (1.790)	0.05326 (1.05)	341 (24)
I90.13** pyrochlore	182.78	0.04240 (0.628)	0.31395 (1.042)	0.05371 (0.424)	359 (10)
I92.35 titanite	56.42	0.05240 (0.653)	0.39188 (2.216)	0.05424 (1.57)	381 (35)
I92.35* titanite	56.42	0.05338 (0.828)	0.39924 (2.582)	0.05424 (1.76)	381 (40)
I90.3 perovskite	182.35	0.05379 (0.956)	0.39963 (1.440)	0.05352 (0.504)	351 (11)
I90.3* perovskite	197.88	0.05383 (0.961)	0.39807 (1.617)	0.05363 (0.672)	356 (15)
I90.4 schorlomite	659.75	0.05670 (0.574)	0.41928 (0.700)	0.05363 (0.147)	356 (6.6)

* these fractions re-cleaned by further hand-picking
** this sample was leached in 10% HF for 10 minutes, and the exterior discarded

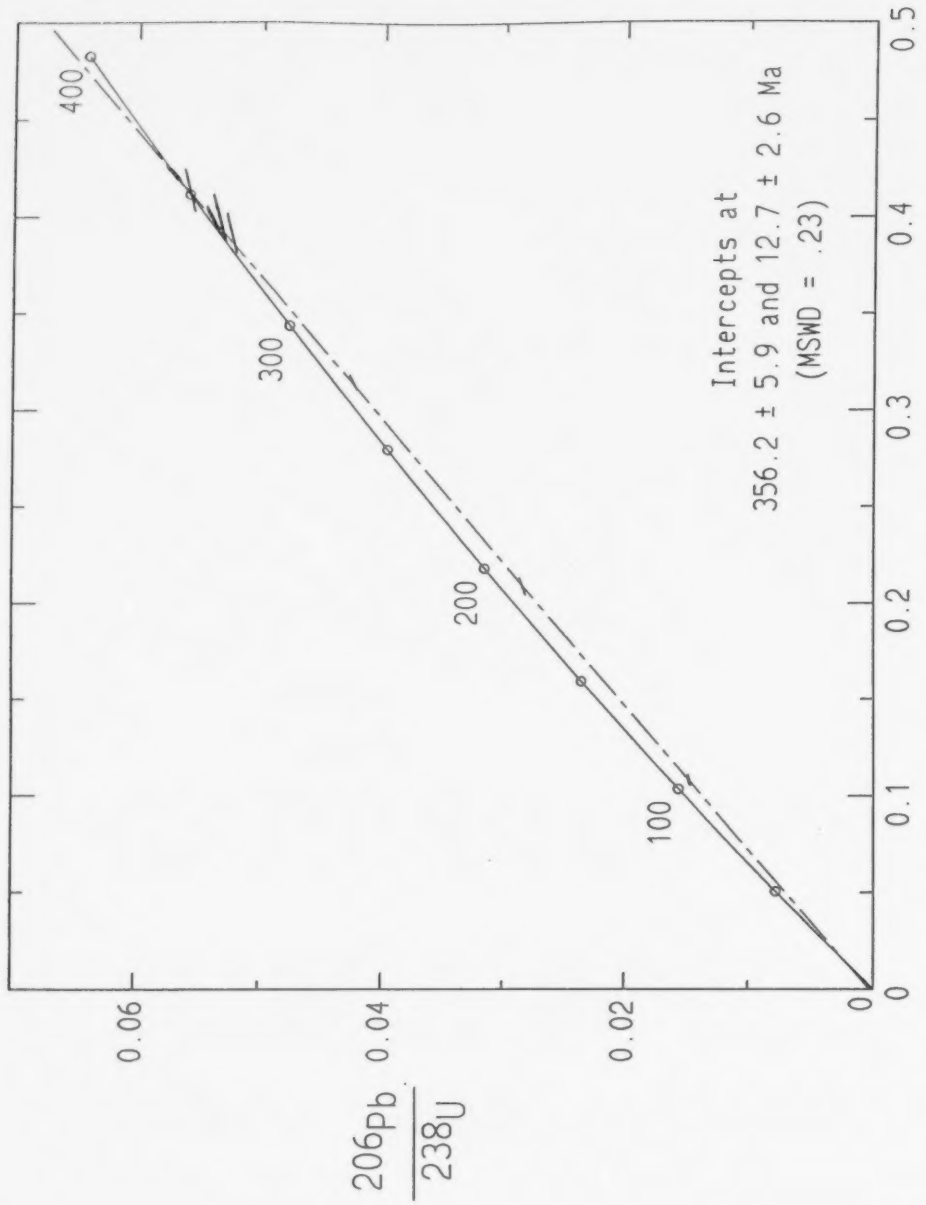

Figure 2.2 U-Pb concordia diagram for the nine sample aliquots. The circles denote the geologic age on concordia, while the ellipses indicate the samples.

the schorlomite datum is concordant (Figure 2.3). Removal of this point would result in an upper intercept of 359 $\pm$ 13 Ma, MSWD = 0.25, for the remaining eight data points - an identical age within error. Because minerals from modally diverse units of the complex lie on the same discordia line, their $^{207}Pb/^{206}Pb$ ages are identical within error (with the exception of the extremely discordant aliquot of pyrochlore, Table 2.3), and therefore all of the different units of the complex are considered to be of the same age. No rock-unit can be said to be older or younger than another on the basis of these results; i.e., a timespan for emplacement of the complex cannot be identified with these U-Pb data.

2.3.2 Rb-Sr

The Rb and Sr isotopic data obtained are listed in Table 2.4. Epsilon Sr values were calculated assuming an age of 356 Ma (see U-Pb results above), a modern bulk earth $^{87}Sr/^{86}Sr$ = 0.7045, and a present $^{87}Rb/^{86}Sr$ = 0.0816 (Faure, 1986). With the exception of sample I92.37 eudialyte syenite (which will be addressed below), the data for thirty-five mineral and whole-rock samples from the complex are shown in Figure 2.4 on a Rb-Sr isochron plot. The expected value of the MSWD for an isochron with n = 35 points is 0.94 $\pm$ 0.49 (Wendt and Carl, 1991). These data define a scatterchron (MSWD = 8.71) when regressed using Model 1 of the Isoplot program (Ludwig, 1990) with errors of $^{87}Rb/^{86}Sr$ = 0.257% ($\pm 1\ \sigma_x$), $^{87}Sr/^{86}Sr$ = 0.0222% ($\pm 1\ \sigma_y$), and a correlation coefficient R = 0.56 (Baadsgaard *et al.*, 1993). Therefore, these data are scattered outside of analytical error, and the uncertainty in the age given by the scatterchron is multiplied by $MSWD^{1/2}$ yielding 369 $\pm$ 17 Ma. No geologically reasonable subset of these data (e.g. whole-rock only) yields an isochron ($0 < MSWD < 2$) upon linear regression.

The calculated Sr initial ratio of the eudialyte syenite corresponds more closely to those of the shales (Table 2.4) and is significantly higher than those of the other rocks of the complex. This can be explained either by extensive

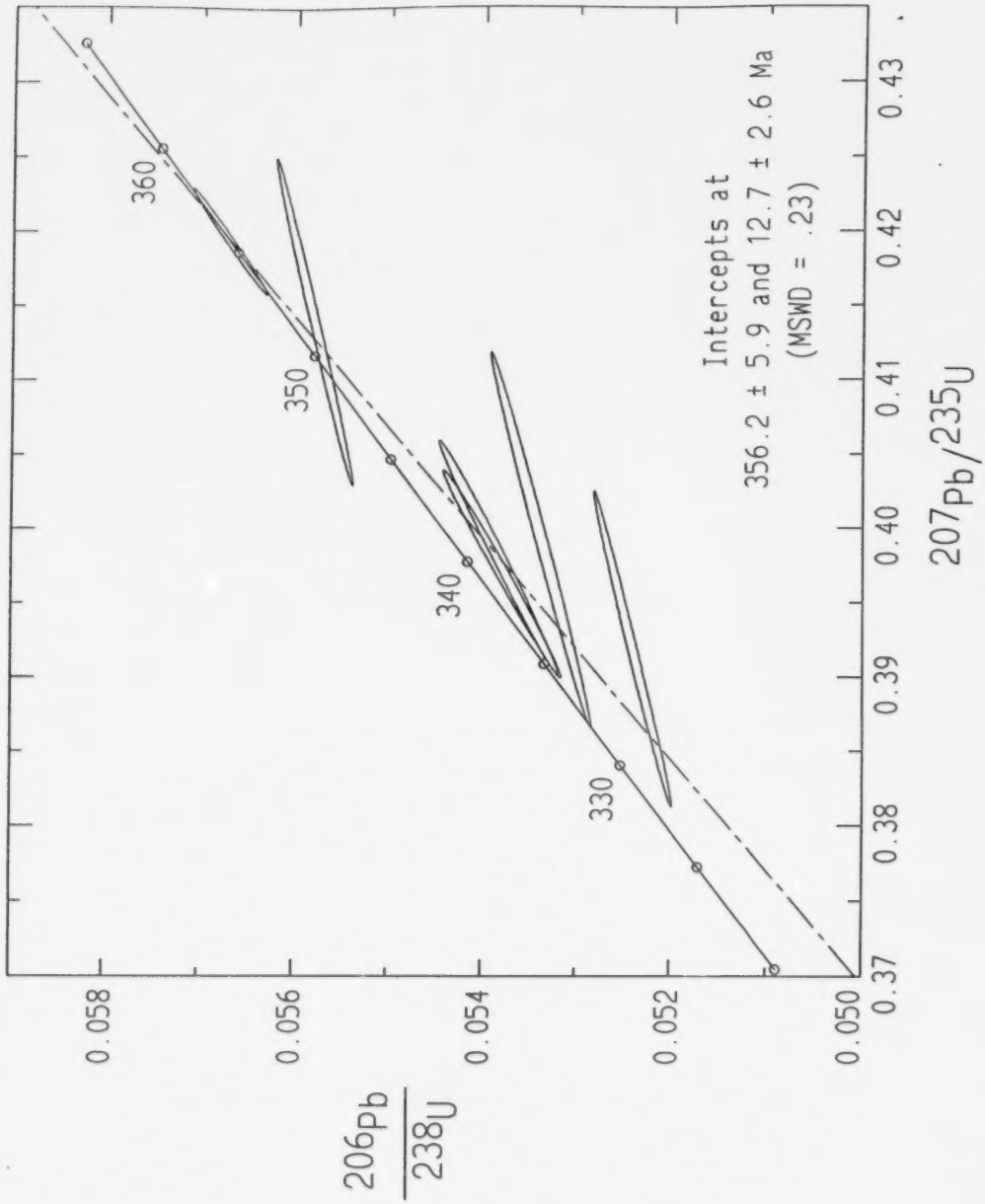

Figure 2.3 Expanded U-Pb concordia diagram in the region 320 -365 Ma, displaying the concordant nature of the schorlomite at 356 Ma.

Table 2.4 Rb-Sr data, Ice River complex

Sample	$\frac{^{87}Sr}{^{86}Sr}$	$\frac{^{87}Rb}{^{86}Sr}$	Rb ppm	Sr ppm	initial ratio at 356 Ma	ϵ^{356}_{UR}
Ice 38 wollastonite urtite	0.70328	0.10710	83.35	2250.73	0.70274	-19
I90.3 perovskite melteigite	0.70415	0.27117	85.05	907.22	0.70277	-19
I90.6 olivine hornblendite	0.70398	0.24552	59.45	700.29	0.70273	-19
I92.8 pyroxenite	0.70302	0.04390	5.05	332.53	0.70279	-18
I92.35 nepheline syenite	0.70467	0.25187	163.07	1872.67	0.70340	-10
I90.13 carbonatite	0.70257	0.02606	20.74	2301.56	0.70244	-23
I90.13 carbonatite*	0.70292	0.00814	30.45	10815.14	0.70288	-17
I90.19 nepheline syenite	0.70661	0.57011	283.56	1438.88	0.70372	-5
I92.35 nepheline syenite*	0.70459	0.25098	163.42	1883.26	0.70332	-11
Sodalite syenite	0.70919	1.30846	194.91	431.05	0.70256	-22
I90.3 magnetite	0.70313	0.02589	0.45	50.11	0.70300	-15
I90.3 apatite	0.70267	0.00112	2.43	6259.02	0.70266	-20
I90.3 diopside	0.70282	0.05646	10.63	544.36	0.70253	-22
I90.4 schorlomite	0.70281	0.02556	0.82	92.78	0.70268	-20
Ice 8 pyroxenite	0.70421	0.07840	28.28	1043.41	0.70382	-4
Ice 22 pargasite ijolite	0.70456	0.16260	71.44	1270.81	0.70373	-5

Table 2.4 - continued

Sample	$\frac{^{87}Sr}{^{86}Sr}$	$\frac{^{87}Rb}{^{86}Sr}$	Rb ppm	Sr ppm	initial ratio at 356 Ma	ϵ_{UR}^{356}
Ice 23 pegmatite syenite	0.71481	2.44267	324.13	384.19	0.70243	-23
I90.7 ijolite	0.70430	0.30441	147.92	1405.39	0.70276	-19
I90.9 melanite ijolite	0.70453	0.33819	103.55	885.64	0.70282	-18
I90.3 nepheline	0.70549	0.58887	112.77	553.96	0.70250	-23
I90.3 residue	0.70375	0.03887	22.76	1693.24	0.70356	-8
I90.3 calcite	0.70300	0.00808	11.63	4163.25	0.70296	-16
Ice 38 wollastonite	0.70303	0.01444	6.45	1291.18	0.70296	-16
Ice 38 hedenbergite	0.70300	0.04942	15.36	898.96	0.70274	-19
I90.13 aegirine-augite	0.70306	0.03035	18.84	1794.80	0.70290	-17
I90.13 calcite	0.70285	0.00012	0.46	11403.63	0.70285	-18
I92.35 nepheline & feldspar	0.70472	0.29085	186.57	1855.36	0.70325	-12
I92.35 hastingsite	0.70397	0.16903	24.52	419.51	0.70312	-14
Ice 38 calcite	0.70328	0.01036	57.26	15992.62	0.70323	-12
Ice 38 nepheline	0.70584	0.61758	216.69	1014.97	0.70271	-20
I90.13 apatite	0.70312	0.00006	0.33	16065.24	0.70312	-14
I92.35 apatite	0.70450	0.10329	153.59	4300.80	0.70398	-2

Table 2.4 - continued

Sample	$\frac{^{87}Sr}{^{86}Sr}$	$\frac{^{87}Rb}{^{86}Sr}$	Rb ppm	Sr ppm	initial ratio at 356 Ma	ϵ_{UR}^{356}
I92.35 hedenbergite	0.70439	0.34337	29.05	244.71	0.70265	-20
I92.35 titanite	0.70341	0.02110	2.02	277.42	0.70330	-11
I90.3 biotite	0.76025	10.83893	596.92	160.16	0.70532	18
I92.37 eudialyte syenite	0.72209	1.75173	250.81	414.84	0.71321	130
Ice 40 Ottertail shale	0.71930	1.42845	141.14	286.20	0.71206	113
RB707 Chancellor shale †	0.71882	0.58412	36.23	496.23	0.71586	167

* repeat of sample using different aliquot; aliquots appear to be heterogeneous
† data from Koffyberg (1994)
The 1 σ uncertainty in $^{87}Sr/^{86}Sr$ varied from 0.000007 to 0.00013.

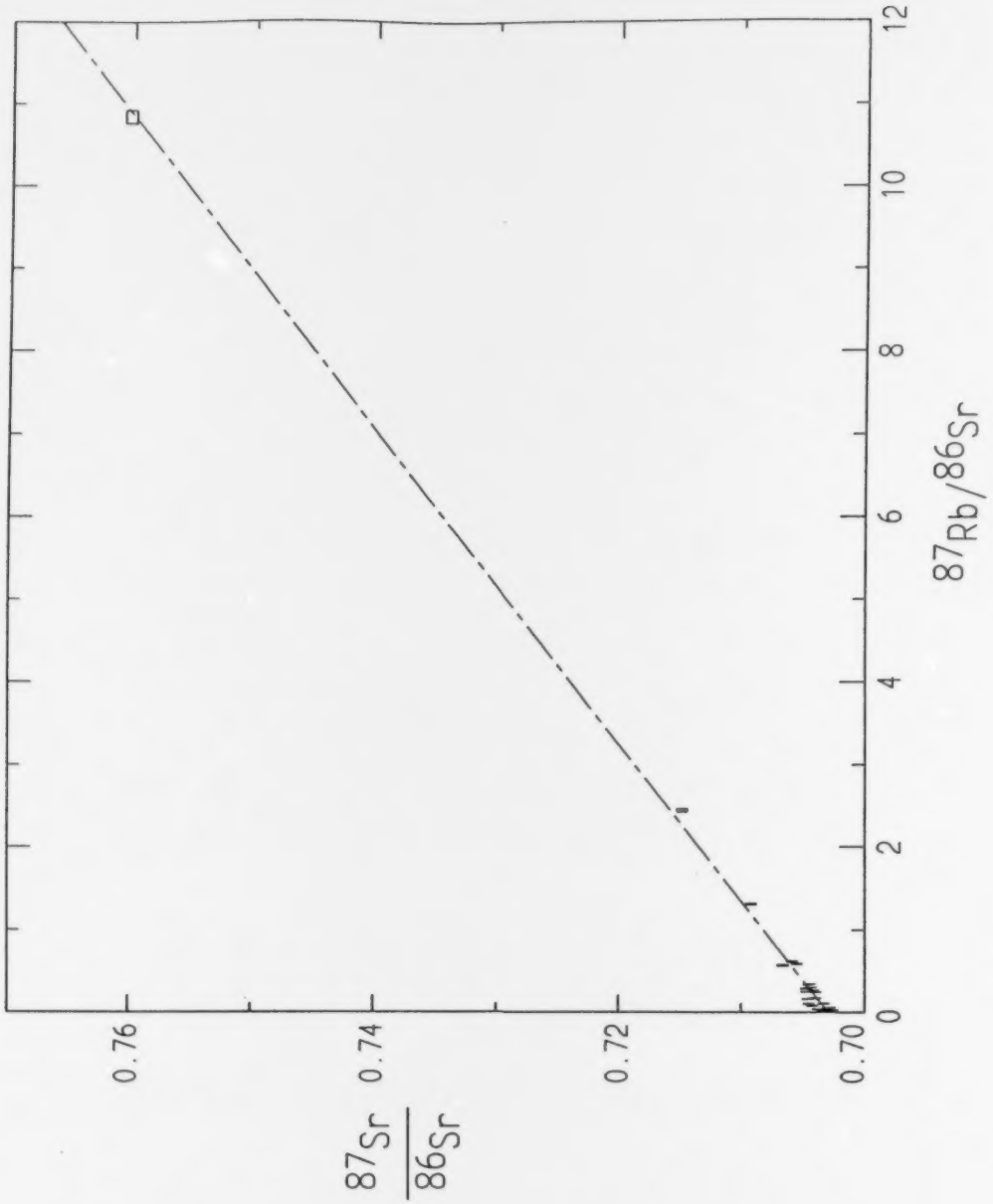

Figure 2.4 Rb-Sr isochron diagram showing the scatter of the data. The best fit line yields an age of 369 ± 17 Ma (2σ *MSWD$^{1/2}$).

interaction between the eudialyte syenite and surrounding shales that have a similar Sr initial ratio (Table 2.4), or by recent Rb loss. The name *eudialyte* is derived from the Greek, and means "easily dissolved". The solubility of eudialyte is consistent with the suggestion that Rb, a mobile alkali metal, could be preferentially leached out of the vulnerable lattice of this mineral. From the equation for the growth of radiogenic ^{87}Sr:

$$^{87}Sr/^{86}Sr = (^{87}Sr/^{86}Sr)_{init} + {}^{87}Rb/^{86}Sr(e^{\lambda t}-1)$$

it can be calculated that if there has been recent loss of Rb, the resulting value for the initial Sr ratio will be anomalously high. As eudialyte comprises roughly forty percent by volume of the eudialyte syenite, and is somewhat altered (Plate 2.1), it is suggested that this rock has lost Rb in geologically recent time (conceivably as a result of weathering upon exposure). However the Sm-Nd and Pb-Pb isotope systematics of the eudialyte syenite are similar to those of the Ice River rocks (see below); minor recent Pb or rare-earth element loss would not significantly affect these isotope systematics.

2.3.3 Sm-Nd

The Sm and Nd isotopic data obtained are listed in Table 2.5. Epsilon Nd values were calculated relative to the chondritic uniform reservoir - CHUR (DePaolo and Wasserburg, 1976), assuming an age of 356 Ma (see U-Pb results above), a present $^{143}Nd/^{144}Nd = 0.512638$, and a modern ratio of $^{147}Sm/^{144}Nd = 0.1967$ (Faure, 1986). The twenty-seven mineral and whole-rock samples from the complex are shown in Figure 2.5 on a Sm-Nd isochron plot. The expected value of the MSWD for an isochron with n = 27 points is 0.92 ± 0.57 (Wendt and Carl, 1991). These data define a scatterchron (MSWD = 5.75) when regressed using Model 1 of the Isoplot program (Ludwig, 1990) with errors of $^{147}Sm/^{144}Nd = 0.1\%$ ($\pm 1\ \sigma_x$), $^{143}Nd/^{144}Nd = 0.004\%$ ($\pm 1\ \sigma_y$) and a correlation coefficient R = 0.5 (Cavell, 1986). The best fit line through the twenty-seven data points yields a slope age of 359 ± 197 Ma ($2\sigma * MSWD^{1/2}$).

A subset of the data shown in Figure 2.5 defines a line subparallel to the

Plate 2.1 Photomicrographs of the eudialyte syenite under plane-polarized (a) and cross-polarized light (b). The eudialyte is quite altered in comparison to the other minerals (aegirine, nepheline, and albite). The magnification was 100 times.

Table 2.5 Sm-Nd data, Ice River complex

Sample	$\frac{^{143}Nd}{^{144}Nd}$	$\frac{^{147}Sm}{^{144}Nd}$	Nd ppm	Sm ppm	$\frac{^{143}Nd}{^{144}Nd}$ initial at 356 Ma	ϵ^{356}_{CHUR}
Ice 40 Ottertail shale‡	0.511236	0.094987	39.68	6.24	0.511015	-22.74
Ice 38 wollastonite urtite	0.512595	0.082933	25.32	3.47	0.512402	4.34
I90.3 perovskite melteigite	0.512627	0.081931	235.92	31.97	0.512436	5.02
I90.6 olivine hornblendite	0.512664	0.105575	46.62	8.14	0.512418	4.66
I90.13 carbonatite	0.512544	0.056840	117.00	11.00	0.512412	4.54
I92.8 pyroxenite	0.512663	0.121062	80.13	16.05	0.512381	3.94
I92.35 nepheline syenite	0.512570	0.093323	33.09	5.11	0.512352	3.38
I90.19 nepheline syenite	0.512507	0.088464	11.05	1.62	0.512301	2.37
I92.35 nepheline syenite*	0.512581	0.090866	33.80	5.08	0.512369	3.71
I92.37 eudialyte syenite	0.512637	0.111850	914.02	169.10	0.512376	3.85
Sodalite syenite	0.512612	0.121235	18.98	3.81	0.512329	2.93
I90.3 apatite	0.512670	0.099659	950.91	156.75	0.512438	5.05
I90.3 diopside	0.512622	0.079883	357.84	47.28	0.512436	5.01
I90.4 schorlomite	0.512987	0.237828	346.42	136.27	0.512433	4.95
Ice 8 pyroxenite	0.512537	0.113572	68.29	12.83	0.512272	1.82

Table 2.5 - continued

Sample	$\frac{^{143}Nd}{^{144}Nd}$	$\frac{^{147}Sm}{^{144}Nd}$	Nd ppm	Sm ppm	$\frac{^{143}Nd}{^{144}Nd}$ initial at 356 Ma	ϵ^{356}_{CHUR}
Ice 22 pargasite ijolite	0.512571	0.099917	109.14	18.04	0.512338	3.10
Ice 23 pegmatite syenite	0.512522	0.072349	23.91	2.86	0.512353	3.40
Ice 35 nepheline syenite	0.512508	0.084495	24.95	3.49	0.512311	2.57
I90.9 melanite ijolite	0.512819	0.169360	51.07	14.31	0.512424	4.78
I90.7 ijolite	0.512641	0.088659	159.40	23.38	0.512434	4.98
I90.13 carbonatite*	0.512553	0.056565	118.54	10.88	0.512421	4.72
I90.3 nepheline	0.512626	0.078742	20.72	2.70	0.512442	5.14
Ice 38 wollastonite	0.512650	0.094098	57.72	8.98	0.512431	4.91
Ice 38 hedenbergite	0.512605	0.089644	12.94	1.92	0.512396	4.23
I90.13 aegirine-augite	0.512586	0.071789	52.27	6.21	0.512419	4.68
I90.13 apatite	0.512591	0.068783	881.91	100.34	0.512431	4.91
I92.35 apatite	0.512528	0.066722	274.24	30.27	0.512372	3.77
I92.35 titanite	0.512609	0.081054	1679.79	225.21	0.512420	4.70

* Repeat of sample using different aliquot.
‡ The CHUR model age of the Ottertail shale is 2040 Ma.
The 1 σ uncertainty in $^{143}Nd/^{144}Nd$ ranged from 0.008 per mil to 0.069 per mil.

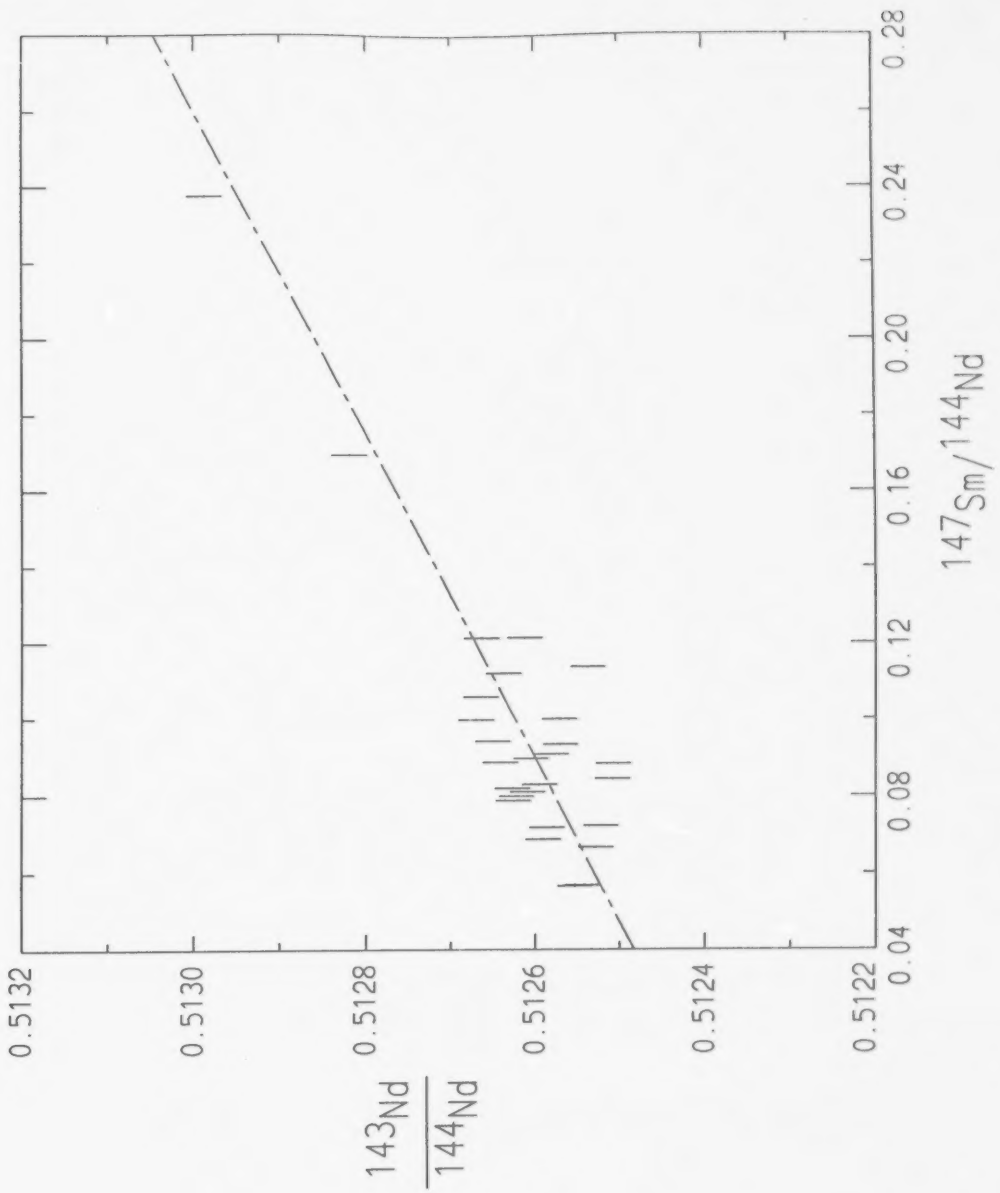

Figure 2.5 Sm-Nd isochron diagram showing the scatter of the data. The best fit line yields an age of 359 ± 197 Ma (2σ *MSWD$^{1/2}$).

best fit regression line for the twenty-seven data points. This fifteen point subset consists of the feldspar-free and carbonatite series of rocks (and their constituent minerals). This subset excludes xenoliths of the feldspar-free series that were stoped into the syenite series. This subset is listed in Table 2.6, and shown in Figure 2.6. Upon linear regression (as above), these data define an isochron (MSWD = 0.46, expected value = 0.85 $\pm$ 0.78, n = 15) yielding an age of 363 $\pm$ 34 Ma. This age is in agreement with that determined by the U-Pb methods (356 $\pm$ 6 Ma), and suggests that this Nd data is of sufficient quality to use as a petrogenetic tracer; this will be addressed in the Discussion below.

2.3.4 Pb-Pb

The Pb data obtained are listed in Table 2.7. These Pb isotopic compositions have not been corrected for their age because U and Th contents were not measured for all samples. With the exclusion of the most radiogenic (and most discordant) pyrochlore aliquot, the remaining samples from the complex yield a scatterchron (MSWD = 22.2) upon linear regression (Model 1, Ludwig, 1990) using 0.1% uncertainty for both axes and a correlation coefficient R = 0.90. The expected value of the MSWD for an isochron with n = 42 points is 0.95 $\pm$ 0.45 (Wendt and Carl, 1991). The best fit line generates a slope age of 346 $\pm$ 52 Ma ($2\sigma * MSWD^{1/2}$). All of the data from Table 2.7 are shown on a $^{207}Pb/^{204}Pb$ vs. $^{206}Pb/^{204}Pb$ diagram in Figure 2.7 with a 356 Ma reference line constrained to run through the schorlomite and the point given for 356 Ma by the model of Stacey and Kramers (1975). Figure 2.8 is an expansion of Figure 2.7 in the region $^{206}Pb/^{204}Pb$ = 18 to 22, with both the Ottertail shale and the Stacey and Kramers point (SK) identified. No geologically reasonable subset of the data yields an isochron upon linear regression.

Table 2.6 Sm-Nd data, feldspar-free and carbonatite series

Sample	$\frac{^{143}Nd}{^{144}Nd}$	$\frac{^{147}Sm}{^{144}Nd}$	Nd ppm	Sm ppm	$\frac{^{143}Nd}{^{144}Nd}$ initial at 356 Ma	ϵ^{356}_{CHUR}
Ice 38 wollastonite urtite	0.512595	0.082933	25.32	3.47	0.512402	4.34
I90.3 perovskite melteigite	0.512627	0.081931	235.92	31.97	0.512436	5.02
I90.6 olivine hornblendite	0.512664	0.105575	46.62	8.14	0.512418	4.66
I90.13 carbonatite	0.512544	0.056840	117.00	11.00	0.512412	4.54
I90.3 apatite	0.512670	0.099659	950.91	156.75	0.512438	5.05
I90.3 diopside	0.512622	0.079883	357.84	47.28	0.512436	5.01
I90.4 schorlomite	0.512987	0.237828	346.42	136.27	0.512433	4.95
I90.9 melanite ijolite	0.512819	0.169360	51.07	14.31	0.512424	4.78
I90.7 ijolite	0.512641	0.088659	159.40	23.38	0.512434	4.98
I90.13 carbonatite*	0.512553	0.056565	118.54	10.88	0.512421	4.72
I90.3 nepheline	0.512626	0.078742	20.72	2.70	0.512442	5.14
Ice 38 wollastonite	0.512650	0.094098	57.72	8.98	0.512431	4.91
Ice 38 hedenbergite	0.512605	0.089644	12.94	1.92	0.512396	4.23
I90.13 aegirine-augite	0.512586	0.071789	52.27	6.21	0.512419	4.68
I90.13 apatite	0.512591	0.068783	881.91	100.34	0.512431	4.91

* Repeat of sample using different aliquot.

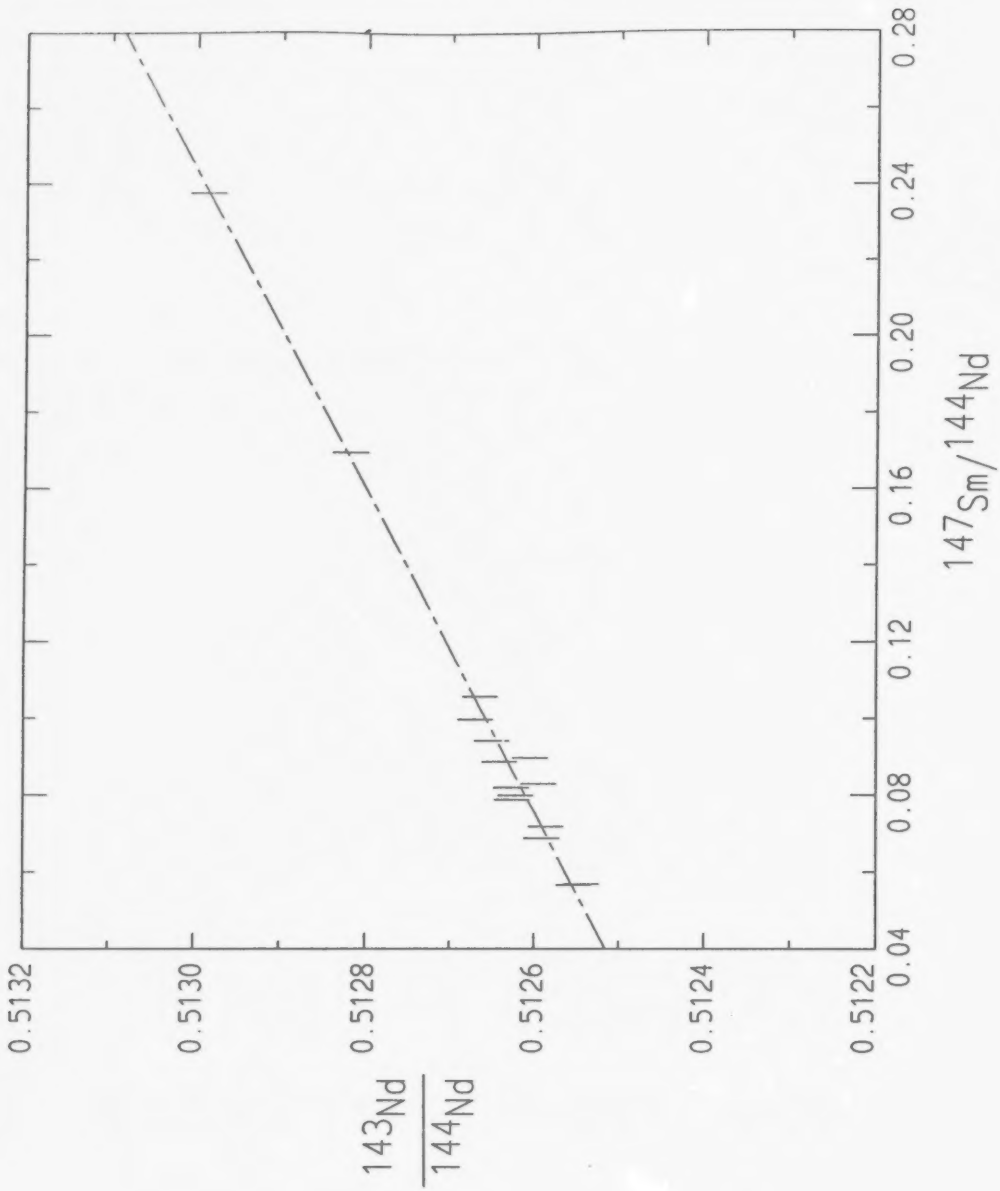

Figure 2.6 Sm-Nd isochron diagram depicting the subset of the feldspar-free and carbonatite series of rocks and minerals. These data yield an isochron with an age of 363 $\pm$ 34 Ma, MSWD = 0.46.

Table 2.7 Pb-Pb data, Ice River complex

Sample	$\frac{^{206}Pb}{^{204}Pb}$	$\frac{^{207}Pb}{^{204}Pb}$	$\frac{^{208}Pb}{^{204}Pb}$
Stacey & Kramers (1975): 356 Ma	18.15	15.60	38.03
Ice 40 Ottertail shale	20.07	15.77	41.55
Sodalite syenite	18.27	15.57	38.36
I90.9 melanite ijolite	18.83	15.53	38.20
I92.8 pyroxenite	18.84	15.65	39.15
I92.37 eudialyte syenite	18.93	15.65	38.86
I90.3 calcite	19.00	15.63	38.66
Ice 38 calcite	19.03	15.58	38.38
Ice 38 hedenbergite	19.36	15.62	38.71
Ice 8 pyroxenite	19.53	15.66	39.30
Ice 35 nepheline syenite	19.54	15.63	39.41
I92.35 nepheline/feldspar	19.62	15.66	39.30
Ice 38 wollastonite	19.63	15.67	39.63
Ice 38 nepheline	19.71	15.64	39.08
I90.3 biotite	19.76	15.76	38.90
I90.3 magnetite	19.79	15.67	39.77
I90.19 nepheline syenite	19.89	15.71	39.66
Ice 23 pegmatite syenite	20.10	15.75	39.48
Ice 38 wollastonite urtite	20.14	15.72	39.63
I90.3 nepheline	20.16	15.64	45.55
I92.35 nepheline syenite	20.17	15.71	40.32
I90.7 ijolite	20.64	15.71	42.80
I92.35 hedenbergite	20.99	15.70	43.01
Ice 22 pargasite ijolite	21.20	15.71	42.13
I90.6 olivine hornblendite	21.41	15.77	44.26

Table 2.7 - continued

Sample	$\frac{^{206}Pb}{^{204}Pb}$	$\frac{^{207}Pb}{^{204}Pb}$	$\frac{^{208}Pb}{^{204}Pb}$
I92.35 apatite	25.67	16.28	51.29
I90.3 perovskite melteigite	26.01	16.01	81.50
I90.3 apatite	27.58	16.04	78.59
I90.3 diopside	28.59	16.13	108.08
I90.13 calcite	51.23	17.43	42.04
I92.35 titanite	55.65	17.77	97.07
I92.35 titanite*	56.42	17.68	98.20
Ice 38 titanite	57.25	17.70	60.68
I90.13 apatite	64.81	18.15	72.28
I90.13 pyrochlore*	88.79	19.41	43.85
I90.13 carbonatite	168.72	23.63	47.76
I90.13 carbonatite*	177.42	24.02	48.29
I90.13 carbonatite*	181.32	24.20	48.61
I90.3 perovskite	182.35	24.39	1361.87
I90.13 carbonatite*	182.45	24.33	48.62
I90.13 pyrochlore**	182.78	24.37	46.72
I90.13 carbonatite*	184.85	24.44	48.54
I90.3 perovskite*	197.87	25.11	1485.70
I90.4 schorlomite	659.75	50.01	185.12
I90.13 pyrochlore	2020.20	121.45	127.17

* repeat of sample using different aliquot

** this sample was leached in 10% HF for 10 minutes, and the exterior discarded

The 1 σ uncertainty in $^{206}Pb/^{204}Pb$ ranged from 0.001 to 0.53.

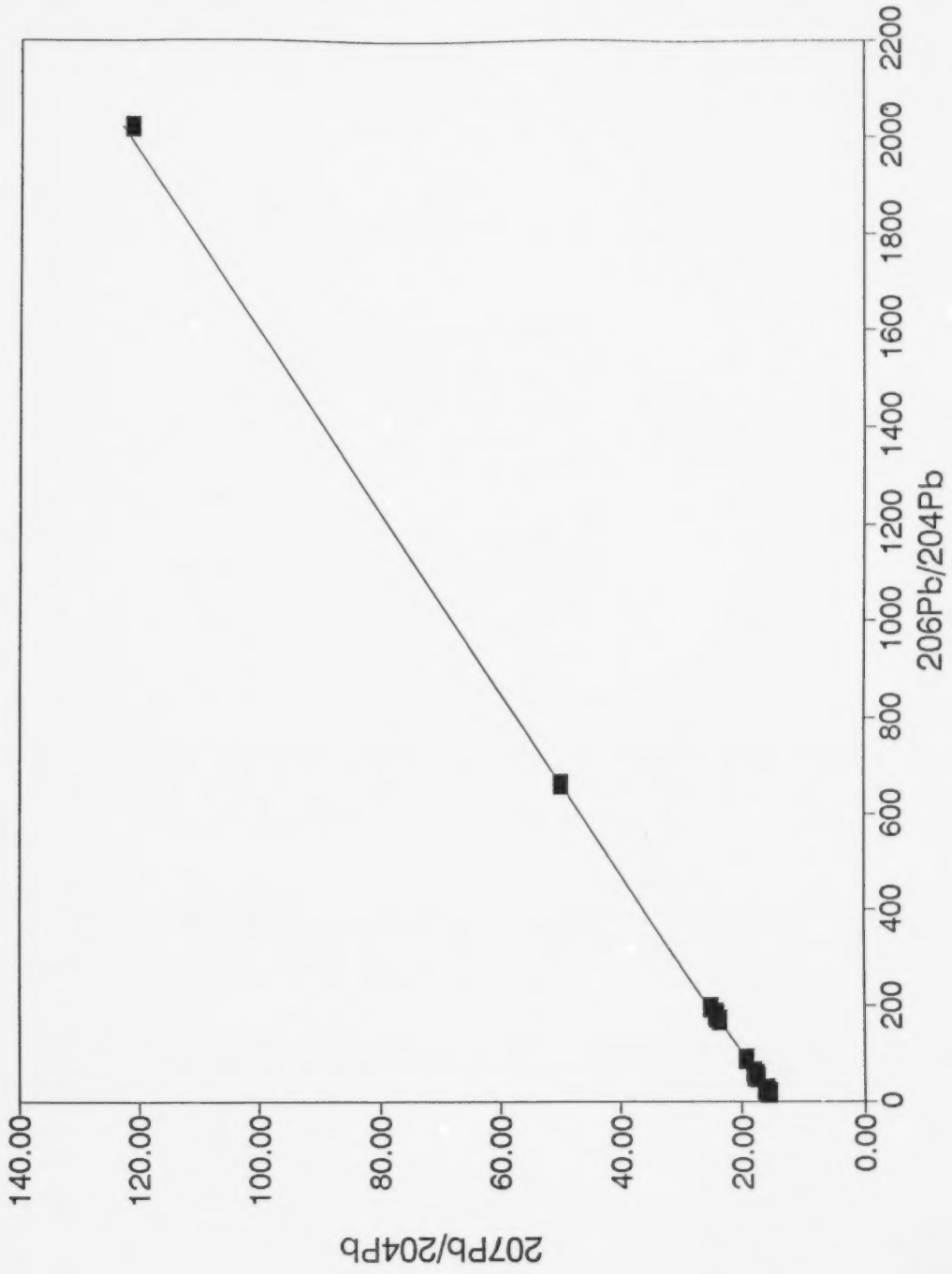

Figure 2.7 Pb-Pb diagram showing a reference line with a slope age of 356 Ma constrained to pass through the schorlomite.

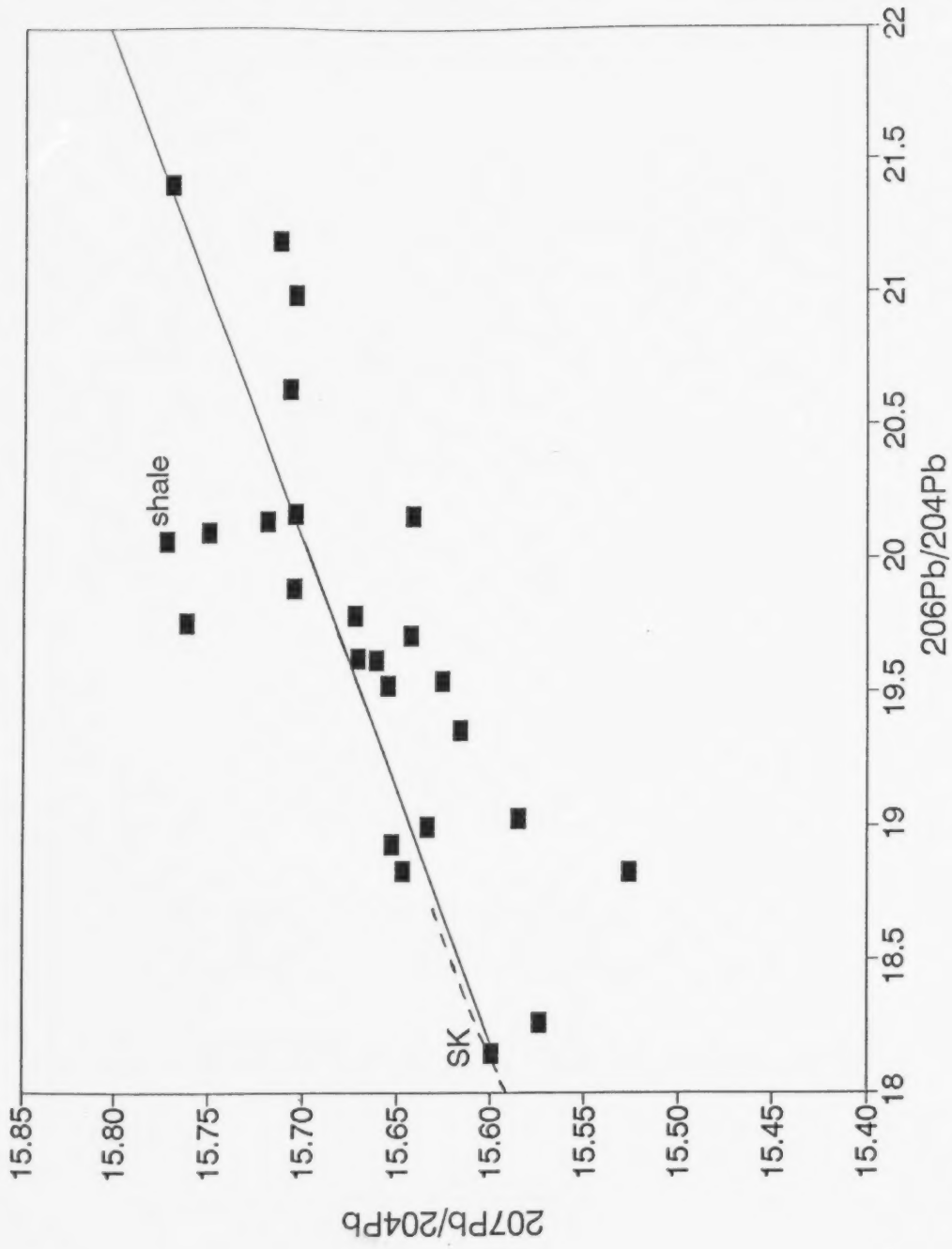

Figure 2.8 Expanded Pb-Pb diagram displaying the scatter of the data. The dashed line is the model curve of Stacey and Kramers (1975).

2.4 DISCUSSION

2.4.1 Age

The age of emplacement of the Ice River complex can be taken to be 356 $\pm$ 6 Ma based on the U-Pb discordia line (pinned on the concordia by the concordant schorlomite) reported above. This places the complex in the earliest part of the Mississippian period, the Tournaisian epoch (363 - 350 Ma) (Harland *et al.*, 1990). The age given by the U-Pb system is consistent with the dates derived from the scatterchrons of the other investigated radioisotope decay systems (Rb-Sr 369 $\pm$ 17, Sm-Nd 359 $\pm$ 197, Pb-Pb 346 $\pm$ 52; uncertainties $\pm 2\sigma * MSWD^{1/2}$). Unfortunately, these systems do not yield isochrons ($0 < MSWD < 2$) upon linear regression, and are therefore interpreted to have been disturbed.

2.4.2 Disturbance of isotope systems

In principle, in a closed magmatic system with homogeneous initial ratios, the Rb-Sr, Sm-Nd, and Pb-Pb systems should all give rise to isochrons. As was noted by Parrish *et al.* (1987), the Rb-Sr system for the Ice River complex is somewhat disturbed, as are decay systems involving argon (K-Ar, Ar-Ar) where the samples may contain excess argon leading to erroneously old dates, or may have lost argon yielding spuriously young ages (Table 2.1). The present author's results indicate that the Sm-Nd and Pb-Pb systems are also disturbed (Figures 2.5 and 2.8).

The radioisotope systems of the Ice River complex could have been disturbed by several different processes including: metamorphism, autometasomatism, crustal contamination, and variability of initial ratios. Because the U-Pb systematics of the minerals of the complex are basically undisturbed (Figure 2.2), no major metamorphic event is considered to have affected the Ice River rocks (to disturb the U-Pb system would require temperatures in excess of 500°C) (Harland *et al.*, 1990). The complex, along with most of the Paleozoic strata of the southern Rocky Mountains, is presumed

to have been metamorphosed to prehnite-pumpellyite facies during the Laramide orogeny (Greenwood *et al.*, 1991). Metamorphism of this grade (2-6 kbar, 200-400°C) would have affected the K-Ar systematics of mica, and the Rb-Sr systematics of biotite and feldspar (Harland *et al.*, 1990; Greenwood *et al.*, 1991). The whole-rock Sm-Nd, Pb-Pb, and Rb-Sr systems would not have been disturbed by the thermal effects of this low grade of metamorphism (Harland *et al.*, 1990). However, Creaser (1989; pp. 260-274) has shown that a low-temperature (< 250°C) fluid can significantly disturb the Rb-Sr system in whole-rock samples of feldspar-rich rocks. By analogy, a low-temperature fluid (circulating during orogenesis) could have disturbed the Rb-Sr system of the feldspar- and feldspathoid-rich rocks of the Ice River complex (evinced perhaps by the alteration of nepheline to cancrinite, and by the turbidity of orthoclase-perthite).

The mineral assemblages present in the syenitic series described above (zeolite syenite, sodalite-rich veins, zeolite/calcite-bearing cavities) were probably a result of autometasomatic activity in the complex. Autometasomatism would have involved the penecontemporaneous alteration of magmatic minerals by reaction with the fluid phase evolved by the crystallizing magma, and the emplacement of veins formed from this fluid. Because this fluid would have the same initial ratios as the rest of the complex, autometasomatism would not change the initial ratios of the isotope systems of the complex, unless the magma-derived fluid also reacted with an external, isotopically different reservoir (such as the surrounding shales and limestones), a form of crustal contamination.

It is difficult to evaluate the possible source(s) of crustal contamination for the Ice River complex. Because the complex was thrust approximately 200 km to the east, roughly 300 million years after its emplacement, few of the rock units with which the parental magma(s) may have interacted with during ascent are known, or exposed nearby. Although it is possible that other rock types in the lower and upper crust interacted with the magma(s), only the shales and

limestones currently surrounding the complex can be investigated as a source of crustal contamination. The complex could have assimilated material from these strata, or interacted with the sedimentary rocks via a fluid (derived either from the cooling intrusion - see above - or from local ground water). It would not be possible to distinguish radioisotopically between the effects of interaction of the Ice River rocks with a fluid bearing the isotopic signature of the surrounding strata, and the direct assimilation of those strata.

Crustal contamination can be evaluated by examining the initial ratios of the complex on a Nd-Sr anticorrelation plot. If all of the rocks and minerals of the complex crystallized in a closed system from a magma with homogeneous initial ratios, the analyzed samples would fall on a single point on Figure 2.9, a plot of epsilon Nd vs. epsilon Sr at 356 Ma (Faure, 1986). A mixing hyperbola would be defined on Figure 2.9 between the complex and a contaminant if the rocks or minerals of the complex interacted (to differing degrees) with a single external reservoir that had initial ratios different from the complex (Faure, 1986). Partial resetting of the Rb-Sr system during orogenic metamorphism would increase the scatter on this diagram. The rocks and minerals of the Ice River complex define a cluster close to the mantle array (except for the eudialyte syenite, whose epsilon Sr is erroneously high, see above), and do not form a mixing hyperbola, even with the Ottertail shale in lower right quadrant (Figure 2.9). No single source of contamination can therefore be identified for the Nd and Sr systematics of the entire Ice River complex. Similarly, the source of the disturbance of the Pb-Pb system (Figure 2.8) is enigmatic; no single contaminant can be identified as the rocks and minerals are scattered roughly equally to either side of the 356 Ma reference line. Crustal contamination is a serious problem in the Pb-Pb system of alkaline rocks because of their lower concentrations of Pb compared to granitic rocks (Kwon *et al.*, 1989).

It is possible that the rocks that compose the Ice River complex crystallized from two (or more) magmas that had differing initial ratios (and

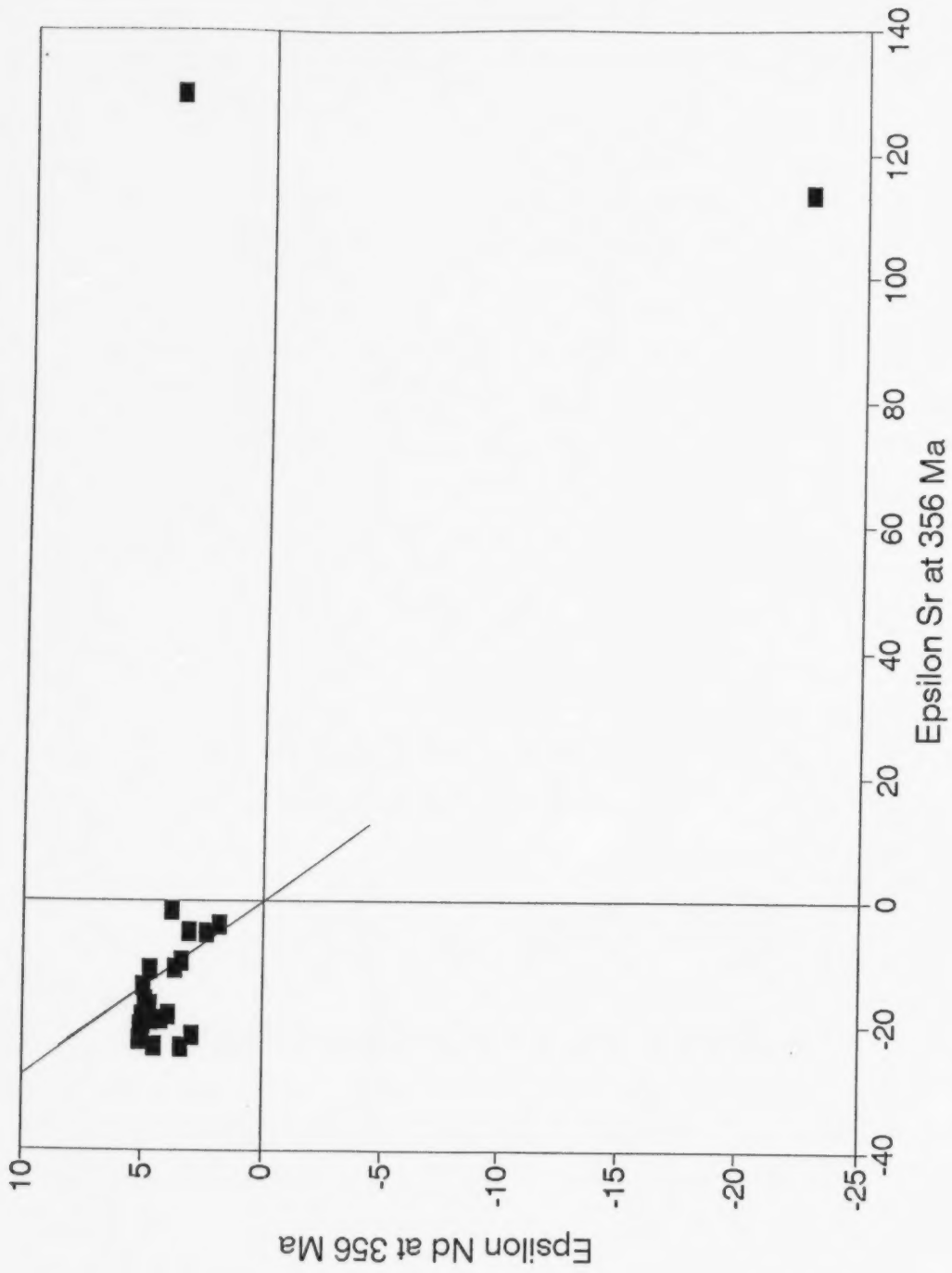

Figure 2.9 Epsilon Nd-Sr anti-correlation plot at 356 Ma. The solid line is the mantle array.

therefore sources). The interaction of two magma pulses would form a mixing array (in a similar manner to that described for crustal contamination above) on the Nd-Sr anti-correlation diagram (Figure 2.9). A mixing hyperbola would also be produced if an initially homogeneous magma split (immiscible magmas), and one of the daughter magmas interacted to a greater degree than the other with a contaminant (the country rocks). The feldspar-free and carbonatite series of rocks consist of a layered mafic-ultramafic assemblage, parts of which occur as xenoliths in the syenitic rocks. The xenolithic rocks are considered to have partially equilibrated isotopically with the host syenitic rocks. If the syenitic and xenolithic rocks are disregarded, the remaining subset (minerals and whole-rocks, Table 2.6) of the feldspar-free and carbonatite series defines a Nd isochron (Figure 2.6) whose age is identical, within error, with that derived from the U-Pb system. The whole rocks of this subset show a restricted range of initial ratios (epsilon Nd = 4.34 to 5.02, epsilon Sr = -17 to -23; the range in epsilon Sr is a result of heterogeneity between the two carbonatite aliquots, the actual range in the feldspar-free series is -18 to -19). In contrast, the whole-rock Nd and Sr systematics of the syenitic series are more scattered (whole rock epsilon Nd = 2.37 to 3.85, epsilon Sr = -5 to -23). The xenolithic rocks (I92.8 pyroxenite, Ice 8 pyroxenite, Ice 22 pargasite ijolite) also exhibit a wide range of initial ratios, epsilon Nd = 1.82 to 3.94, and epsilon Sr = -4 to -18. These results could be interpreted as indicating that: the Nd isochron of the subset of feldspar-free rocks is a fortuitous artifact of sampling; the syenitic series crystallized from a magma that was derived from a different source than the feldspar-free series; the syenitic series crystallized from the same magma (or immiscible daughter magma) but interacted more heavily with crustal rocks. Because the Nd and Sr systematics of the feldspar-free series are well correlated, the first suggestion is discounted. However, the isotopic data does not allow a choice to be made between either of the other interpretations.

2.4.3 Origin

The rocks and minerals of the Ice River complex form a cluster, slightly to the left of the mantle array, in the upper left quadrant of the Nd - Sr anticorrelation diagram (Figure 2.9). This is consistent with the parental magma(s) of the complex having been derived from a source reservoir that had been depleted (for a long time) in large-ion lithophile elements relative to the bulk earth and chondritic uniform reservoir (Bell and Blenkinsop, 1989). This is despite the observation that alkaline rocks contain high concentrations of large-ion lithophile elements (Fitton and Upton, 1987). The depleted source is considered to be the mantle because of the similarity between the isotopic data of most carbonatites (including the Ice River complex) and some ocean island basalts (Bell and Blenkinsop, 1989). Whether the depleted source is the subcontinental lithospheric mantle or the asthenospheric mantle is still a matter of debate (Bell and Blenkinsop, 1989; Kwon *et al.*, 1989). The magma(s) that formed the Ice River complex could have been derived by small degrees of partial melting of a previously depleted mantle source that was metasomatized (large-ion lithophile elements were added) shortly before melting took place (Fitton and Upton, 1987). These circumstances would explain the "depleted" isotopic signature, and the high large ion lithophile element content of the complex.

The Pb isotope systematics of the Ice River complex corroborate the interpretation, based on Nd - Sr results, that the complex was derived from a previously depleted mantle source. Although the Pb isotopes of the complex have not been corrected to initial ratios, the least radiogenic data can be assumed to approximate the Pb ratios at the time of crystallization. The least radiogenic Pb data of the complex, like mid-ocean ridge basalts and ocean island basalts (Kwon *et al.*, 1989), plots below the Stacey-Kramers evolution curve for lead (Figure 2.8). This is consistent with the derivation of the Ice River magma(s) from a large-ion lithophile element depleted mantle source that was also depleted in U (Kwon *et al.*, 1989).

The Ice River complex appears to be temporally associated with a suite of Devonian-Mississippian alkaline complexes, carbonatites, and ultramafic diatremes dispersed along the length of the Rocky Mountain thrust and fold, and Omineca crystalline belts (Pell, 1987a). In the northern Rocky Mountains the Aley carbonatite complex has K-Ar ages (determined on biotite) of 339 $\pm$ 12 and 349 $\pm$ 12 Ma (Pell, 1987a). A few hundred metres from the Aley complex is the Ospika alnöitic composite diatreme; Rb-Sr studies with mica yielded 334 $\pm$ 7 Ma, while K-Ar results for the same sample gave 323 $\pm$ 10 Ma (Pell, 1987a). Just to the west of the Aley complex are the syenites and carbonatites of the Manson Creek area; interpreted zircon (U-Pb) ages for these rocks are 350 $\pm$ 10 and 370 $\pm$ 20 Ma (Pell, 1987a). In central eastern British Columbia are the carbonatites, nepheline and sodalite syenites, and melteigites of the Blue River area. Zircons from this area have yielded U-Pb dates of 350 $\pm$ 5, 328 $\pm$ 30 Ma, and 325 $\pm$ 25 Ma (Pell, 1987a; Pell and Höy, 1989). Preliminary U-Pb analyses of zircon from the nearby Trident Mountain nepheline syenite gneisses gave an age of 378 $\pm$ 7 Ma (Pell and Höy, 1989). Biotite from the numerous alnöitic diatremes in the Golden-Columbian Icefields area, 90 to 130 km north of the Ice River complex, yielded a Rb-Sr age of 348 $\pm$ 7 Ma, and K-Ar dates of 391 $\pm$ 12 and 396 $\pm$ 10 Ma (Pell, 1987a; Pell, 1987b). This suite of alkaline intrusions forms a northwest trending belt, subparallel to the ancient continental margin. Correcting for the eastward displacement of these rocks during the Laramide orogeny, the suite would have been emplaced into the miogeoclinal succession on the Devonian-Mississippian continental shelf. The reasons for the roughly synchronous emplacement of these rocks, whose origins appear to lie in the mantle, are somewhat enigmatic. The crustal rifting and extensional events necessary to the generation and intrusion of these magmas may have taken place in response to middle-late Devonian orogenesis to the west (Pell and Höy, 1989; Gabrielse and Yorath, 1991; Pell and Hora, 1993; Geldsetzer and Upitis, 1993). Cordilleran middle-late Devonian orogeny is thought to have been controlled by early Proterozoic

structures that extended into the Precambrian basement (Price and Welbon, 1993). Therefore, during extension, alkaline magmas generated in the mantle could have migrated along deep-seated faults into the crust.

2.5 CONCLUSIONS

The Ice River alkaline intrusive complex has an age of emplacement of 356 $\pm$ 6 Ma. It was derived from a source in the upper mantle previously depleted in large-ion lithophile elements. The complex may have originated as a result of extension and rifting in response to mid-Devonian orogenesis. The Nd and Pb isotope systems may have been disturbed by crustal contamination during intrusion of the complex, while the Sr system may have been upset by interaction with fluids during Laramide orogenesis.

2.6 REFERENCES CITED

Allan, J.A. (1914) Geology of Field Map-area, B.C. and Alberta. Memoir 55, 312 p. Geological Survey of Canada, Ottawa.

Baadsgaard, H., Folinsbee, R.E., and Lipson, J. (1961) Potassium-argon dates of biotites from Cordilleran granites. Geological Society of America Bulletin, 72, 689-702.

Baadsgaard, H., and Lerbekmo, J.F. (1983) Rb-Sr and U-Pb dating of bentonites. Canadian Journal of Earth Sciences, 20, 1282-1290.

Baadsgaard, H., Lerbekmo, J.F., Wijbrans, J.R., Swisher III, C.C., and Fanning, M. (1993) Multimethod radiometric age for a bentonite near the top of the *Baculites reesidei* Zone of southwestern Saskatchewan (Campanian-Maastrichtian stage boundary?). Canadian Journal of Earth Sciences, 30, 769-775.

Bell, K., and Blenkinsop, J. (1989) Neodymium and strontium isotope geochemistry of carbonatites. In K. Bell, Ed., Carbonatites, Genesis and Evolution, p. 278-300. Unwin Hyman, London.

Cavell, P.A. (1986) The geochronology and petrogenesis of the Big Spruce Lake Alkaline Complex, 448 p. Ph.D. thesis, University of Alberta, Edmonton, Alberta.

Creaser, R.A. (1989) The geology and petrology of middle Proterozoic felsic magmatism of the Stuart Shelf, South Australia, 434 p. Ph.D. thesis, LaTrobe University, Bundoora, Victoria.

Currie, K.L. (1975) The Geology and Petrology of the Ice River Alkaline Complex, British Columbia. Bulletin 245, 68 p. Geological Survey of Canada, Ottawa.

Dawson, G.M. (1886) Geological and Natural History Survey of Canada Annual Report, Volume 1, 122B-124B.

DePaolo, D.J., and Wasserburg, G.J. (1976) Nd isotopic variations and petrogenetic models. Geophysical Research Letters, 3, 249-252.

Duke, M.J.M. (1993) The geochronology, geochemistry and isotope geology of the type-Nûk gneisses of the Akia terrane, southern West Greenland, 286 p. Ph.D. thesis, University of Alberta, Edmonton, Alberta.

Ellsworth, H.V. and Walker, J.F. (1925) Knopite and magnetite occurrence, Moose Creek, southeastern British Columbia. Geological Survey of Canada, Summary Report, 1925, Part A, 230A-232A.

Faure, G. (1986) Principles of isotope geology (2nd edition), 589 p. Wiley & Sons, New York.

Fitton, J.G., and Upton, B.G.J. (1987) Introduction. In J.G. Fitton & B.G.J. Upton, Eds., Alkaline Igneous Rocks. Blackwell Scientific Publications, London.

Gabrielse, H. (Compiler) (1991) Structural styles, Chapter 17. In Geology of the Cordilleran Orogen in Canada, H. Gabrielse and C.J. Yorath (ed.). Geological Survey of Canada, Geology of Canada, No.4, 571-675.

Gabrielse, H., and Yorath, C.J. (1991a) Tectonic synthesis, Chapter 18. In Geology of the Cordilleran Orogen in Canada, H. Gabrielse and C.J. Yorath (ed.). Geological Survey of Canada, Geology of Canada, No.4, 677-705.

Geldsetzer, H.H.J., and Upitis, G.W. (1993) The Sassenach Formation, indirect evidence of Late Devonian tectonism. Joint Annual Meeting of the Geological Association of Canada and Mineralogical Association of Canada Program and Abstracts, A34.

Greenwood, H.J., Woodsworth, G.J., Read, P.B., Ghent, E.D., and Evenchick, C.A. (1991) Metamorphism, Chapter 16. In Geology of the Cordilleran Orogen in Canada, H. Gabrielse and C.J. Yorath (ed.). Geological Survey of Canada, Geology of Canada, No.4, 533-570.

Grice, J.D., and Gault, R.A. (1981) Edingtonite and natrolite from Ice River, British Columbia. Mineralogical Record, July-August, 221-226.

Grice, J.D., Gault, R.A. and Ansell, H.G. (1984) Edingtonite: the first two Canadian occurrences. Canadian Mineralogist, 22, 253-258.

Gussow, W.C., and Hunt, C.W. (1959) Age of the Ice River Complex, Yoho National Park, British Columbia. Journal of the Alberta Society of Petroleum Geologists, 7, 62.

Gussow, W.C. (1977a) The Ice River Complex, British Columbia, *is* Precambrian basement. Bulletin of Canadian Petroleum Geology, 25, 505-517.

———— (1977b) Review of: Geology and Petrology of the Ice River Alkaline Complex, British Columbia, by K. L. Currie. Bulletin of Canadian Petroleum Geology, 25, 707-709.

Harland, W.B., Armstrong, R.L., Cox, A.V., Craig, L.E., Smith, A.G., and Smith, D.G. (1990) A geologic time scale 1989, Cambridge University Press, Cambridge.

Hunt, P.A., and Roddick, J.C. (1987) A compilation of K-Ar ages, Report 17. In Radiogenic Age and Isotopic Studies: Report 1, Geological Survey of Canada, Paper 87-2, 143-210.

———— (1988) A compilation of K-Ar ages, Report 18. In Radiogenic Age and Isotopic Studies: Report 2, Geological Survey of Canada, Paper 88-2, 127-153.

Koffyberg, A.M. (1994) Strontium isotopic constraints on the geochemistry and origins of regional vein-forming fluids in the southern Canadian Cordillera, 103 p. M.Sc. thesis, University of Alberta, Edmonton, Alberta.

Kwon, S.-T., Tilton, G.R., and Grünenfelder, M.H. (1989) Lead isotope relationships in carbonatites and alkalic complexes: an overview. In K. Bell, Ed., Carbonatites, Genesis and Evolution, p. 360-387. Unwin Hyman, London.

Lowdon, J.A. (1960) Age determinations by the Geological Survey of Canada. Geological Survey of Canada, Paper 60-17, 6-7.

Ludwig, K.R. (1990) Isoplot, a plotting and regression program for radiogenic-isotope data, for IBM-PC compatible computers (Version 2.10), 44 p. United States Geological Survey open-file report 88-557.

Lugmair, G.W., and Marti, K. (1978) Lunar initial $^{143}Nd/^{144}Nd$: Differential evolution of the lunar crust and mantle. Earth and Planetary Science Letters, 39, 349-357.

Parrish, R.R., Heinrich, S., and Archibald, D. (1987) Age of the Ice River complex, southeastern British Columbia. In Radiogenic Age and Isotopic Studies: Report 1, Geological Survey of Canada, Paper 87-2, 33-37.

Pell, J.A. (1987a) Alkalic ultrabasic diatremes in British Columbia: petrology, geochronology and tectonic significance (82G, J, N; 83C; 94B). British Columbia Ministry of Energy, Mines and Petroleum Resources, Geological Fieldwork, 1986, Paper 1987-1, 259-272.

———————— (1987b) Open File 1987-17 Alkaline ultrabasic rocks in British Columbia. Province of British Columbia, Ministry of Energy, Mines and Petroleum Resources, Mineral Resources Division, Geological Survey Branch.

Pell, J.A., and Hora, Z.D. (1993) Devonian carbonatites and related rocks in the Canadian Cordillera. Joint Annual Meeting of the Geological Association of Canada and Mineralogical Association of Canada Program and Abstracts, A82.

Pell, J.A., and Höy, T. (1989) Carbonatites in a continental margin environment - the Canadian Cordillera. In K. Bell, Ed., Carbonatites, Genesis and Evolution, p. 200-220. Unwin Hyman, London.

Phillips, A.H. (1916) Some new forms of natrolite. American Journal of Science, 42 (whole number 192), 472-474.

Price, R.A., and Welbon, A.I. (1993) Devonian reactivation of Proterozoic and early Paleozoic transverse, northeast-trending faults and associated volcanism in the southern Canadian Rockies. Joint Annual Meeting of the Geological Association of Canada and Mineralogical Association of Canada Program and Abstracts, A85.

Rapson, J.E. (1963) Age and aspects of metamorphism associated with the Ice River Complex, British Columbia. Bulletin of Canadian Petroleum Geology, 11, 116-124.

———— (1966) Carbonatite in the Alkaline Complex of the Ice River area, southern Canadian Rocky Mountains. Mineralogical Society of India, IMA volume, 9-22.

Romer, R.L., and Wright, J.E. (1992) U-Pb dating of columbites: A geochronologic tool to date magmatism and ore deposits. Geochimica et Cosmochimica Acta, 56, 2137-2142.

Stacey, J.S., and Kramers, J.D. (1975) Approximation of terrestrial lead isotope evolution by a two-stage model. Earth and Planetary Science Letters, 26, 207-221.

Steiger, R.H., and Jäger, E. (1977) Subcommission on Geochronology: Convention on the use of decay constants in geo- and cosmochronology. Earth and Planetary Science Letters, 36, 359-362.

Stevens, R.D., Delabio, R.N., and Lachance, G.R. (1982) Age determinations and geological studies. K-Ar isotopic ages, Report 16, Geological Survey of Canada, Paper 82-2, 1-14.

Wendt, I., and Carl, C. (1991) The statistical distribution of the mean squared weighted deviation. Chemical Geology (Isotope Geoscience Section), 86, 275-285.

3. CHEMICAL RELATIONS OF THE ROCKS AND MINERALS OF THE ICE RIVER COMPLEX

3.1 INTRODUCTION

The Ice River alkaline intrusive complex is the largest plutonic body in the Canadian Rocky Mountains. It is an undersaturated, alkaline intrusion consisting generally of miaskitic nepheline syenite, calcite-carbonatite, and ijolite-pyroxenite. The purpose of this paper is to examine the magmatic evolution of the major units of the complex through study of the chemical relationships of the whole-rocks (both major and trace elements) and the chemical compositions of the minerals.

The Ice River complex is situated in the western Main Ranges, 40 km east-southeast of Golden, and 23 km south of Field, British Columbia. The bulk of the complex outcrops in Yoho and Kootenay National Parks with the remainder exposed in the valley of Moose Creek between the parks. The complex is exposed as an arcuate body approximately 19 km in length, with a maximum width of 4 km; it covers about 29 km^2 (Currie, 1975). The complex is 356 $\pm$ 6 Ma in age (Chapter 2), and intruded the Cambrian shales and limestones of the Chancellor and Ottertail Formations and the Cambrian-Ordovician shales of the McKay Group (Currie, 1975). Skarn and widespread hornfels resulted from the contact metamorphism of these host rocks. Metasomatized and deformed/brecciated rocks (agmatite, and aegirine-feldspar fenite, often with a strong gneissic texture) are also found close to the border of the intrusion (Currie, 1975; Pell, 1987). Approximately 300 million years after intrusion, during Cretaceous-Paleocene (Laramide) orogenesis, the Ice River complex and its host Paleozoic strata were thrust eastwards about 200 km along a west-dipping décollement surface (Gabrielse, 1991). Therefore, the complex is no longer situated at its original geographic site of intrusion (the Devonian-Mississippian western continental shelf). In addition to being thrust to the east during orogenesis, the complex and its host strata were metamorphosed to

prehnite-pumpellyite facies at that time (Currie, 1975; Pell and Höy, 1989; Greenwood *et al.*, 1991). This metamorphic overprinting does not appear to have affected significantly the chemical composition or modal mineralogy of the rocks of the complex (Currie, 1975). The igneous rocks are relatively undisturbed in comparison to the surrounding penetratively deformed strata. The rigid mass of the complex is inferred to have behaved more competently during deformation than the host sedimentary rocks (Currie, 1975).

3.1.1 Geological units of the complex

The geology of the Ice River complex is thoroughly described in the work of Allan (1914) and Currie (1975), a summary of which can be found in Pell (1987). A synopsis of the geology from these sources and the present author's observations follows. The rocks of the Ice River complex comprise three major series: a feldspar-free ultramafic-mafic series, a carbonatite series, and a syenitic series (Figure 3.1). In addition, several types of dykes (lamprophyres, carbonatite, nepheline syenite) and sodalite-bearing veins cross-cut units of the complex and its host strata (Allan, 1914; Currie, 1975; Pell, 1987).

The feldspar-free series of rocks consists of repetitive layers of sequences of graded cumulates (clinopyroxenite, melteigite, olivine hornblendite, ijolite, pargasite ijolite, melanite ijolite, urtite, and wollastonite urtite) (Currie, 1975). Ijolite is the major unit in this series; the other rock-units are subordinate in their abundance. The rock units are mesocratic to melanocratic, and are characterized by a general lack of feldspar, and the presence of primary calcite as an accessory phase. The layers range in thickness from roughly 10 to 200 m, and increase in nepheline content towards the top of each layer (Currie, 1975). The thickness or occurrence of a rock-unit is variable from layer to layer, as is its grain size. Pegmatitic patches, schlieren and veins are common; modal and grain size heterogeneities are sometimes as within rock-units as between them. In general, boundaries between the units are completely

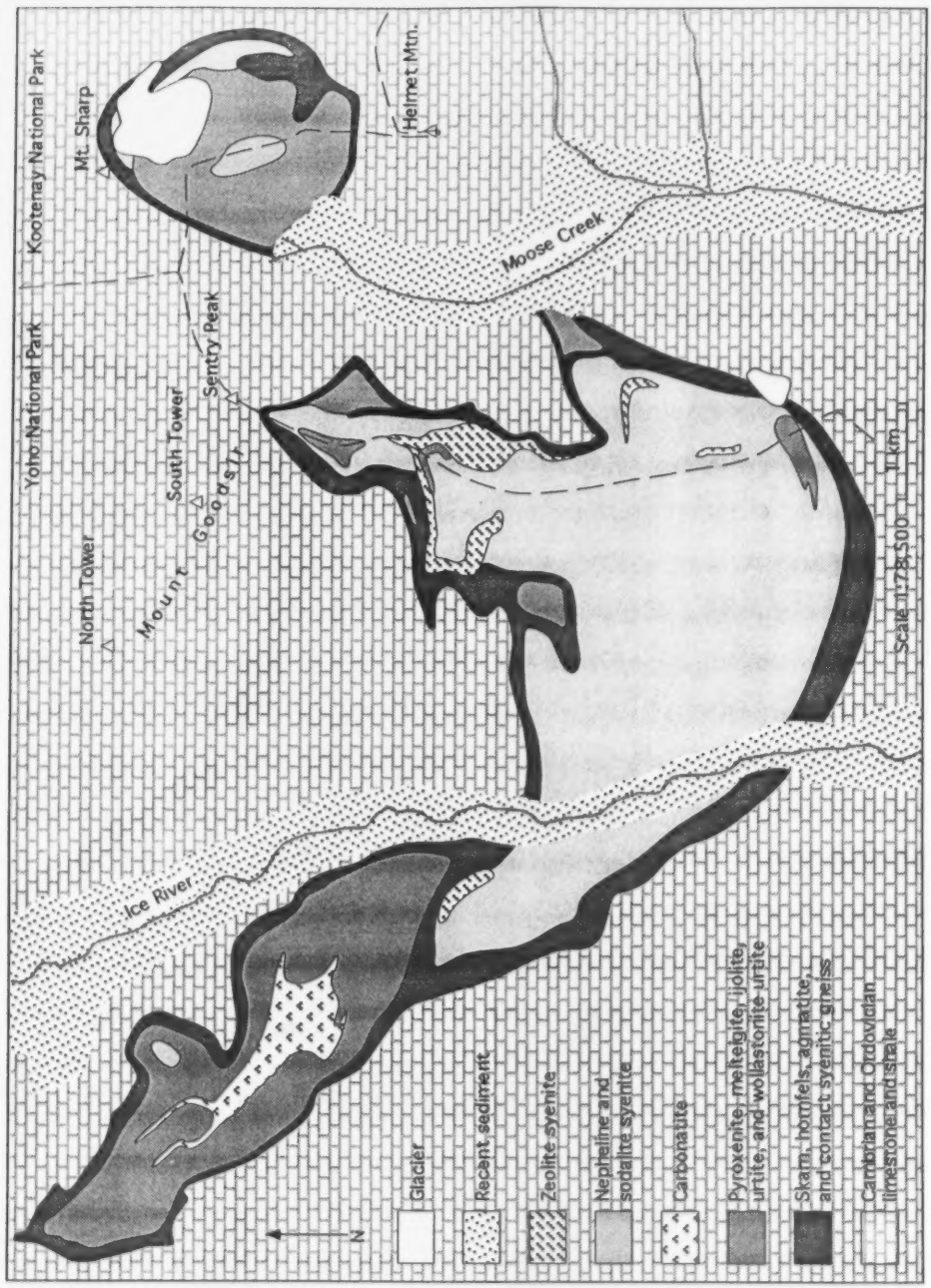

Figure 3.1 Geological map of the Ice River complex (after Currie, 1975).

gradational (with some exceptions). Contacts between the layers are sharp and display sedimentary-type structures (channel scouring, disconformable layering) (Currie, 1975). The stratigraphically lowest layers start with clinopyroxenite; higher in the complex the base of successive layers is rarely more mafic than ijolite (Currie, 1975).

There are three major types of carbonatite in the Ice River complex: a main body of buff-weathering calcite-carbonatite, a black-weathering iron-rich variety that occurs as siderite-rich carbonatite dykes associated with the main body, and a red-weathering variety that cross-cuts the buff carbonatite (Pell, 1987). The main body of carbonatite is a lenticular mass (400 m by 1500 m in dimensions) that is roughly concordant with the ijolitic rocks, but transects them in detail (Currie, 1975). Carbonatite dykes occur most frequently in the layered feldspar-free series, but are found throughout the complex. The dykes are more abundant toward the margin of the main carbonatite body (Currie, 1975). The physical relationships of the carbonatites with the syenitic series preclude determination of an order of emplacement. Some carbonatite dykes are reported to contain syenitic xenoliths and to cross-cut the syenitic rocks, but nepheline syenite is described as having intruded the main carbonatite mass (Currie, 1975; Pell, 1987).

The syenitic series of rocks consists chiefly of melanocratic to leucocratic miaskitic nepheline syenite, with subordinate sodalite syenite, and rare peralkaline nepheline syenite pegmatites, zeolite syenite, and eudialyte syenite (Currie, 1975; Pell, 1987). The syenites form an elliptical mass, zoned from a pale green sodalite syenite core through leucocratic nepheline syenite to melanocratic nepheline syenite at the margin. Nepheline syenite dykes were observed to cross-cut the ijolitic rocks of the feldspar-free series. The zeolite syenite, and peralkaline nepheline syenite pegmatites are located near the stratigraphic top of the complex. Sodalite veins are common throughout the complex. Rare late-stage pneumatolytic pockets and seams occur in the nepheline syenite, often bearing a low-temperature, agpaitic mineral

assemblage which may include calcite, natrolite, edingtonite, ancylite, catapleiite, aegirine, zircon, magnetite, ilmenite, pyrite, and galena (Phillips, 1916; Currie, 1975; Grice and Gault, 1981; Grice *et al.*, 1984).

3.1.2 Petrographic features

This section presents general mineral assemblages of the rock-units that were investigated in this study. All of the rocks are medium to coarse grained. Only the rocks of the feldspar-free series have cumulate textures.

The clinopyroxenite consists dominantly of diopside, (constituting up to 90% of the rock), along with nepheline, and kaersutite or hastingsite. Accessories may include apatite, magnetite, titanite, biotite-phlogopite, calcite, cancrinite, pyrrhotite and chlorite.

The melteigite consists mainly of diopside (40%), and nepheline (30%), with minor perovskite, apatite, and biotite-phlogopite. Accessories may include schorlomite, cancrinite, magnetite, pyrrhotite, calcite and titanite.

The olivine hornblendite is made up chiefly of hastingsite (50%), olivine (chrysolite, 30%), and phlogopite, with accessory diopside, magnetite, ilmenite, apatite and calcite.

The ijolite consists chiefly of nepheline and diopside in roughly equal quantities. Minor phases include apatite, calcite, pyrrhotite, magnetite, cancrinite, biotite-phlogopite series mica, and titanite.

The pargasite ijolite is made up of nepheline, pargasite, and diopside, with accessory titanite, calcite, apatite, cancrinite and zoisite.

The melanite ijolite consists mainly of diopside and nepheline in roughly equal quantities and up to 15% melanite (titanian andradite). Minor phases may include calcite, apatite and cancrinite.

The wollastonite urtite is chiefly made up of nepheline (up to 70%), hedenbergite, and wollastonite. Accessory phases include titanite, calcite, sodalite, cancrinite, biotite-phlogopite, apatite, pyrite and pectolite.

The carbonatite consists dominantly of calcite, constituting up to 90% of

the rock, and aegirine-augite, biotite and apatite. Trace minerals include pyrochlore, hematite, ilmenite and strontianite.

The nepheline syenite is made up chiefly of orthoclase microperthite (up to 50%), nepheline (up to 30%), hastingsite, and hedenbergite. Minor phases may include biotite-phlogopite, sodalite, cancrinite, titanite, apatite, melanite, pyrite, trace barite and zircon.

The nepheline syenite pegmatite is similar to the nepheline syenite in containing mainly orthoclase microperthite, and nepheline. Minor and accessory phases include sodalite, cancrinite, aegirine, andradite, fluorite, zircon, ilmenite, magnetite and hematite.

The sodalite syenite consists mainly of orthoclase microperthite, sodalite, aegirine, and nepheline. Minor minerals include cancrinite, natrolite, biotite-phlogopite and ilmenite.

The eudialyte syenite is made up chiefly of eudialyte (up to 40%), aegirine, nepheline, sodalite, and albite. Accessory minerals include calcite and amphibole.

This brief description of the geology of the Ice River complex shows the rock-units to be modally diverse, and complicated in their interrelationships. It was hoped that investigation of the chemical relations of the rock-units and the chemical compositions of their minerals would lead to a better understanding of the petrogenesis of the complex.

3.2 MATERIALS AND METHODS

During reconnaissance sampling in 1989, 1990, and 1992, specimens were collected from the major rock-units of the Ice River complex. Whole-rock powders were prepared following the methods of Duke (1993; p. 212). The carbon dioxide contents of selected whole-rock samples were determined using a gas analyzer in the Department of Soil Science at the University of Alberta. The amounts of ferrous iron in selected whole-rock and mineral samples were measured by titration with potassium permanganate (Appendix 1). Polished

thin sections were prepared, using conventional techniques, for petrographic and electron microprobe analysis.

3.2.1 X-ray fluorescence analysis (XRF)

Selected whole-rock powders were analyzed, for the author, by X-ray fluorescence spectrometry using an automated Rigaku 3370 spectrometer at the Department of Geology, Washington State University, under the supervision of Dr. Peter Hooper. The methods used followed those described in Duke (1993; pp. 213-214). The following were determined by XRF and reported as weight percent oxides: SiO_2, TiO_2, Al_2O_3, FeO (total iron), MnO, MgO, CaO, Na_2O, K_2O, P_2O_5. Elements determined by XRF and reported as parts per million by weight (ppm) included: V, Ni, Cu, Zn, Ga, Rb, Sr, Y, Zr, Nb, Ba, and Pb.

Silicate standards were used to determine quantitative abundances of elements in the samples. This led to a problem with the carbonatite because it is composed of about 90% calcite. The carbonatite XRF analysis was corrected based on the abundance and composition of its non-carbonate minerals. The modal abundance of the minerals of the carbonatite are listed in Chapter 2, Table 2.2. The composition of the aegirine-augite is listed below in Table 3.2; average compositions of fluorapatite and biotite were assumed (from Deer *et al.*, 1985) for these minerals in the carbonatite. The compositions of these three minerals (aegirine-augite, biotite, apatite) were subtracted from the original analysis of the carbonatite and the remaining CaO, FeO, and MgO summed and assumed to represent calcite. A stoichiometric equivalent amount of carbon dioxide was added and the four "minerals" summed to 100%. The original XRF analysis was recalculated based on the amount of carbon dioxide needed to form the calcite. The trace elements determined by XRF were also multiplied by this factor. The applicability of this arbitrary procedure will be discussed below.

3.2.2 Instrumental neutron activation analysis (INAA)

All of the whole-rock samples reported here were analyzed, for the author, by instrumental neutron activation analysis using the SLOWPOKE II reactor facility at the University of Alberta, by Dr. M. John M. Duke. The methods used followed those described by Duke (1993; pp. 227-231). The following elements were determined by INAA and reported as parts per million by weight (ppm): Sc, Cr, Co, Ni, Br, Cs, La, Ce, Nd, Sm, Eu, Tb, Yb, Lu, Hf, Ta, W, and Th. U was determined in selected samples by delayed neutron counting at the SLOWPOKE facility using the techniques of Duke (1993; pp. 231-232).

3.2.3 Electron microprobe analysis

Analyses of clinopyroxene, clinoamphibole, garnet, wollastonite, pectolite, zoisite, and olivine were performed using an ARL SEMQ microprobe with a Tracor Northern 5600 automation package. Following preliminary examination by energy dispersive analysis, elemental analyses were performed using the wavelength dispersive mode, with an excitation voltage of 15 kV, a probe current of 12 nA, and a beam diameter of 1 μm rastered over an 100 μm^2 area. Peak and background counting times were 20 and 10 s, respectively for both the samples and standards. Reduction of data was carried out with the use of a Phi-Rho-Z program included with the Tracor Northern software. Standards used for the analysis of the pyroxenes, amphiboles, and zoisite included willemite (Mn), tugtupite (Cl), kaersutite (Na, K, Ti), augite (Ca, Mg, Al, Si), apatite (F), chromian augite (Cr), and hypersthene (Fe). Standards used in the analysis of garnet included kaersutite (Na), pyrope (Mg, Al, Si), grossular (Ca), rutile (Ti), willemite (Mn), chromite (Fe), and zircon (Zr). The standards that were used for the analysis of the wollastonite and pectolite included kaersutite (Na, K, Ti), wollastonite (Ca, Si), willemite (Mn), augite (Mg, Al, Fe), and chromian augite (Cr). Olivine analyses were performed using the standards olivine (Mg, Fe, Si, Ni), grunerite (Ca), kaersutite (Na, Ti), augite

(Al), chromian augite (Cr), and willemite (Mn).

3.3 RESULTS

3.3.1 Whole-rock compositions

The numerous rock-units of the Ice River complex are modally diverse and heterogeneous on scales from the hand-specimen to outcrop, and chemically variable because of cumulate layering, localized magmatic processes and autometasomatic activity. Together with the extremely variable exposure of the rock-units in the complex (and their often indeterminable field relationships), these factors make it difficult to obtain specimens (and therefore chemical compositions) that are representative of the major rock-units. The analyses presented here are not intended to proxy the compositions of the magma(s) from which the rocks formed. Instead, these chemical compositions should allow qualitative interpretations to be made of the relationships amongst the rock-units and the general evolution of the complex.

The whole-rock chemical compositions are reported in Table 3.1 and include major, minor, and trace elements for most of the samples, and only trace elements for the remainder. Where FeO and Fe_2O_3 are reported, the FeO has been determined by titration; in all other cases total iron is reported as FeO. The carbon dioxide content of the carbonatite was calculated (see above); the other reported CO_2 values were measured using a gas analyzer.

The silicate rocks of the Ice River complex span a wide range of chemical compositions (Table 3.1): they are ultrabasic to intermediate, containing 38 - 56 wt% SiO_2. The syenitic rocks are generally miaskitic and occasionally mildly peralkaline. In the silicate rocks, concentrations of CaO, MgO, FeO, TiO_2, and P_2O_5 generally decrease and concentrations of Al_2O_3, Na_2O, and K_2O increase, with increasing SiO_2 (Figures 3.2b and 3.3). These trends are in agreement with the observed changes in silicate mineralogy - increasing content of nepheline (followed by feldspar and sodalite), and decreasing content of clinopyroxene and other mafic minerals. However, the

Table 3.1 Whole-rock major, minor and trace element compositions

	I90.13 carbonatite	I92.8 pyroxenite	I90.3 melteigite	I90.6 ol hblndite	Ice 8 pyroxenite
	wt %	wt %	wt %	wt %	wt %
SiO_2	4.59		38.53	39.24	41.59
TiO_2	0.26		3.01	2.14	5.47
Al_2O_3	0.35		20.05	8.52	6.97
Fe_2O_3					6.32
FeO	2.75		7.80	14.95	7.80
MnO	0.17		0.16	0.34	0.18
MgO	0.29		4.30	22.37	9.70
CaO	50.67		11.68	8.20	19.88
Na_2O	0.75		9.04	1.62	1.53
K_2O	0.12		3.26	1.63	0.96
P_2O_5	1.40		1.14	0.47	0.32
CO_2	38.44				1.25
Total	99.81		98.97	99.48	101.97
	ppm	ppm	ppm	ppm	ppm
Sc	0.24	15	5.23	24.6	70.5
V	77		278	204	386
Cr	4.7		9.6	264	70.0
Co	2.48	81	30.4	98.6	56.7
Ni				270	101
Cu	17		76	34	61
Zn	52		61	107	101
Ga			7	11	15
Br	2.8		2.0		2.0

Table 3.1 - continued

	I90.13 carbonatite	I92.8 pyroxenite	I90.3 melteigite	I90.6 ol hblndite	Ice 8 pyroxenite
	ppm	ppm	ppm	ppm	ppm
Rb	22		85	58	28
Sr	17000		886	680	1118
Y	8		32	22	30
Zr	684		236	190	389
Nb	1959		296.0	94.0	82.4
Cs	0.19		0.78	0.78	1.39
Ba	1681	400	278	774	677
La	287	70	277	56.9	55.3
Ce	417	130	534	101	122
Nd	95	60	216	41.0	61.4
Sm	16.3	16.4	32.0	7.72	13.5
Eu	3.02	5.1	8.94	2.48	4.22
Tb	0.65	2.4	2.37	0.97	1.82
Yb	5.34	2.6	1.63	1.65	2.38
Lu	0.84		0.24	0.24	0.25
Hf	0.35	10	6.70	4.32	14.2
Ta	36.8	3.3	37.8	4.85	6.13
W			7.0		
Pb	28				7
Th	72	2.8	93.8	6.76	3.15
U	379		5.59	1.05	0.85

Table 3.1 - continued

	Ice 22 parg ijolite	I90.7 ijolite	I90.9 mel ijolite	Ice 38 woll urtite	I92.35 ne syenite
	wt %	wt %	wt %	wt %	wt %
SiO_2	41.96		43.89	45.29	
TiO_2	3.76		1.79	0.71	
Al_2O_3	16.62		17.22	10.33	
Fe_2O_3	3.11			3.40	
FeO	9.13		9.35	7.12	
MnO	0.28		0.36	0.56	
MgO	4.22		2.75	1.58	
CaO	12.95		13.07	21.18	
Na_2O	5.19		7.65	6.06	
K_2O	2.68		3.41	2.29	
P_2O_5	0.92		0.30	0.07	
CO_2	0.31			4.29	
Total	101.12		99.78	102.87	
	ppm	ppm	ppm	ppm	ppm
Sc	6.14	2.6	0.53	0.25	0.34
V	278		219	108	
Cr	5.8	17	5	1.8	6
Co	32.4	34	17	20.6	4.9
Ni					
Cu	40			61	
Zn	128		155	221	60
Ga	19		24	30	
Br	3.4			4.1	

Table 3.1 - continued

	Ice 22 parg ijolite	I90.7 ijolite	I90.9 mel ijolite	Ice 38 woll urtite	I92.35 ne syenite
	ppm	ppm	ppm	ppm	ppm
Rb	69	155	103	86	170
Sr	1224	1100	845	1830	1570
Y	46		82	18	
Zr	382		696	681	
Nb	324.8		177.7	454.4	
Cs	0.90	2.1	1.2	0.56	1.5
Ba	1486		62	1210	4850
La	141	267	43	55.5	54
Ce	247	430	84	82.6	93
Nd	102	185	52	21.4	50
Sm	17.8	25.5	14.4	3.53	5.2
Eu	5.45	6.7	5.7	1.15	2.4
Tb	1.98	1.8	2.5	0.47	0.5
Yb	3.39	5.0	8.1	2.00	1.4
Lu	0.45			0.37	
Hf	8.13	6.4	13	8.47	3.6
Ta	19.2	25	9.7	12.5	7.8
W					
Pb	7		1	7	
Th	15.9	44	7.4	2.79	11
U	3.20			1.13	

Table 3.1 - continued

	Ice 35 ne syenite	I90.19 ne syenite	Ice 23 pegmatite	Sodalite syenite	I92.37 eud syenite
	wt %	wt %	wt %	wt %	wt %
SiO_2	53.25		56.79		
TiO_2	0.50		0.16		
Al_2O_3	24.65		21.55		
Fe_2O_3	1.19		3.10		
FeO	1.99		0.50		
MnO	0.13		0.15		
MgO	0.10		0.15		
CaO	2.60		1.69		
Na_2O	9.77		10.24		
K_2O	7.52		7.13		
P_2O_5	0.05		0.02		
CO_2	0.34		1.16		
Total	102.09		102.63		
	ppm	ppm	ppm	ppm	ppm
Sc	0.13	0.13	0.24	3.0	1.7
V			5		
Cr	1.4		1.5	29	41
Co	2.76	2.6	0.75	3.0	3.9
Ni	7		10		
Cu	12		7		
Zn	78	55	106	68	260
Ga	15		32		
Br	7		10		

Table 3.1 - continued

	Ice 35 ne syenite	I90.19 ne syenite	Ice 23 pegmatite	Sodalite syenite	I92.37 eud syenite
	ppm	ppm	ppm	ppm	ppm
Rb	260	305	325	195	240
Sr	1858	1230	382	470	460
Y	13		18		
Zr	263		774		
Nb	163.1		355.8		
Cs	7.36	4.2	8.4	5.1	3.8
Ba	2363	1350	237	710	
La	49.7	31	94.6	44	3200
Ce	74.3	46	146	58	3520
Nd	22.6	15	27.3		900
Sm	3.47	2.2	4.21	3.9	160
Eu	1.22	0.87	0.79	1.4	34
Tb	0.35	0.4	0.41	0.6	33
Yb	0.77	1	1.42	1.5	180
Lu	0.10		0.19		
Hf	3.46	1.7	11.0	3.8	310
Ta	8.96	1.7	10.4	9.5	215
W	4.5		9		
Pb	19		55		
Th	15.0	8.7	45.6	10	51
U	3.57		16.1		

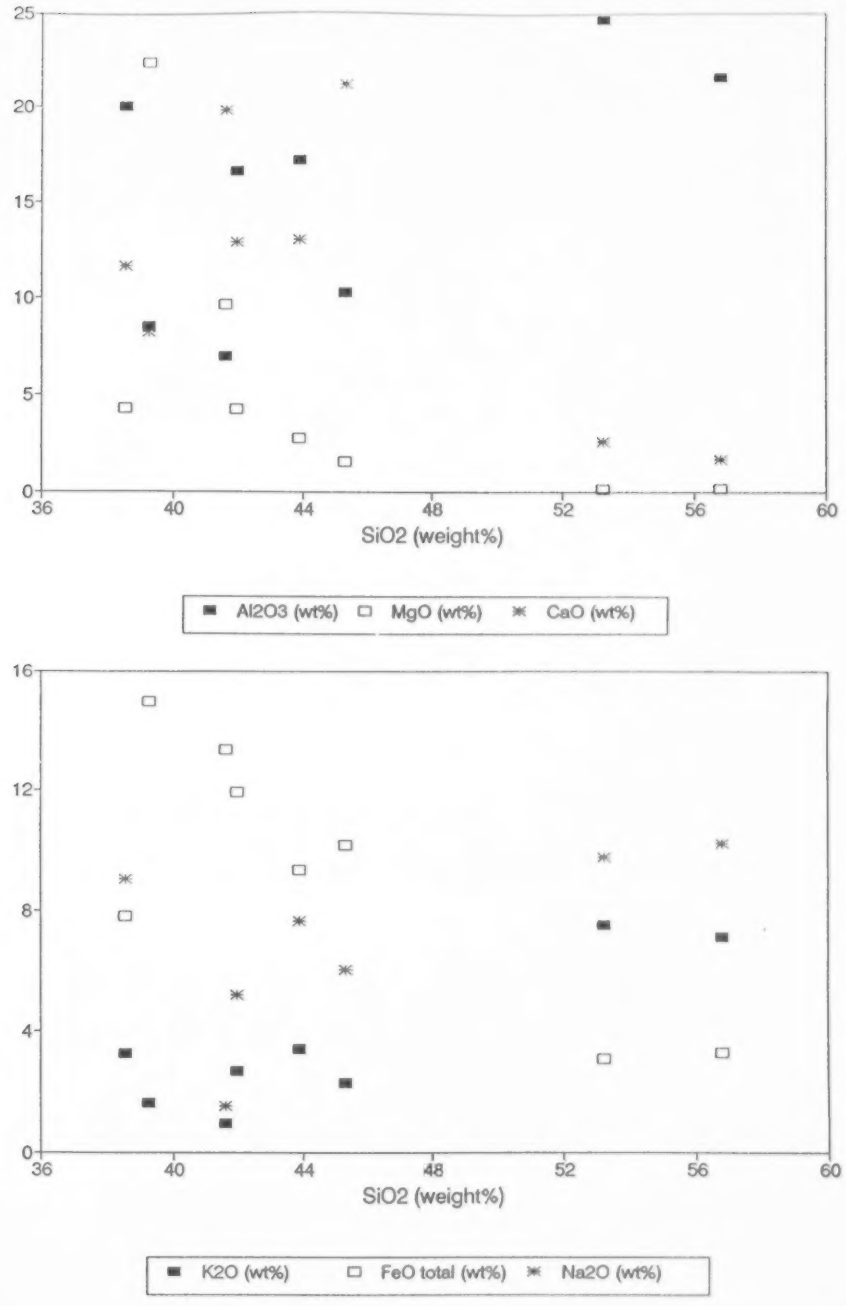

Figure 3.2 Oxide variation diagrams for the Ice River complex.

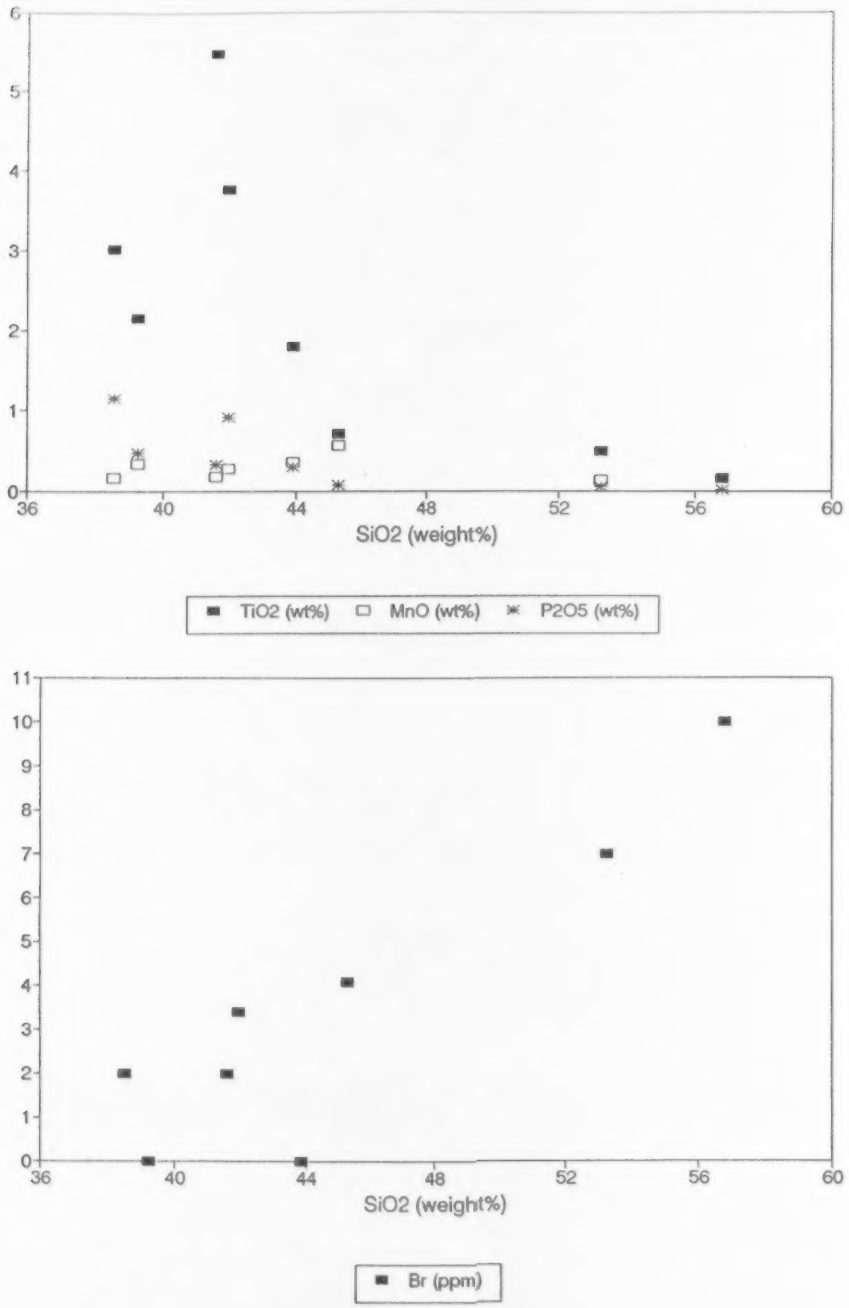

Figure 3.3 Oxide and halogen variation diagrams for the Ice River complex.

data points do not form smooth trends on these variation diagrams. This is consistent with the cumulate nature of several of the rock-units, and the suggestion that not all of the rock-units are related to each other by simple, closed-system differentiation (fractional crystallization) (Wilson, 1993). The increase of Br with SiO_2 concentration (Figure 3.3) is consistent with the generally observed trend of increasing volatile (halogen) content in alkaline magmas with silica content or differentiation (Bailey and Hampton, 1990). In detail, the Br data forms two clusters corresponding to the two silicate rock series presented: low Br contents (0 - 4.1 ppm) are typical of the ultramafic-mafic feldspar-free series of rocks, while high Br contents (7 - 10 ppm) characterize the syenitic rocks. Most of the other trace element data do not form recognizable patterns on variation diagrams, or provide useful information on discrimination plots (a common problem in alkaline rocks, cf. Rock, 1978; Cavell, 1986) and are therefore not discussed in detail.

The carbonatite is not expected to form trends in chemical composition with the silicate rocks because it is radically different in chemical and mineralogic composition from them. The analysis of carbonatite presented in Table 3.1, although arbitrarily corrected (see above), is quite similar to the average composition of calciocarbonatite calculated by Woolley and Kempe (1989). Therefore, this analysis is assumed to be valid for the purposes of this study.

In order to compare the carbonatite to the other rocks of the complex, rare-earth element patterns were plotted using the chondrite normalization values of Evensen *et al.* (1978), and are shown in Figures 3.4 and 3.5. The rare earth patterns of all the different rock-units are broadly similar, showing linear trends that are considerably richer in light rare earth elements than heavy rare earth elements. Absolute abundances of the rare earth elements, and the slight variations in the shapes of the patterns, appear to be controlled by the modal mineralogy of the rock units (i.e., the amounts of the rare-earth element-rich minerals apatite, titanite, perovskite, pyrochlore, zircon or

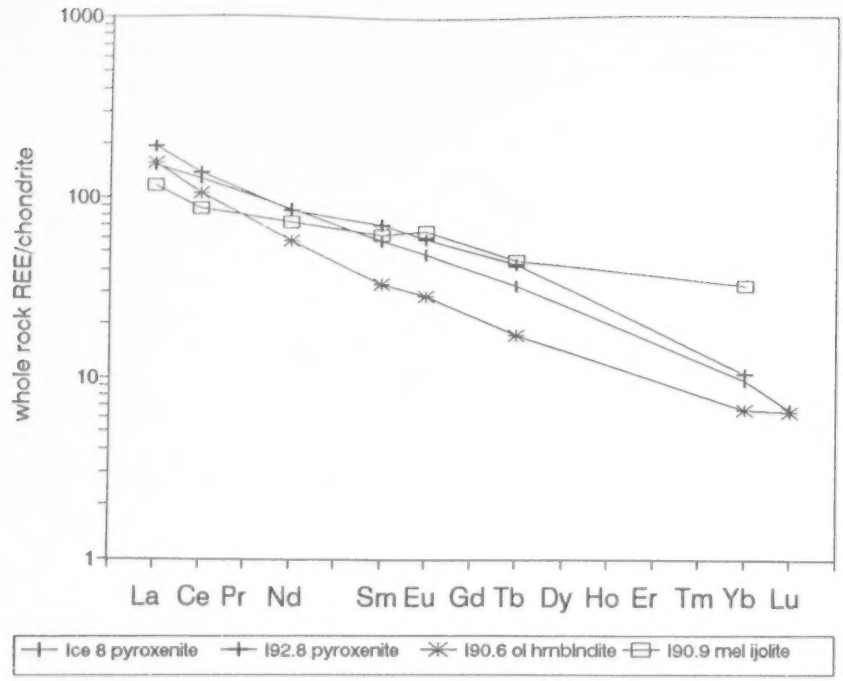

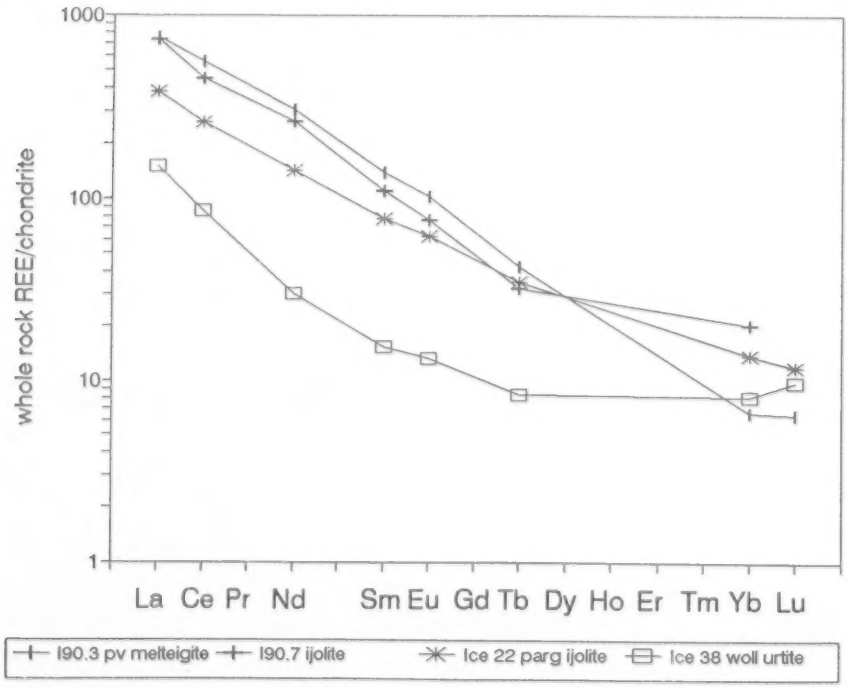

Figure 3.4 Rare earth element diagrams for the cumulate rocks.

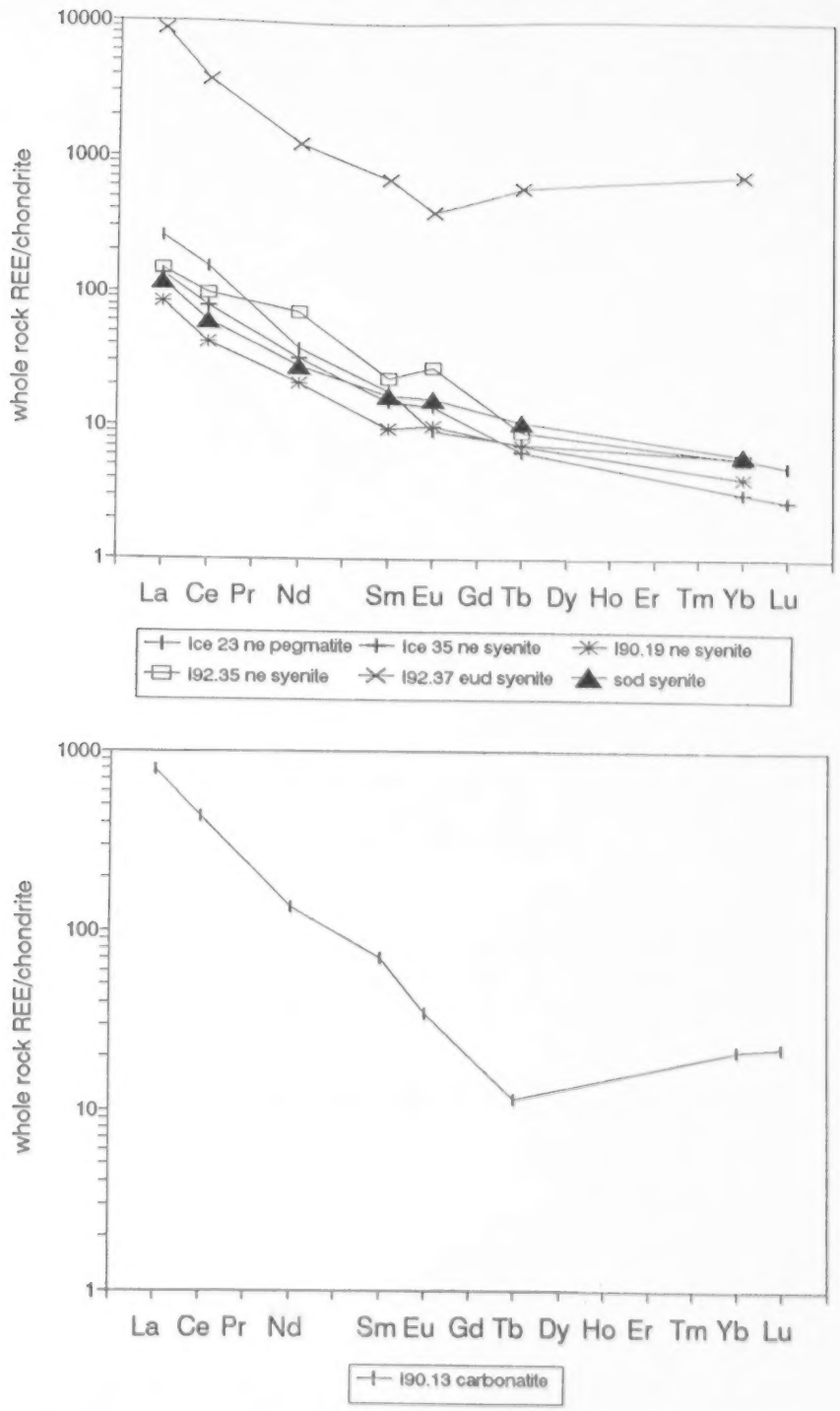

Figure 3.5 Rare earth element plots for the syenitic and carbonatite series.

eudialyte that are present). The rock-units of the syenitic series (with the exception of the eudialyte syenite) show small positive Eu anomalies (Figure 3.5), interpreted to be a result of feldspar accumulation. The eudialyte syenite exhibits a minor negative europium anomaly and is interpreted to represent the end phase of the differentiation of the syenitic series. The broad similarity of the rare earth patterns of the different rock-units of the Ice River complex is most consistent with their generation from single source. However, different magma sources for the different series cannot be ruled out on the basis of this similarity, because of sampling and analytical uncertainties, and the cumulate nature of many of the rocks analyzed.

3.3.2 Mineral compositions

The evolution of alkaline complexes may be investigated through examination of the variations in the chemical compositions of the mafic minerals (Rock, 1982; Platt and Woolley, 1986; Mitchell, 1990). Representative analyses of clinopyroxene, clinoamphibole and garnet are reported in Tables 3.2, 3.3, and 3.4 respectively. Structural formulae were calculated using the stoichiometric number of oxygen anions (6, 23, and 12 respectively).

The clinopyroxene analyses were classified (Table 3.2) using the IMA approved nomenclature of Morimoto (1989). The majority of the analyses fall within the field of the Ca-Mg-Fe quadrilateral (Figure 3.6); the Ca-Na pyroxene is the aegirine-augite of the carbonatite, and the Na pyroxene is the aegirine found in the nepheline syenite pegmatite. The pyroxenes in the feldspar-free cumulates range in composition from subsilicic diopside (pyroxenite) to sodian hedenbergite (wollastonite urtite), while those in the syenitic rocks range from hedenbergite to aegirine (Table 3.2). Compositional trends of the clinopyroxenes are depicted in Figure 3.7, plotted against molar Na minus Mg, the pyroxene differentiation index (Rock, 1982). The two Na-rich pyroxenes are clearly divided from the Ca-Mg-Fe pyroxenes. The latter show decreasing Ca, and increasing Mn and Fe with increasing Na-Mg. The

Table 3.2 Chemical compositions of clinopyroxene from the Ice River complex

Sample	192.8 pyroxenite		190.7 ijolite		190.9 mel ijolite	
oxide	wt %	1 σ n=6	wt %	1 σ n=9	wt %	1 σ n=7
SiO_2	42.80	0.61	52.03	0.87	50.96	0.38
TiO_2	4.52	0.31	0.62	0.44	0.29	0.09
Al_2O_3	9.36	0.30	1.57	1.00	0.90	0.13
Fe_2O_3	4.67		1.67		2.33	
FeO	3.80*	0.24	8.10*	1.71	14.55*	1.64
MnO	0.11	0.03	0.36	0.09	0.69	0.07
MgO	10.72	0.16	12.42	1.00	7.84	1.09
CaO	22.60	0.14	22.31	0.86	20.87	1.17
Na_2O	0.71	0.02	0.78	0.50	1.13	0.52
Total	99.28	0.22	99.86	0.59	99.55	0.30
element	cations per 6 O		cations per 6 O		cations per 6 O	
Si	1.621		1.952		1.979	
Ti	0.129		0.017		0.008	
Al	0.418		0.070		0.041	
Fe^{3+}	0.133		0.047		0.068	
Fe^{2+}	0.120		0.254		0.473	
Mn	0.004		0.011		0.023	
Mg	0.606		0.695		0.454	
Ca	0.917		0.897		0.869	
Na	0.052		0.057		0.085	
Total	4.000		4.000		4.000	
	subsilicic ferrian titanian diopside		diopside		hedenbergite	

* FeO calculated by stoichiometry, standard deviation is of total Fe measured as FeO
\# FeO measured titrimetrically, Fe_2O_3 by difference

Table 3.2 - continued

Sample	190.3 melteigite		Ice 38 woll urtite		Ice 23 ne pegmatite	
oxide	wt %	1 σ n=6	wt %	1 σ n=3	wt %	1 σ n=2
SiO_2	47.08	0.79	49.80	0.13	52.09	0.36
TiO_2	2.59	0.27	0.36	0.02	0.53	0.06
Al_2O_3	6.69	0.58	0.91	0.02	1.16	0.01
Fe_2O_3	3.53		3.60		28.00	
FeO	4.32#	0.46	18.02#	0.84	3.20*	0.04
MnO	0.18	0.03	0.89	0.01	0.71	0.08
MgO	12.55	0.41	4.58	0.47	0.41	0.07
CaO	23.01	0.19	19.74	0.40	1.84	0.12
Na_2O	0.56	0.02	1.58	0.16	12.03	0.23
Total	100.50	0.16	99.49	0.16	99.95	0.53
element	cations per 6 O		cations per 6 O		cations per 6 O	
Si	1.749		1.977		2.002	
Ti	0.072		0.011		0.015	
Al	0.293		0.043		0.052	
Fe^{3+}	0.099		0.108		0.810	
Fe^{2+}	0.134		0.598		0.103	
Mn	0.006		0.030		0.023	
Mg	0.695		0.271		0.023	
Ca	0.916		0.840		0.076	
Na	0.041		0.122		0.896	
Total	4.004		3.998		4.000	
	subsilicic diopside		sodian ferrian hedenbergite		ferroan aegirine	

* FeO calculated by stoichiometry, standard deviation is of total Fe measured as FeO
\# FeO measured titrimetrically, Fe_2O_3 by difference

Table 3.2 - continued

Sample	Ice 22 parg ijolite		I90.13 carbonatite		I90.19 ne syenite	
oxide	wt %	1 σ n=4	wt %	1 σ n=6	wt %	1 σ n=3
SiO_2	45.52	1.37	51.88	0.41	46.72	0.09
TiO_2	1.86	0.43	0.40	0.06	0.63	0.05
Al_2O_3	6.25	0.89	0.46	0.07	3.12	0.24
Fe_2O_3	5.00		26.71		5.76	
FeO	10.23*	0.34	2.47#	0.24	18.32*	0.14
MnO	0.41	0.03	0.25	0.04	1.06	0.03
MgO	7.45	0.21	2.15	0.07	2.76	0.11
CaO	21.67	0.27	5.56	0.33	19.76	0.06
Na_2O	0.96	0.05	10.41	0.30	1.47	0.04
Total	99.34	0.72	100.29	0.54	99.60	0.10
element	cations per 6 O		cations per 6 O		cations per 6 O	
Si	1.766		1.984		1.877	
Ti	0.054		0.012		0.019	
Al	0.286		0.021		0.148	
Fe^{3+}	0.146		0.769		0.174	
Fe^{2+}	0.332		0.079		0.616	
Mn	0.014		0.008		0.036	
Mg	0.431		0.123		0.165	
Ca	0.901		0.228		0.850	
Na	0.072		0.772		0.115	
Total	4.000		3.995		4.000	
	ferrian diopside		aegirine-augite		ferrian sodian hedenbergite	

* FeO calculated by stoichiometry, standard deviation is of total Fe measured as FeO

\# FeO measured titrimetrically, Fe_2O_3 by difference

Table 3.2 - continued

Sample	192.35 ne syenite		Ice 35 ne syenite		Ice 8 pyroxenite		190.6 ol hornblendite
oxide	wt %	1 σ n=4	wt %	1 σ n=4	wt %	1 σ n=4	wt %
SiO_2	46.51	0.53	46.79	0.88	47.74	1.47	52.31
TiO_2	0.80	0.43	0.49	0.08	3.29	0.57	0.90
Al_2O_3	3.22	0.43	2.52	0.14	5.02	1.20	1.71
Fe_2O_3	5.37		6.20		4.00		4.19
FeO	16.36*	0.52	17.84*	0.22	2.52*	0.55	0.70*
MnO	0.98	0.06	1.17	0.05	0.08	0.04	0.13
MgO	3.61	0.18	2.46	0.07	13.93	0.80	16.19
CaO	21.29	0.72	19.66	0.63	23.77	0.27	24.69
Na_2O	1.14	0.06	1.68	0.24	0.46	0.08	0.44
Total	99.27	0.72	98.81	0.91	100.81	0.16	101.26
element	cations per 6 O		cations per 6 O		cations per 6 O		cations per 6 O
Si	1.863		1.896		1.761		1.897
Ti	0.024		0.015		0.091		0.025
Al	0.152		0.120		0.218		0.073
Fe^{3+}	0.162		0.189		0.111		0.114
Fe^{2+}	0.548		0.605		0.078		0.021
Mn	0.033		0.040		0.003		0.004
Mg	0.216		0.149		0.766		0.875
Ca	0.914		0.854		0.940		0.959
Na	0.088		0.132		0.033		0.031
Total	4.000		4.000		4.000		4.000
	ferrian hedenbergite		ferrian sodian hedenbergite		ferrian diopside		ferrian diopside

* FeO calculated by stoichiometry, standard deviation is of total Fe measured as FeO

\# FeO measured titrimetrically, Fe_2O_3 by difference

Table 3.3 Chemical compositions of amphibole from the Ice River complex

Sample	192.8 pyroxenite		Ice 22 parg ijolite		190.19 ne syenite		192.35 ne syenite	
oxide	wt %	1 σ n=5	wt %	1 σ n=4	wt %	1 σ n=6	wt %	1 σ n=4
SiO_2	36.98	0.33	36.13	0.69	36.83	0.20	37.02	0.27
TiO_2	5.60	0.23	3.54	0.77	1.52	0.23	3.22	0.98
Al_2O_3	14.30	0.19	14.28	0.48	11.45	0.14	12.93	0.63
Fe_2O_3			1.24		5.78		3.22	
FeO	11.75*	0.32	19.93*	0.89	24.05*	0.36	21.08#	3.38
MnO	0.15	0.03	0.45	0.04	0.92	0.04	0.67	0.10
MgO	11.93	0.18	6.22	0.10	2.43	0.26	4.56	1.33
CaO	11.80	0.08	11.06	0.07	9.97	0.23	10.86	0.33
Na_2O	2.13	0.05	1.98	0.07	2.58	0.16	2.52	0.10
K_2O	1.88	0.05	2.20	0.12	2.01	0.06	1.82	0.15
F								
Cl			0.08	0.01			0.05	0.01
Total	96.52	0.46	97.11	0.20	97.52	0.46	97.94	0.34
element	cations per 23 O		cations per 23 O		cations per 23 O		cations per 23 O	
Si	5.621		5.702		5.979		5.847	
Ti	0.640		0.420		0.185		0.383	
Al	2.562		2.657		2.190		2.408	
Fe^{3+}			0.147		0.706		0.383	
Fe^{2+}	1.494		2.630		3.265		2.785	
Mn	0.020		0.059		0.127		0.090	
Mg	2.703		1.463		0.587		1.074	
Ca	1.921		1.870		1.733		1.837	
Na	0.627		0.607		0.812		0.770	
K	0.364		0.443		0.416		0.366	
Total	15.953		16.000		16.000		15.943	
	subsilicic potassian kaersutite		subsilicic potassian pargasite		potassian hastingsite		titanian potassian hastingsite	

* FeO calculated by stoichiometry, standard deviation is of total Fe measured as FeO

\# FeO measured titrimetrically, Fe_2O_3 by difference

Table 3.3 - continued

Sample	Ice 35 ne syenite		190.6 ol hornblendite		Ice 8 pyroxenite	
oxide	wt %	1 σ n=4	wt %	1 σ n=4	wt %	1 σ n=4
SiO_2	36.00	0.85	42.14	0.51	39.93	0.24
TiO_2	1.83	0.34	2.52	0.03	1.31	0.77
Al_2O_3	11.49	0.34	12.47	0.52	12.78	0.60
Fe_2O_3	6.20		1.99		4.75	
FeO	24.86*	2.54	6.85*	0.81	14.40*	2.55
MnO	0.91	0.05	0.12	0.03	0.19	0.01
MgO	1.64	0.15	16.57	0.01	9.93	1.26
CaO	9.85	0.24	12.18	0.22	11.48	0.47
Na_2O	2.45	0.04	2.97	0.08	2.86	0.26
K_2O	2.16	0.01	1.10	0.07	1.49	0.15
F			0.16	0.10	0.26	0.08
Cl	0.05	0.01	0.02	0.00	0.04	0.04
Total	97.44	0.96	99.10	0.26	99.41	0.36
element	cations per 23 O		cations per 23 O		cations per 23 O	
Si	5.898		6.076		6.010	
Ti	0.225		0.274		0.148	
Al	2.218		2.118		2.267	
Fe^{3+}	0.764		0.216		0.538	
Fe^{2+}	3.407		0.826		1.813	
Mn	0.127		0.015		0.024	
Mg	0.401		3.560		2.227	
Ca	1.730		1.882		1.851	
Na	0.779		0.831		0.835	
K	0.451		0.203		0.287	
Total	16.000		16.000		16.000	
	potassian hastingsite		titanian magnesio-hastingsite		potassian magnesian hastingsite	

* FeO calculated by stoichiometry, standard deviation is of total Fe measured as FeO
\# FeO measured titrimetrically, Fe_2O_3 by difference

Table 3.4 Chemical compositions of garnet from the Ice River complex

Sample	I90.9 mel ijolite		I90.19a ne syenite		I90.19b ne syenite	
oxide	wt %	1 σ n=4	wt %	1 σ n=4	wt %	1 σ n=3
SiO_2	29.14	0.16	34.18	0.10	34.20	0.23
TiO_2	13.64	0.46	2.50	0.47	1.86	0.14
ZrO_2	0.51	0.08			0.24	0.07
Al_2O_3	1.11	0.07	4.28	0.39	4.04	0.05
Fe_2O_3	17.90	0.18	24.91	0.60	25.26	0.31
FeO	3.95*		0.54*		0.37*	
MnO	0.49	0.03	0.69	0.07	0.67	0.06
MgO	0.58	0.03	0.10	0.03	0.12	0.02
CaO	31.91	0.05	32.27	0.29	31.98	0.11
Na_2O	0.23	0.02	0.08	0.03	0.10	0.07
Total	99.46	0.32	99.54	0.56	98.84	0.34
element	cations per 12 O		cations per 12 O		cations per 12 O	
Si	2.489		2.856		2.880	
Ti	0.877		0.157		0.118	
Zr	0.021				0.010	
Al	0.112		0.422		0.401	
Fe^{3+}	1.151		1.566		1.601	
Fe^{2+}	0.282		0.038		0.026	
Mn	0.035		0.049		0.048	
Mg	0.074		0.012		0.015	
Ca	2.921		2.888		2.886	
Na	0.038		0.013		0.016	
Total	8.000		8.000		8.000	
	melanite		melanite		melanite	

* FeO calculated by stoichiometry, standard deviation is of total Fe measured as Fe_2O_3

\# FeO measured titrimetrically, Fe_2O_3 by difference

melanite is a varietal name for titanian andradite, (TiO_2 = 1 - 15 wt%)

Table 3.4 - continued

Sample	192.34 ne pegmatite		190.4 melteigite	
oxide	wt %	1 σ n=3	wt %	1 σ n=33
SiO_2	35.02	0.09	27.42	0.61
TiO_2	0.93	0.80	16.43	0.85
ZrO_2			0.93	0.12
Al_2O_3	2.03	0.16	1.36	0.14
Fe_2O_3	28.92	0.75	15.05	0.55
FeO			5.14#	0.03
MnO	0.72	0.03	0.44	0.04
MgO	0.15	0.05	1.06	0.11
CaO	33.19	0.10	31.24	0.27
Na_2O	0.09	0.03	0.23	0.04
Total	101.05	0.26	99.54§	

element	cations per 12 O	cations per 12 O
Si	2.915	2.348
Ti	0.058	1.058
Zr		0.039
Al	0.199	0.137
Fe^{3+}	1.811	0.970
Fe^{2+}		0.368
Mn	0.051	0.032
Mg	0.019	0.135
Ca	2.960	2.866
Na	0.014	0.038
Total	8.028	8.010†
	andradite	schorlomite

* FeO calculated by stoichiometry, standard deviation is of total Fe measured as Fe_2O_3

\# FeO measured titrimetrically, Fe_2O_3 by difference

§ Analysis includes V_2O_3 0.20 (0.01) and H_2O 0.036 (0.003)

† Analysis includes V 0.014 and H_2 0.005

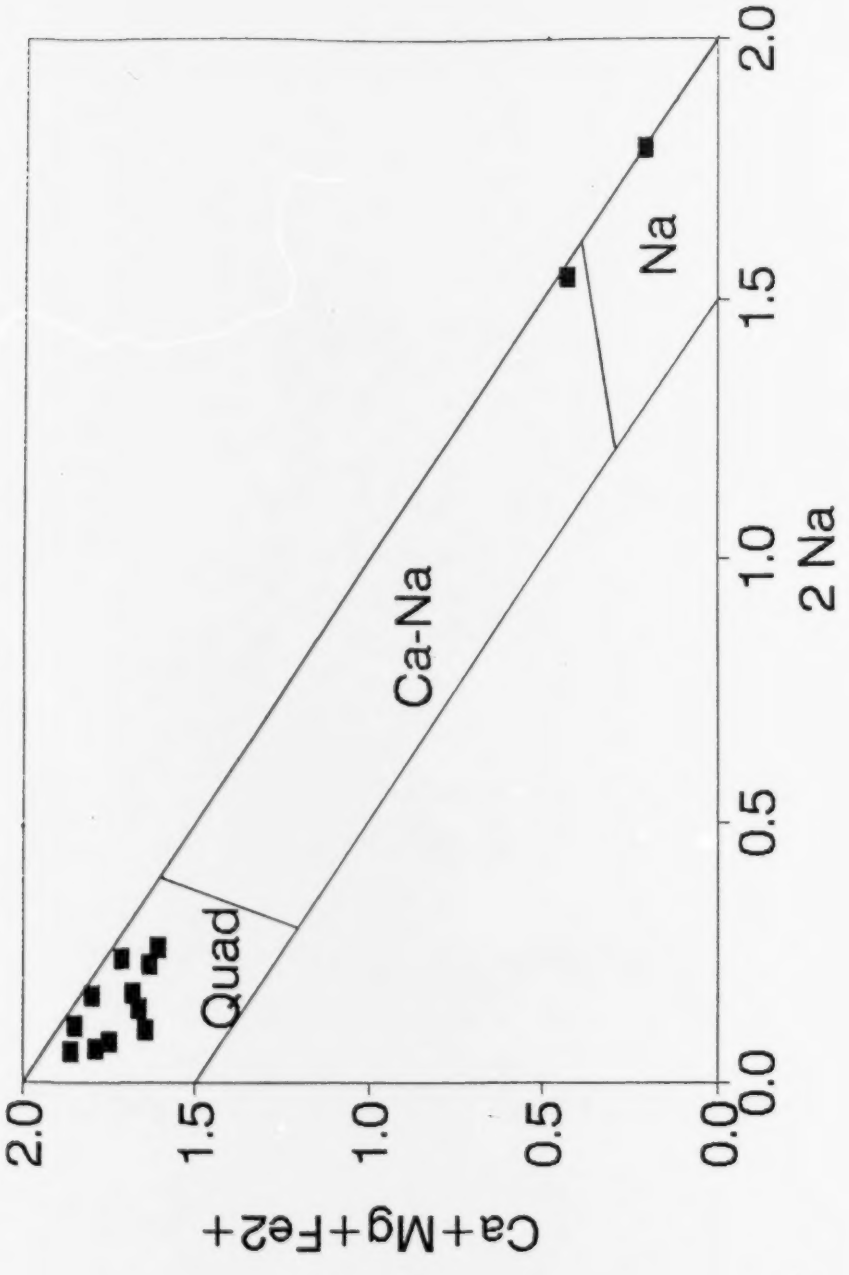

Figure 3.6 Pyroxene classification diagram (after Morimoto, 1989).

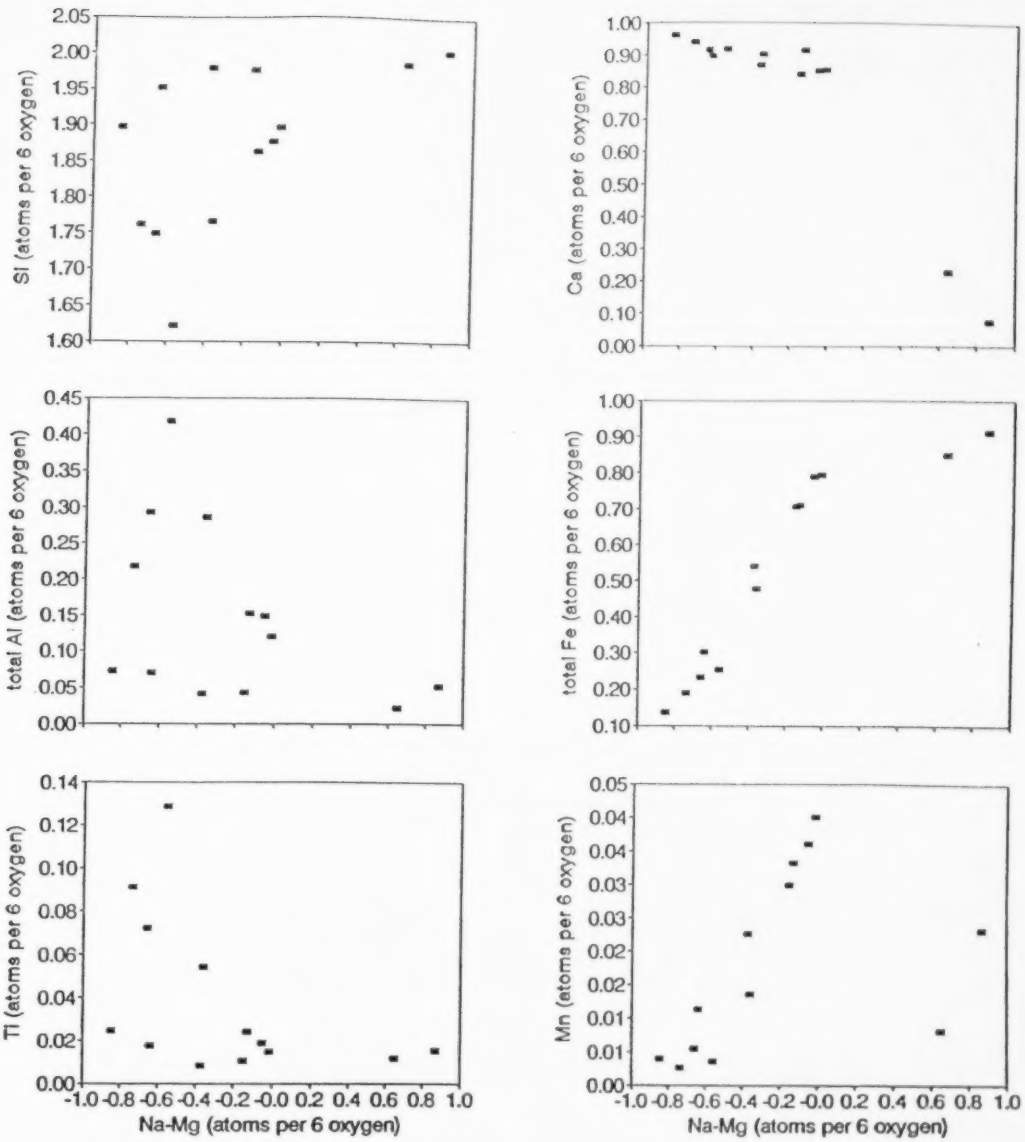
Si (atoms per 6 oxygen)
Ca (atoms per 6 oxygen)
total Al (atoms per 6 oxygen)
total Fe (atoms per 6 oxygen)
Ti (atoms per 6 oxygen)
Mn (atoms per 6 oxygen)
Na-Mg (atoms per 6 oxygen)
Na-Mg (atoms per 6 oxygen)

Figure 3.7 Compositional variation trends of the clinopyroxenes.

pyroxenes in the silicate rocks show a clear narrow trend of initial enrichment in Fe before subsequent enrichment in Na with increasing differentiation (Figure 3.8). This trend is broadly similar to those of other alkaline rocks (Platt and Woolley, 1986; Flohr and Ross, 1990).

The clinoamphibole analyses were classified according to the guidelines of Hawthorne (1981). All of the amphiboles analyzed were calcic amphiboles (Table 3.3); no alkali amphiboles were observed. The complete range of amphibole analyses is depicted in Figure 3.9, showing the compositional variation against Mg/(Mg+Fe). The chemical relationships in this figure are generally scattered, with the exception of decreasing K and Mn, and increasing Ca with increasing Mg/(Mg+Fe). Figure 3.10 represents the amphibole compositions in terms of molar Ca + Al^{iv} (tetrahedrally coordinated Al) and molar Si + Na + K, (Platt and Woolley, 1986). This figure depicts a linear sequence of amphibole evolution from subsilicic ({Ca + Al^{iv}} > 4) to compositions richer in (Si + Na + K). The amphiboles range in composition from subsilicic kaersutite through pargasite to hastingsite, following the primary miaskitic magmatic trend of Mitchell (1990). This amphibole differentiation trend is characteristic of complexes that contain miaskitic nepheline syenite and associated basic rocks (Mitchell, 1990).

Garnet is a minor modal phase in many of the rock-units of the Ice River complex, and a major phase in the melanite ijolite (Currie, 1975). The garnets examined range in composition along the solid solution series schorlomite-melanite-andradite. Melanite, although a varietal term, is used here as a convenient synonym for titanian andradite (TiO_2 = 1.0 - 15.0 wt%; Chapter 4). The garnet compositions show decreasing Ti and Zr, and increasing Fe and Si with differentiation (Table 3.4); schorlomite occurs in the ultrabasic melteigite, melanite (TiO_2 = 14 wt%) is found in the melanite ijolite, Ti-poor melanite (TiO_2 = 2 - 3 wt%) occurs in nepheline syenite, and andradite is found in the nepheline syenite pegmatite.

Several other mineral species (olivine, wollastonite, pectolite, and zoisite)

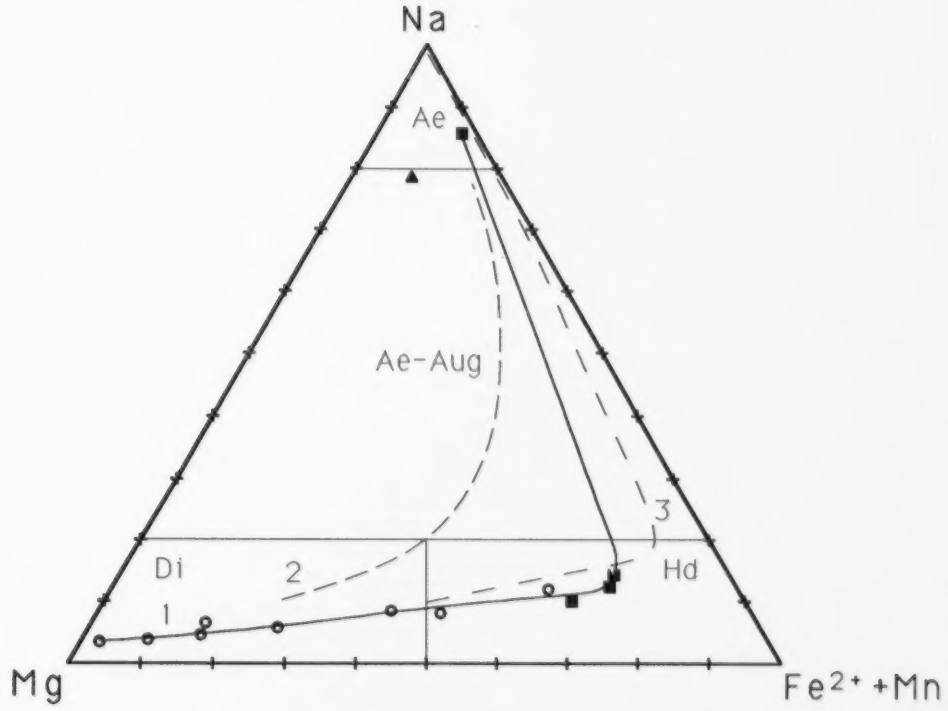

Figure 3.8 Electron microprobe analyses of clinopyroxenes from the Ice River complex plotted in the system Na-Mg-(Fe^{2+}+Mn) (cations). The trend labelled 1 is that defined by the pyroxenes of the Ice River complex. The pyroxenes of the feldspar-free cumulates are defined by open circles, those of the syenitic series by solid squares, and that of the carbonatite by a solid triangle. Trends 2 and 3 are from the Chambe and the Main alkaline complexes, respectively, of the Mulanje massif (Platt and Woolley, 1986). The clinopyroxene fields are Di - diopside, Hd - hedenbergite, Ae-Aug - aegirine-augite, Ae - aegirine.

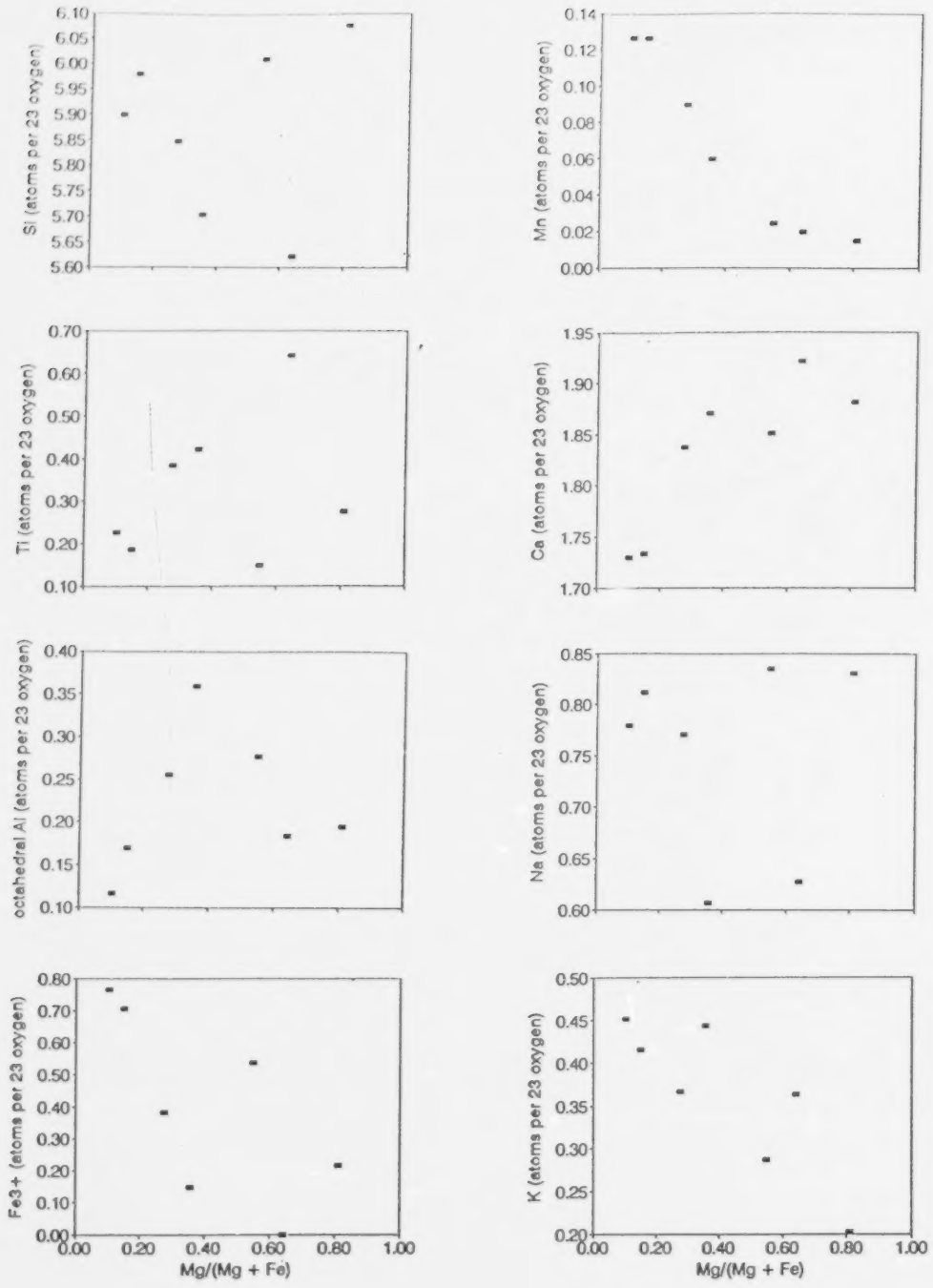
Si (atoms per 23 oxygen)
Mn (atoms per 23 oxygen)
Ti (atoms per 23 oxygen)
Ca (atoms per 23 oxygen)
octahedral Al (atoms per 23 oxygen)
Na (atoms per 23 oxygen)
Fe3+ (atoms per 23 oxygen)
K (atoms per 23 oxygen)
Mg/(Mg + Fe)
Mg/(Mg + Fe)

Figure 3.9 Compositional variation of the amphiboles of the complex.

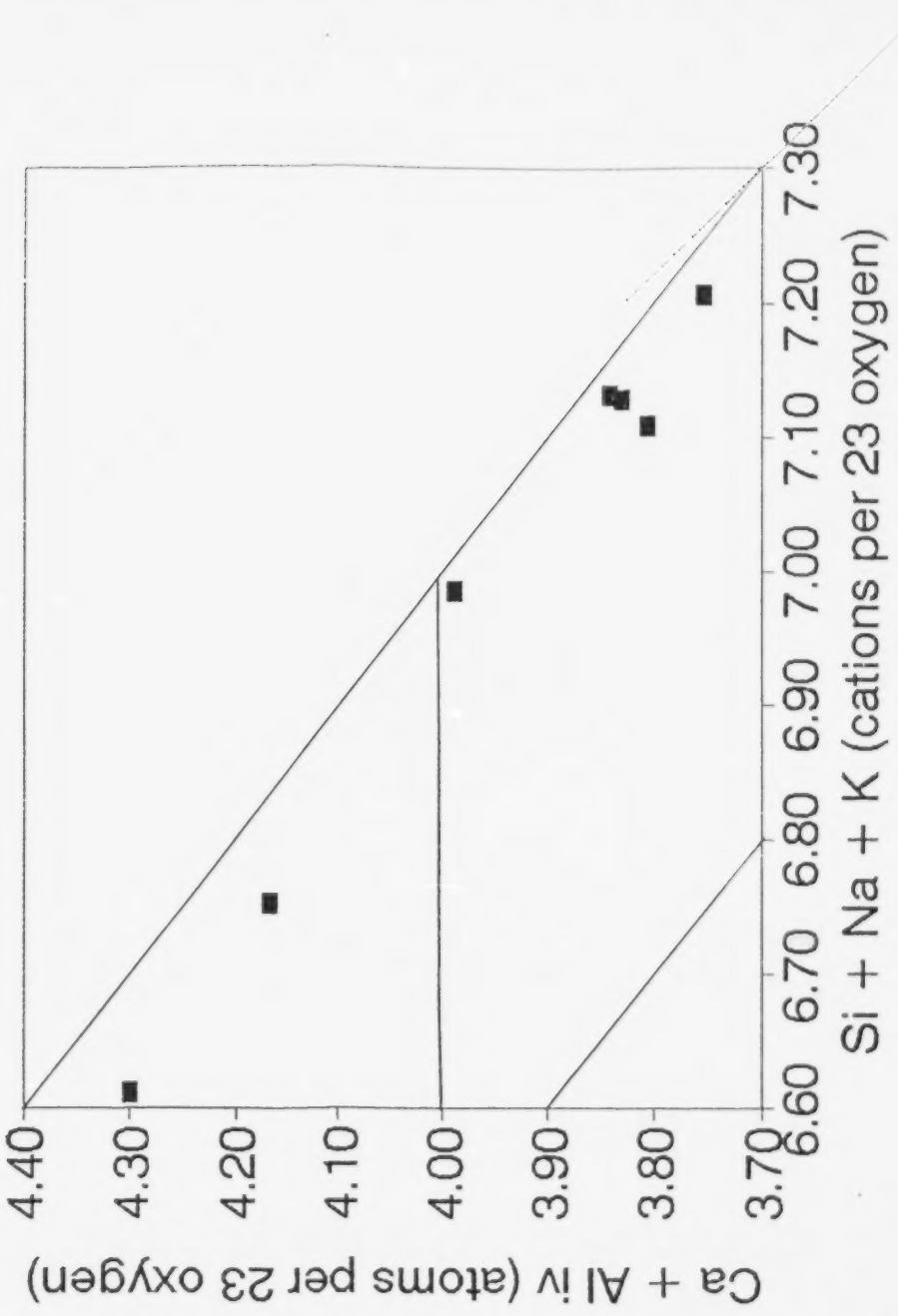

Figure 3.10 Amphibole evolution diagram (after Platt and Woolley, 1986). The field above $(Ca+Al^{iv}) > 4$ defines subsilicic amphiboles.

were examined, using the electron microprobe, in the course of this study to resolve uncertainties in the published descriptions of the Ice River complex as to their existence, composition, or identity. Structural formulae were calculated using the stoichiometric number of oxygen anions (4, 9, 9, and 13 respectively).

Prior to this study, olivine was not considered to be, "... a significant phase in any of the Ice River rocks, appearing in trace amounts only in a few dyke rocks..." (Currie, 1975). The olivine hornblendite, described briefly above, is a rare cumulate in the Ice River complex. It was observed in only one location, where it forms a semi-concordant band in melteigite. The olivine hornblendite contains roughly 30% olivine; the composition of this olivine is Fo_{76} (Table 3.5), similar to the compositions reported for olivine-bearing cumulates from other alkaline complexes (Beccaluva *et al.*, 1992).

Primary magmatic wollastonite is known from both intrusive and extrusive alkalic rocks (Deer *et al.*, 1978; Peterson, 1989a; Peterson, 1989b). The original description of wollastonite from the wollastonite urtite of the Ice River complex reported the FeO content (total iron) to be 9.47 wt% (16 atomic percent Fe) (Currie, 1975). This prompted later authors (Woolley, 1987) to refer to the Ice River material as ferrobustamite in view of the limited solubility of iron in the wollastonite structure (12 atomic percent); higher amounts of iron should force a transition to the bustamite structure (Deer *et al.*, 1978). Ferrobustamite is not known to occur as a magmatic phase in igneous rocks (Deer *et al.*, 1978). Re-examination of the wollastonite from the Ice River complex revealed that it contains only 0.98 wt% FeO (total iron, Table 3.5). Investigation of the material using X-ray powder diffraction techniques showed that it has the structure of wollastonite-1*A*, the most common triclinic polytype (Deer *et al.*, 1978). It is suggested that the original electron microprobe results (Currie, 1975) resulted from the accidental excitation of a sample volume that contained both wollastonite and hedenbergite.

In the course of the investigation of the Ice River wollastonite, pectolite was observed to form minute, acicular (roughly 5 by 50 micrometers) crystals at

Table 3.5 Chemical compositions of olivine, wollastonite, pectolite and zoisite

Sample	190.6 olivine ol hornblendite n=7		Ice 38 wollastonite woll urtite n=6		Ice 38 pectolite woll urtite n=3		Ice 22 zoisite parg ijolite
oxide	wt %	1 σ	wt %	1 σ	wt %	1 σ	wt %
SiO_2	37.82	0.64	51.05	0.19	53.19	1.13	39.29
Al_2O_3					0.04	0.01	34.43
Fe_2O_3			1.00		0.09		
FeO	21.52	0.34	0.08*	0.37	0.19‡	0.18	0.16
MnO	0.79	0.03	0.67	0.05	1.22	0.24	0.03
MgO	38.68	0.39	0.05	0.01	0.04	0.02	0.17
CaO	0.36	0.13	46.84	0.40	32.74	0.20	22.96
NiO	0.05	0.03					
Na_2O			0.08	0.03	8.98	0.12	0.29
K_2O					0.03	0.02	0.20
H_2O+ calc					2.66†		1.94†
Total	99.22	1.32	99.78	0.21	99.17	1.31	99.47

element	cations per 4 O	cations per 9 O	cations per 9 O	cations per 13 O
Si	0.993	2.979	2.983	2.981
Al			0.003	3.079
Fe^{3+}		0.044	0.004	
Fe^{2+}	0.472	0.004	0.009	0.010
Mn	0.018	0.033	0.058	0.002
Mg	1.514	0.005	0.003	0.019
Ca	0.010	2.929	1.967	1.866
Ni	0.001			
Na		0.009	0.976	0.043
K			0.002	0.019
H			0.995	0.982
Total	3.007	6.003	7.001	9.001

* FeO calculated by stoichiometry, standard deviation is of total Fe measured as FeO
‡ Fe^{2+}/Fe^{3+} taken from average value in Deer *et al.* (1978)
† H_2O+ calculated by stoichiometric constraints

the boundaries of some wollastonite aggregates. The composition of the pectolite is reported in Table 3.5. Pectolite is also known to occur as a primary mineral in some alkaline igneous rocks (Deer *et al.*, 1978; Horvath and Gault, 1990).

The nepheline in the rocks of the Ice River complex frequently contains microlites in the form of minute, randomly oriented acicular inclusions (Plate 3.1). These have been interpreted to be rosenbuschite (Barlow, 1902; Allan, 1914), apatite and/or aegirine (Allan, 1914). Apatite and clinopyroxene microlites in nepheline were observed by the author in several different samples, but rosenbuschite could not be identified. Rosenbuschite is a complex calcium-sodium-titanium-zirconium silicate characteristic of agpaitic nepheline syenite pegmatites (Deer *et al.*, 1985) and is therefore unlikely to occur throughout the rock-units of a miaskitic complex. In the course of electron microprobe investigation of the pargasite in the pargasite ijolite (sample Ice 22), the author analyzed some of the microlites in the nearby nepheline (Plate 3.1). The composition of these microlites (Table 3.5) matches that of zoisite or clinozoisite. The microlites were assumed to be zoisite rather than clinozoisite because the former is more stable in the temperature range 350 - 600°C (Jenkins *et al.*, 1985).

It is suggested here that the zoisite microlites were formed by exsolution (coupled with cation exchange) from the host nepheline upon subsolidus cooling. Nepheline may be viewed as a solid solution series of the form:

$$Na_xK_yCa_zV_{3-(x+y+z)}Al_{(x+y+2z)}Si_{6-(x+y+2z)}O_{12}$$

where *V* are vacant sites resulting from the substitution of Si for Al (Deer *et al.*, 1985). Although nepheline can contain up to 35 molar percent anorthite in solid solution at 1295°C (Bowen, 1912), most natural nepheline contains only small amounts of calcium (Deer *et al.*, 1985). Even nepheline formed in calcium-rich environments does not contain significantly greater amounts (Deer *et al.*, 1985). Deer *et al.* (1985) suggest that this may be a result of the lesser solubility of calcium in nepheline at lower temperatures. Exsolution of zoisite

Plate 3.1 Photomicrographs of zoisite microlites in nepheline taken under plane-polarized (a) and cross-polarized (b) light. The magnification was 200 times.

(with concomitant addition of alkali-metal and hydroxyl) from nepheline upon cooling could explain the low calcium contents of natural nepheline. The structural formula of zoisite may be written as $Ca_2(OH)Al_3Si_3O_{12}$ in order to facilitate comparison with the Na and K endmembers of the nepheline solid solution series: $Na_3Al_3Si_3O_{12}$ and $K_3Al_3Si_3O_{12}$. All three formulae have the same Al:Si ratio; Ca and OH replace (Na,K) in this comparison. The following reaction may be written:

$$4\ (Na,K)_2Ca_{0.5}V_{0.5}Al_3Si_3O_{12} + 1\ (Na,K)^+ + 1\ (OH)^- =$$
$$3\ (Na,K)_3Al_3Si_3O_{12} + Ca_2(OH)Al_3Si_3O_{12}$$

Natural nepheline contains very little water (Deer *et al.*, 1985) and thus a source outside of the nepheline must be postulated for the hydroxyl necessary to form the zoisite during exsolution. Oxygen diffuses rapidly through nepheline (Connolly and Muehlenbachs, 1988) and therefore the similarly sized hydroxyl or water molecules should also diffuse rapidly through the nepheline structure (Muehlenbachs, personal communication, 1994). The nearby pargasite could act as a source for both the hydroxyl that is necessary to form the zoisite, and the alkali-metal necessary to charge balance the remaining nepheline. The zoisite is proposed to form during subsolidus cooling because of its minute crystal size, occurrence solely in nepheline, and because zoisite decomposes above 620°C at 3 kbar (calculated with the thermodynamic dataset of Holland and Powell, 1990) - the complex is thought to have been emplaced at 700 - 1000°C and 2 - 3.5 kbar (Currie, 1975).

3.4 DISCUSSION

There are several hypotheses regarding the evolution of alkaline complexes that contain both carbonatite and silicate rocks, but most authors consider the carbonatite to form by immiscibility from a silicate magma, and to be the last unit emplaced (Barker, 1989). Barker (1989) suggests that the sequence of emplacement, from oldest to youngest, is nepheline syenite, to nepheline-clinopyroxene rocks, to carbonatite. An opposing arrangement of

clinopyroxenite, followed by nepheline-clinopyroxene rocks, then nepheline syenite, and finally carbonatite, is favored by Kapustin (1986). The reader is directed to the compilation volumes of Fitton and Upton (1987), and Bell (1989), and the paper of Bailey (1993) for reviews of recent opinions on the genesis and evolution of these complexes.

The hypothesis that will be considered here (albeit based on a quite limited data set) is that a single carbonate-bearing silicate magma generated the Ice River complex. This magma precipitated silicate and oxide minerals, forming the feldspar-free cumulates, and increasing its carbonate:silicate ratio. At some point in the cumulate precipitating process, the magma became critically saturated in carbonate, and split into immiscible daughter carbonate and silicate liquids. The daughter silicate magma was considerably more felsic than its parent, and gave rise to the nepheline syenite (and the other rock-units of the syenitic series). The carbonatite magma generally remained liquid to lower temperatures than the immiscible silicate magma, and formed the calcite-carbonatite.

The cumulate textures of the feldspar-free rocks, and the ubiquitous occurrence of primary magmatic calcite within the cumulates, are both consistent with the suggestion that the rocks of the feldspar-free series crystallized from a carbonate-bearing silicate magma. In contrast, the rocks of the syenitic series (nepheline and sodalite syenites and pegmatites) do not display cumulate textures or contain primary calcite; this is in agreement with their derivation from a carbonate-free magma of intermediate (although undersaturated) composition. Ijolite blocks are hosted by nepheline syenite (Figure 19 of Currie, 1975) and nepheline syenite dykes cross-cut the cumulates. Therefore, the syenitic series post-date the crystallization of the feldspar-free series. The field relationships depicted in Figure 25 of Currie (1975) - rounded syenite inclusion in 3-metre carbonatite dyke cutting ijolite - are consistent with the late position of the carbonatite in the order of emplacement, post-dating even the syenitic rocks. This is contradicted by the

observation of Currie (1975) that the carbonatite is cut by younger syenite elsewhere in the complex. The complex relationships between the carbonatite and the syenitic series would not be unreasonable if the two immiscible magmas were penecontemporaneously evolving and crystallizing.

The scatter on oxide variation diagrams (Figures 3.2 and 3.3) is consistent with the cumulate nature of the feldspar-free rocks, and the lack of a simple fractional crystallization mechanism relating them with the rocks of the syenitic series. The clustering of the Br data (Figure 3.3) is indicative of the separated nature of the two series. The broad similarity of the rare-earth patterns of all of the rock-units of the complex (Figures 3.4 and 3.5) is consistent with the suggestion that they were derived from a single source.

The compositional trends of the mafic minerals are also consistent with the interpretation that the cumulates, feldspathoidal syenites, and carbonatite of the Ice River Complex are comagmatic. In the silicate rocks, with increasing differentiation, the garnets increase in Fe and Si, and decrease in Ti (schorlomite to melanite to andradite), while the amphiboles follow the primary miaskitic trend from kaersutite through pargasite to hastingsite (Mitchell, 1990). The pyroxenes show a narrow trend of iron enrichment preceding sodium enrichment (Figure 3.8).

3.5 CONCLUSIONS

The Ice River alkaline complex resulted from the evolution of a single parental magma. The ultramafic-mafic, feldspar-free, nepheline-bearing cumulates were the first to crystallize. Immiscible separation of the remaining magma into an intermediate, undersaturated liquid, and a carbonatite magma followed. These two magmas evolved and crystallized penecontemporaneously, resulting in dykes and veins that cross-cut the cumulates, and locally each other.

3.6 REFERENCES CITED

Allan, J.A. (1914) Geology of Field Map-area, B.C. and Alberta. Memoir 55, 312 p. Geological Survey of Canada, Ottawa.

Bailey, D.K. (1993) Carbonate magmas. Journal of the Geological Society, 150, 637-651.

Bailey, D.K., and Hampton, C.M. (1990) Volatiles in alkaline magmatism. Lithos, 26, 157-165.

Barker, D.S. (1989) Field relations of carbonatites. In K. Bell, Ed., Carbonatites, Genesis and Evolution, p. 38-69. Unwin Hyman, London.

Barlow, A.E. (1902) On the nepheline rocks of Ice River, British Columbia. The Ottawa Naturalist, June, 70-76.

Beccaluva, L., Barbieri, M., Born, H., Brotzu, P., Coltorti, M., Conte, A., Garbarino, C., Gomes, C.B., Macciotta, G., Morbidelli, L., Ruberti, E., Siena, F., and Traversa, G. (1992) Fractional crystallization and liquid immiscibility processes in the Alkaline-Carbonatite Complex of Juquiá (São Paulo, Brazil). Journal of Petrology, 33, 1371-1404.

Bell, K. (1989) editor, Carbonatites, Genesis and Evolution, Unwin Hyman, London.

Bowen, N.L. (1912) The binary system $Na_2Al_2Si_2O_8$ (Nephelite, Carnegieite) - $CaAl_2Si_2O_8$ (Anorthite). Abstract of thesis, 14 p. Massachusetts Institute of Technology.

Cavell, P.A. (1986) The geochronology and petrogenesis of the Big Spruce Lake Alkaline Complex, 448 p. Ph.D. thesis, University of Alberta, Edmonton, Alberta.

Connolly, C., and Muehlenbachs, K. (1988) Contrasting oxygen diffusion in nepheline, diopside and other silicates and their relevance to isotopic systematics in meteorites. Geochimica et Cosmochimica Acta, 52, 1585 -1591.

Currie, K.L. (1975) The Geology and Petrology of the Ice River Alkaline Complex, British Columbia. Bulletin 245, 68 p. Geological Survey of Canada, Ottawa.

Deer, W.A., Howie, R.A., and Zussman, J. (1985) An introduction to the rock -forming minerals (15th impression), 528 p. Longman, Harlow.

———————— (1978) Single-Chain Silicates: Non-Pyroxenes. In Rock-forming minerals, volume 2A: Single-Chain Silicates (2nd edition), p. 547-668. Longman, London.

Duke, M.J.M. (1993) The geochronology, geochemistry and isotope geology of the type-Nûk gneisses of the Akia terrane, southern West Greenland, 286 p. Ph.D. thesis, University of Alberta, Edmonton, Alberta.

Evensen, N.M., Hamilton, P.J., and O'Nions, R.K. (1978) Rare earth abundances in chondritic meteorites. Geochimica et Cosmochimica Acta, 42, 1199-1212.

Fitton, J.G., and Upton, B.G.J. (1987) editors, Alkaline Igneous Rocks, Blackwell Scientific Publications, London.

Flohr, M.J.K., and Ross, M. (1990) Alkaline igneous rocks of Magnet Cove, Arkansas: Mineralogy and geochemistry of syenites. Lithos, 26, 67-98.

Gabrielse, H. (Compiler) (1991) Structural styles, Chapter 17. In Geology of the Cordilleran Orogen in Canada, H. Gabrielse and C.J. Yorath (ed.). Geological Survey of Canada, Geology of Canada, No.4, 571-675.

Greenwood, H.J., Woodsworth, G.J., Read, P.B., Ghent, E.D., and Evenchick, C.A. (1991) Metamorphism, Chapter 16. In Geology of the Cordilleran Orogen in Canada, H. Gabrielse and C.J. Yorath (ed.). Geological Survey of Canada, Geology of Canada, No.4, 533-570.

Grice, J.D., and Gault, R.A. (1981) Edingtonite and natrolite from Ice River, British Columbia. Mineralogical Record, July-August, 221-226.

Grice, J.D., Gault, R.A. and Ansell, H.G. (1984) Edingtonite: the first two Canadian occurrences. Canadian Mineralogist, 22, 253-258.

Hawthorne, F.C. (1981) Crystal chemistry of the amphiboles. In Mineralogical Society of America Reviews in Mineralogy, 9A, 1-102.

Holland, T.J.B., and Powell, R. (1990) An enlarged and updated internally consistent thermodynamic data set with uncertainties and correlations: the system K_2O-Na_2O-CaO-MgO-FeO-Fe_2O_3-Al_2O_3-TiO_2-SiO_2-C-H_2-O_2. Journal of Metamorphic Geology, 8, 89-124.

Horvath, L., and Gault, R.A. (1990) Mont Saint-Hilaire. The Mineralogical Record, 21, 284-392.

Jenkins, D.M., Newton, R.C., and Goldsmith, J.R. (1985) Relative stability of Fe-free zoisite and clinozoisite. Journal of Geology, 93, 663-672.

Kapustin, Y.L. (1986) The origin of early calcitic carbonatites. International Geology Review, 28, 1031-1044.

Mitchell, R.H. (1990) A review of the compositional variation of amphiboles in alkaline plutonic complexes. Lithos, 26, 135-156.

Morimoto, N. (1989) Nomenclature of pyroxenes. Canadian Mineralogist, 27, 143-156.

Pell, J.A. (1987) Open File 1987-17 Alkaline ultrabasic rocks in British Columbia. Province of British Columbia, Ministry of Energy, Mines and Petroleum Resources, Mineral Resources Division, Geological Survey Branch.

Pell, J.A., and Höy, T. (1989) Carbonatites in a continental margin environment - the Canadian Cordillera. In K. Bell, Ed., Carbonatites, Genesis and Evolution, p. 200-220. Unwin Hyman, London.

Peterson, T.D. (1989a) Peralkaline nephelinites. I. Comparative petrology of Shombole and Oldoinyo L'engai, East Africa. Contributions to Mineralogy and Petrology, 101, 458-478.

———— (1989b) Peralkaline nephelinites. II. Low pressure fractionation and the hypersodic lavas of Oldoinyo L'engai. Contributions to Mineralogy and Petrology, 102, 336-346.

Phillips, A.H. (1916) Some new forms of natrolite. American Journal of Science, 42 (whole number 192), 472-474.

Platt, R.G., and Woolley, A.R. (1986) The mafic mineralogy of the peralkaline syenites and granites of the Mulanje complex, Malawi. Mineralogical Magazine, 50, 85-99.

Rock, N.M.S. (1978) Petrology and petrogenesis of the Monchique Alkaline Complex, Southern Portugal. Journal of Petrology, 19 Part 2, 171-214.

———— (1982) Chemical mineralogy of the Monchique Alkaline Complex, Southern Portugal. Contributions to Mineralogy and Petrology, 81, 64-78.

Wilson, M. (1993) Magmatic differentiation. Journal of the Geological Society, 150, 611-624.

Woolley, A.R. (1987) Alkaline Rocks and Carbonatites of the World, Part 1: North and South America, 216 p. British Museum of Natural History, London.

Woolley, A.R. and Kempe, D.R.C. (1989) Carbonatites: nomenclature, average chemical compositions, and element distribution. In K. Bell, Ed., Carbonatites, Genesis and Evolution, p. 1-14. Unwin Hyman, London.

4. SPECTROSCOPY OF THE CATION DISTRIBUTION IN THE SCHORLOMITE SPECIES OF GARNET

4.1 INTRODUCTION

The general formula of silicate garnets may be written $\{X\}_3[Y]_2(Si)_3O_{12}$ where {} represents triangular dodecahedral coordination, [] indicates octahedral coordination, and () denotes tetrahedral coordination (Hawthorne, 1981; Leigh, 1990). The garnet structure usually crystallizes in the cubic space group *Ia3d*.

Schorlomite is a species of silicate garnet containing more than one atom of titanium per formula unit. Melanite is the complementary varietal name for titanian andradite that has less than one titanium atom per formula unit (Deer *et al.*, 1982). Unlike most other natural silicate garnets the tetrahedral site in schorlomite is not fully occupied by silicon. This deficiency, together with the large concentrations of titanium and both ferric and ferrous iron in the mineral, has given rise to contention about the cation distribution between the different crystallographic sites in schorlomite. Numerous studies have investigated the crystal chemistry of schorlomite and titanian andradite in attempts to resolve the roles of titanium and iron. The results of chemical studies have shown an inverse correlation between silicon and titanium and have been used as evidence that Ti^{4+} replaces Si^{4+} in the tetrahedral site, with any excess titanium allocated to the octahedral site (often as Ti^{3+}) (Koenig, 1886; Hoffmann, 1902; Howie and Woolley, 1968; Basso *et al.*, 1981; Onuki *et al.*, 1981; Dingwell and Brearley, 1985; Sawaki, 1988; Lueck and Russell, 1994). Optical and near infrared spectroscopic studies have produced several interpretations of the crystal chemistry of schorlomite including $^{[6]}Ti^{3+}$ (Manning and Harris, 1970; Moore and White, 1971), $^{[4]}Fe^{2+}$ (Manning and Harris, 1970; Dowty, 1971; Huggins *et al.*, 1977b; Smith, 1978), and various charge-transfer mechanisms (Dowty, 1971; Moore and White, 1971; Huggins *et al.*, 1977b). From the numerous ^{57}Fe Mössbauer studies of schorlomite no

consensus has been reached about the distribution of iron (and indirectly titanium). Interpretations have included $^{[4]}Ti^{4+}$ in slight amounts (Huggins *et al.*, 1977b; Koritnig *et al.*, 1978; Kühberger *et al.*, 1989), slight quantities of $^{[6]}Ti^{3+}$ (Huggins *et al.*, 1977b; Schwartz *et al.*, 1980; Onuki *et al.*, 1982; Wu and Mu, 1986; Kühberger *et al.*, 1989), exclusive $^{[6]}Ti^{4+}$ (Dowty, 1971; Amthauer *et al.*, 1977), significant $^{[4]}Fe^{2+}$ (Dowty, 1971; Huggins *et al.*, 1977b; Amthauer *et al.*, 1977; Koritnig *et al.*, 1978; Kühberger *et al.*, 1989) and various charge-transfer or electron delocalization mechanisms (Huggins *et al.*, 1977b; Schwartz *et al.*, 1980; Yupu and Ruiying, 1985; Wu and Mu, 1986).

Most of the above studies indirectly constrained the valence state(s) and site distribution of titanium by using general crystal-chemical guidelines and by determining the site occupancies and oxidation states of the other constituent cations (mainly iron). Stoichiometric constraints were then used to fix the distribution of titanium and its valence state(s). This approach, which assumes perfect stoichiometry, propagates all the analytical uncertainties into the calculation of the titanium distribution.

Studies, using X-ray absorption near-edge spectroscopy (XANES), that investigated directly the coordination and valence state of titanium in schorlomite concluded that titanium was exclusively tetravalent and octahedrally coordinated within experimental error (Waychunas, 1987; de Groot *et al.*, 1992).

There are several analytical difficulties involved in investigating schorlomite or titanian andradite. Customary wet-chemical determination of the ferrous iron content is hampered by the relative insolubility of garnet, and will give misleading results in the presence of other reduced cations such as V^{3+} and Ti^{3+} (Groves, 1937). Optical and near infrared spectral assignments may be equivocal given the presence of several different transition metals. The results of ^{57}Fe Mössbauer spectroscopy may be difficult to evaluate because of the possibility of differing recoil-free fractions between the disparate crystallographic sites, as well as the variation of the hyperfine parameters with

temperature and composition. Perhaps the most serious analytical challenge is the compositional zoning found in many garnet specimens; if present, this zoning precludes rational characterization of a sample by analytical methods requiring bulk portions.

This study used several different analytical techniques to investigate aliquots of a single homogeneous megacryst of schorlomite. Methods included optical microscopy, powder X-ray diffractometry (XRD), electron microprobe analysis, instrumental neutron activation analysis (INAA), synchrotron-based X-ray absorption near-edge spectroscopy (XANES), volumetric Fe^{2+} determination, Fourier transform infrared spectroscopy (FTIR), ^{57}Fe Mössbauer spectroscopy (at 295 and 80 K), and optical absorption spectroscopy. These techniques are more fully described below. A multi-analytical approach provides mutually supporting evidence, thereby increasing the confidence of the interpretations. The valence states and site occupancies of titanium and iron in schorlomite are the major concerns addressed by this study.

4.2 MATERIAL AND METHODS

An anhedral schorlomite megacryst was collected from the melteigite unit of the Ice River Alkaline Complex, Yoho National Park, British Columbia, Canada. The specimen is opaque and pitch-black in color at thicknesses greater than 20 μm and has an adamantine luster. A strong red-brown color is evinced by sections thinner than 20 μm. No zoning was observed by transmitted or reflected light microscopy. Density measurements were determined using a VDF torsion balance and toluene as an immersion liquid. The index of refraction of the sample was measured using fresh Cargille Laboratories immersion liquids and standard immersion techniques.

To prepare a purified mineral separate, schorlomite fragments were ground in a tungsten carbide swing mill along with carbon dioxide pellets (to prevent oxidation). The resulting material was dry-sieved and the size fraction between 120 and 170 U.S. sieve mesh collected and washed with acetone.

Impurities (apatite, biotite, calcite, diopside, nepheline, and pyrite) were removed from by settling in diiodomethane followed by magnetic separation. The purity of the mineral separate was estimated to be > 99.9%.

To examine a ferric-only end-member of schorlomite, a doubly polished wafer and an aliquot of the sample powder were placed into individual alumina crucibles and heated in air for 594 hours at 1050°C. The resulting samples were investigated using Mössbauer, optical and infrared spectroscopic methods, and X-ray powder diffraction techniques.

4.2.1 X-ray powder diffraction

An aliquot of the unheated purified separate was prepared for X-ray diffraction by grinding it in an alumina ball mill with carbon dioxide pellets. An X-ray powder diffraction pattern from 2 to 90° 2Θ was recorded on a Rigaku Geigerflex automated powder diffractometer using Co radiation, a graphite monochromator and a scan speed of 0.6° 2Θ/min. Using these data the unit cell dimension was calculated using the least-squares program of Appleman and Evans (1973) as revised for the microcomputer by Benoit (1987). The uncertainty in the X-ray peak positions is estimated to be 0.003° 2Θ based on repeated scans of a quartz standard.

4.2.2 Electron microprobe analyses

Analyses were performed using an ARL SEMQ electron microprobe with a Tracor Northern 5600 automation package. Following preliminary examination by energy dispersive analysis, elemental analyses were performed using the wavelength dispersive mode, with an excitation voltage of 15 kV, a probe current of 12 nA, and a beam diameter of 1 μm rastered over an 100 μm^2 area. Peak and background counting times were 20 and 10 s, respectively for both the standards and samples. Standards used included kaersutite (Na), pyrope (Mg, Al, Si), grossular (Ca), rutile (Ti), willemite (Mn), chromite (Fe), and zircon (Zr). Vanadium was the only other element observed in the energy

dispersive spectrum and was quantified with reference to a vanadium metal standard. These microprobe vanadium results were subsequently shown to be consistently higher by ~50% than those from duplicate ICP and INAA analyses (on separate aliquots from the same megacryst) and are therefore not presented. Reduction of data was carried out with the use of a Phi-Rho-Z program included with the Tracor Northern software. Total iron was calculated as ferric iron. Thirty-three quantitative analyses were acquired at 250 μm intervals along a traverse.

4.2.3 Instrumental neutron activation analysis (INAA)

Selected minor and trace elements were determined by instrumental neutron activation analysis of two aliquots of the purified schorlomite separate. Short-lived radionuclides were determined by irradiating a 30 mg aliquot for 5 min at a nominal thermal neutron flux of 1 x 10^{11} n cm^{-2} s^{-1} in an inner site of the SLOWPOKE II nuclear reactor at the University of Alberta. The irradiated sample was counted for 5 min live time at a sample-to-detector distance of 6 cm after a 20 min decay period. For the determination of the long-lived radionuclides, a 500 mg aliquot was irradiated for 2 h at 1 x 10^{12} n cm^{-2} s^{-1}. This aliquot was counted twice: initially for 50 min at a sample-to-detector distance of 3 cm following a decay of 6 days, and a second time for 6.94 h at a geometry of 1 cm after a total decay of 21 days. All measurements were performed in a 10 cm thick Pb cave with a graded shield of Cu and Perspex®.

The gamma-ray spectroscopy system included a 20% efficiency hyperpure Ge detector (that has a full width at half maximum peak height (FWHM) of 1.9 keV for the 1332.5 keV photopeak of ^{60}Co) coupled to a multichannel analyzer. Elemental concentrations were determined by the semi-absolute method of NAA (Bergerioux *et al.*, 1979). Reference materials included: USGS BCR-1 (basalt), USGS W-1 (diabase), USGS RGM-1 (rhyolite), NIST NBS 1633a (fly ash), and GIT-IWG AC-E (microgranite).

4.2.4 X-ray absorption near-edge spectroscopy

Table 4.1 lists the minerals used as model compounds in this study. The samples were ground finely, and those for transmission studies were intimately mixed with boron nitride and mounted with Mylar® tape onto sample holders. The sample for fluorescence study was mounted directly onto Mylar®. Absorption spectra of the Ti and V K-edges were acquired at room temperature using the (1.8 T, 8 pole) wiggler on beamline 4-1 of the Stanford Synchrotron Radiation Laboratory in transmission mode for all the model minerals and for Ti in schorlomite. Measurements were made in the fluorescence mode in the case of V in the schorlomite using a Lytle detector (Lytle *et al.*, 1984). Five fluorescence scans were acquired and averaged to improve the signal to noise ratio. A Si (220) double crystal monochromator was used, with no focussing optics, and a 1 mm upstream vertical aperture to produce a monochromatic synchrotron X-ray beam trimmed to dimensions of approximately 1 mm x 10 mm. The energy scales were calibrated relative to the first inflection point in either Ti or V foils as appropriate (4966.0 and 5465.0 eV respectively).

Table 4.1 Mineral standards used for synchrotron study

Mineral	Source	Formula
Vanadinite	Mibladen, Morocco	$Pb_5(VO_4)_3Cl$
Descloizite	Grootfontein Mine, Berg Aukas, Namibia	$PbZn(VO_4)OH$
Cavansite	Poona, Maharashtra, India	$Ca(VO)Si_4O_{10} \cdot 4H_2O$
Titanite	Ice River Complex, Yoho National Park, British Columbia, Canada	$CaTiSiO_5$
Rutile	Ibitiara, Bahia, Brazil	TiO_2

4.2.5 Ferrous iron determination

Ferrous iron content was determined by titration against a standardized potassium permanganate solution after sample dissolution in a boiling mixture of sulfuric and hydrofluoric acids (modified after Groves, 1937). This volumetric procedure used a portion of the purified schorlomite separate that had been finely ground in an alumina ball mill with CO_2 pellets.

Vanadium present in the Ice River schorlomite was shown to be trivalent by XANES (see Results below). The presence of trivalent vanadium leads to an over-estimation of ferrous iron (Groves, 1937). A correction was applied to the ferrous iron content using the vanadium concentration determined by INAA. For the measured 0.20 wt% V_2O_3 content of the schorlomite, it was calculated that 0.38 wt% FeO must be subtracted from the FeO value initially determined by titration.

4.2.6 Hydroxyl content

To determine the hydroxyl content of the specimen a doubly polished wafer of schorlomite measuring 85 $\pm$ 3 μm in thickness (measured with a Logitech two-dial micrometer) was prepared and dried at 60°C. Unpolarized FTIR spectra were recorded using a Nicolet 60SX spectrometer. The hydroxyl content was calculated using the absorption coefficient for low-OH grossular of Rossman and Aines (1991). Such a relationship has not yet been determined for schorlomite, but the absorption coefficient for grossular should give comparable results at these hydroxyl concentrations (Lager *et al.*, 1989; Rossman, personal communication, 1993).

4.2.7 Mössbauer spectroscopy

Room-temperature Mössbauer (^{57}Fe) spectra were obtained for the unheated powdered sample, the unheated single crystal wafer and the heated schorlomite powder using a nominal 50-mCi (1.85 GBq) ^{57}Co source in Rh at the University of Alberta. The amount of sample powder sandwiched between

two layers of Mylar® was adjusted to give an absorber thickness of ~5 mg Fe/cm^2 to avoid saturation effects (Bancroft, 1973). Mirror-image Mössbauer spectra were recorded using a microcomputer-based multi-channel analyzer. Between one- and five million off-resonance counts per channel were collected. A velocity range of 4 mm/s was used; this velocity was calibrated with iron foil, with values of g_o = 3.9156 mm/s and g_1 = 2.2363 (Stevens and Stevens, 1972). The isomer shifts are reported relative to metallic iron at room temperature.

Data from the two sides of the mirror-imaged spectrum were folded, and then fitted with Lorentzian doublets by a least-squares procedure with the program PCMOS. Spectra of unheated schorlomite were fitted with equal-area, equal half-width doublets for both ferric and ferrous iron. The spectrum of heated schorlomite was fitted with equal-area, equal half-width doublets for ferric iron only as ferrous iron was not detectable.

The 80 K spectrum was obtained through the courtesy of Dr. D. Canil at the Bayerisches Geoinstitut, Germany. The apparatus is similar to that used for the room-temperature experiments at the University of Alberta; this spectrum was collected over a 5 mm/s velocity range.

4.2.8 Infrared and optical spectroscopy

Room temperature FTIR spectra in the region 1000-3000 nm were recorded on a Nicolet Nic-Plan Magna-IR 750 series microscope. Optical absorption spectra were recorded at room temperature using a Hewlett Packard 8450A spectrophotometer. Doubly polished sections of unheated and heated schorlomite mounted on glass slides with epoxy were examined.

4.3 RESULTS

The physical properties of the unheated Ice River schorlomite specimen are listed in Table 4.2. The refractive index and cell edge are in agreement with the values determined by Howie and Woolley (1968) and the measured and calculated densities agree with the more recent work of Wu and Mu

(1986). The X-ray lines are very similar to those listed by JCPDS card 33-285 for schorlomite from Oka, Quebec, Canada.

Table 4.2 Physical parameters of Ice River schorlomite

Index of refraction n	Density g/cm^3	Unit cell dimension a (Å)	Mohs hardness	X-ray lines (Å)§
1.940	3.77*	12.153	6.5 - 7	2.716 (100)
	3.80**			3.037 (55)
				1.624 (54)
				2.481 (41)
				1.686 (23)

* mean of five measurements
** calculated with the cell dimension and chemical analysis
§ numbers in parentheses are relative intensities

In the heated powder sample, the schorlomite decomposed to a mixture of rutile, ferric oxide and a garnet with a slightly expanded unit cell (to 12.167 Å). The wafer of heated schorlomite was optically anisotropic and polycrystalline. However, the X-ray powder pattern could still be fitted to the space group *Ia3d*.

4.3.1 Chemical composition

The electron microprobe analyses of the schorlomite are given in Table 4.3. The uniformity of the 33 analyses over an aggregate distance of 8250 μm is consistent with a homogeneous specimen. Therefore, unlike compositionally zoned garnets, bulk analytical techniques may be used upon different aliquots of this sample to determine additional aspects of its composition.

Table 4.3 Electron microprobe analyses of Ice River schorlomite

	1	2	3	4	5	6	7
SiO_2	28.22	28.70	28.12	28.06	28.20	28.41	28.79
TiO_2	15.00	14.19	15.23	15.45	14.87	15.16	15.06
ZrO_2	0.91	0.77	0.83	0.82	0.93	0.84	0.68
Al_2O_3	1.04	1.37	1.07	1.20	1.11	1.21	1.21
Fe_2O_3*	21.54	21.55	21.65	21.43	21.94	21.83	21.57
MnO	0.46	0.36	0.43	0.44	0.49	0.48	0.48
MgO	0.81	0.82	0.82	0.99	0.94	1.01	0.98
CaO	31.75	31.72	31.52	30.80	30.95	30.94	31.48
Na_2O	0.30	0.17	0.25	0.29	0.24	0.22	0.27
Total	100.03	99.65	99.92	99.48	99.67	100.10	100.52

	8	9	10	11	12	13	14
SiO_2	28.76	27.62	27.20	27.41	27.10	27.05	27.05
TiO_2	14.89	16.98	16.99	16.71	16.88	17.18	16.83
ZrO_2	1.06	0.94	1.05	0.79	0.94	0.93	0.82
Al_2O_3	1.00	1.37	1.35	1.48	1.41	1.42	1.43
Fe_2O_3*	21.69	20.71	20.25	20.35	20.77	20.03	20.51
MnO	0.35	0.43	0.42	0.47	0.45	0.46	0.43
MgO	0.86	1.09	1.10	0.99	1.17	1.14	1.16
CaO	31.45	31.51	31.29	30.98	31.38	31.39	31.19
Na_2O	0.22	0.24	0.25	0.27	0.20	0.27	0.18
Total	100.28	100.89	99.90	99.45	100.30	99.87	99.60

Table 4.3 - continued

	15	16	17	18	19	20	21
SiO_2	27.34	27.00	27.29	27.05	26.98	26.96	27.35
TiO_2	17.02	16.69	16.84	16.94	16.86	16.86	16.84
ZrO_2	1.03	0.97	0.85	0.96	0.95	0.91	1.18
Al_2O_3	1.50	1.42	1.43	1.42	1.47	1.41	1.46
Fe_2O_3*	20.69	20.67	20.73	20.24	20.56	20.61	20.62
MnO	0.44	0.42	0.37	0.35	0.38	0.47	0.49
MgO	1.04	1.12	1.14	1.10	1.06	1.11	1.08
CaO	31.29	31.56	31.07	30.94	30.96	31.26	31.14
Na_2O	0.24	0.26	0.23	0.13	0.25	0.25	0.21
Total	100.59	100.11	99.95	99.13	99.47	99.84	100.37

	22	23	24	25	26	27	28
SiO_2	27.24	27.01	27.06	27.09	26.81	27.00	26.87
TiO_2	16.89	16.90	16.82	17.02	16.83	16.86	16.94
ZrO_2	0.72	1.02	1.14	1.09	1.00	0.92	1.00
Al_2O_3	1.48	1.51	1.45	1.39	1.38	1.37	1.45
Fe_2O_3*	20.26	20.60	20.21	20.31	20.52	20.52	20.73
MnO	0.46	0.46	0.47	0.44	0.45	0.44	0.45
MgO	1.15	1.14	1.08	1.17	1.13	1.08	1.11
CaO	31.21	31.24	31.44	30.80	30.59	31.11	31.48
Na_2O	0.23	0.22	0.25	0.25	0.24	0.21	0.23
Total	99.64	100.10	99.92	99.56	98.95	99.51	100.26

Table 4.3 - continued

	29	30	31	32	33
SiO_2	26.93	26.90	27.18	27.01	26.95
TiO_2	16.78	16.88	16.81	16.92	16.93
ZrO_2	1.01	0.74	0.92	0.99	0.85
Al_2O_3	1.47	1.39	1.41	1.38	1.49
Fe_2O_3*	20.59	20.61	20.48	20.18	20.29
MnO	0.44	0.46	0.40	0.39	0.49
MgO	1.06	1.14	1.18	1.08	1.14
CaO	31.41	31.31	31.09	31.20	31.51
Na_2O	0.18	0.25	0.22	0.18	0.23
Total	99.87	99.68	99.69	99.33	99.88

* total iron presented as ferric iron

Table 4.4 lists the chemical analysis and calculated cation proportions of the schorlomite. The chemical data presented include the mean results of the microprobe analyses, the minor elements (including vanadium) and trace elements measured by INAA, the ferrous iron content (the mean of 5 volumetric analyses) and the hydroxyl content (determined by FTIR, Figure 4.1). The one sigma standard deviations for the mean microprobe results and the mean volumetric ferrous iron content in Table 4.4 were calculated from the variations of the analyses. The standard deviations for the results of the other techniques were either derived from counting statistics and replicate analyses of standard materials (INAA), or estimated (FTIR).

The cation proportions of the major and minor elements, based on 12 oxygen atoms, were calculated assuming divalent manganese; vanadium was shown to be trivalent and titanium to be tetravalent by XANES (see below).

Table 4.4 Chemical analysis and cation proportions of schorlomite

oxide	wt %	std dev 1 σ	cation	atoms/ 12 O	std dev 1 σ	trace elements	ppm	std dev 1 σ
SiO_2	27.42	0.610	Si	2.348	0.0402	Sc	6.4	0.2
TiO_2	16.43	0.852	Ti	1.058	0.0463	Cr	7.3	1.2
ZrO_2	0.93	0.118	Zr	0.039	0.0049	Co	22.2	0.3
Al_2O_3	1.36	0.139	Al	0.137	0.0139	Zn	218	10
Fe_2O_3	15.05	0.546	Fe^{3+}	0.970	0.0333	Rb	25	5
FeO	5.14	0.033	Fe^{2+}	0.368	0.0055	Sr	130	28
V_2O_3	0.20	0.008	V	0.014	0.0006	Ba	247	12
MnO	0.44	0.040	Mn	0.032	0.0029	La	68	2
MgO	1.06	0.106	Mg	0.135	0.0135	Ce	321	8
CaO	31.24	0.274	Ca	2.866	0.0432	Nd	377	10
Na_2O	0.23	0.036	Na	0.038	0.0060	Sm	128	2
H_2O+	0.036	0.003	H_t	0.005	0.0004	Eu	58	1
Rem*	0.25		No. cations	8.010	0.0275	Tb	27.4	0.3
Total	99.79		$Fe^{3+}/\Sigma Fe$	0.725	0.031	Dy	139	7
						Yb	68	2
						Lu	8.8	0.5
						Hf	145	6
						Ta	71	1
						Th	31	1
						U	35	1.5

* Rem = Remainder, includes trace elements as oxides; lanthanides calculated as sesquioxides (R_2O_3)

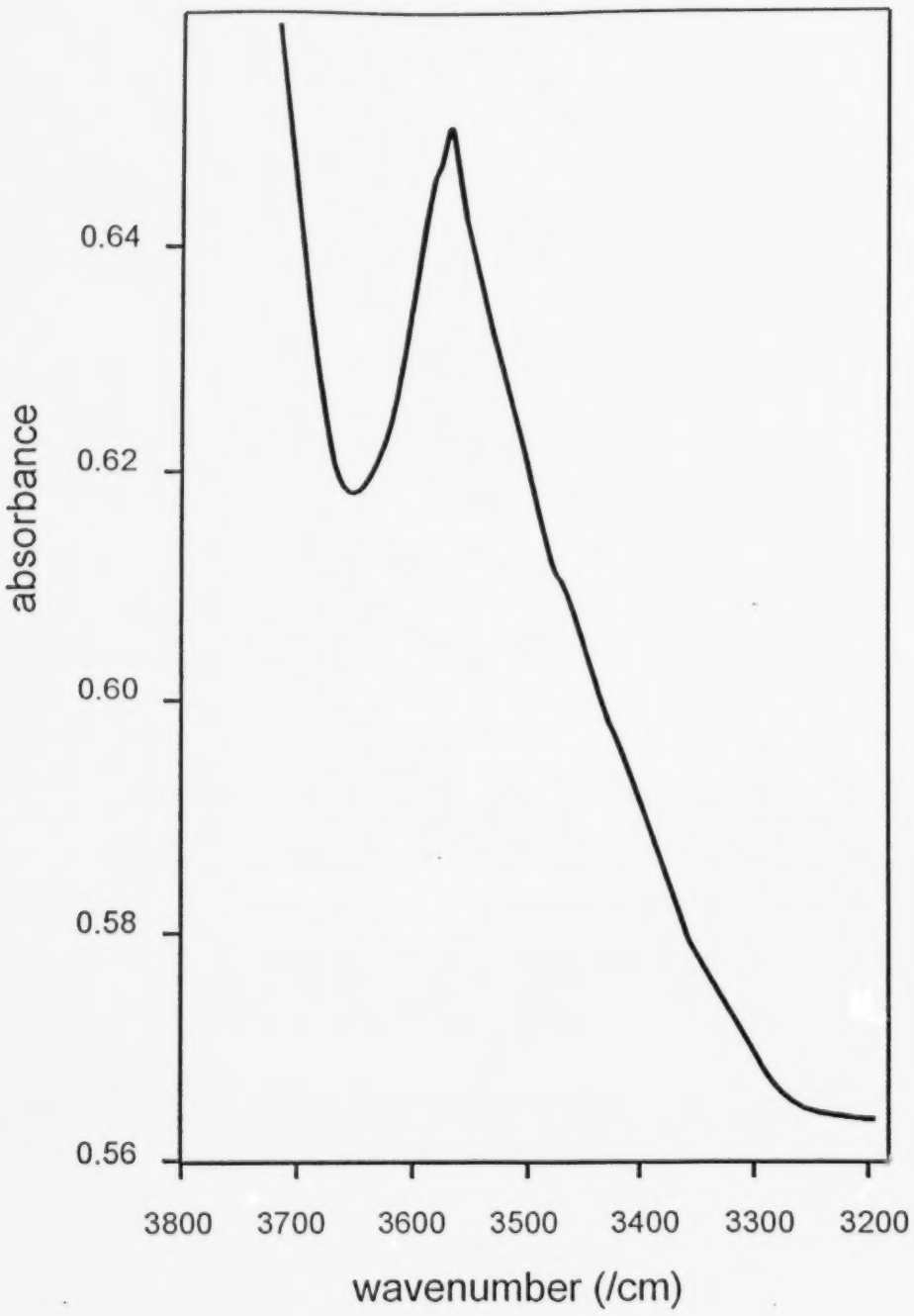

Figure 4.1 Unpolarized infrared absorption spectrum of hydroxyl in Ice River schorlomite, 85 μm thick, with strongest peak at 3564 cm^{-1}.

The trace elements were excluded as their contribution to the cation sum was calculated to be negligible. The ferrous iron content was taken from the corrected mean volumetric analysis and the ferric iron calculated by difference from the mean total iron as determined from the microprobe analyses. The hydroxyl content was assumed to occur in the tetrahedral hydrogarnet substitution (Lager *et al.*, 1989; Geiger *et al.*, 1991), although it is possible that the hydroxyl may substitute in all three cation sites (Rossman and Aines, 1991). Uncertainties in the cation proportions and sum were calculated by partial error propagation methods (Giaramita and Day, 1990). The cation sum agrees within error to the stoichiometric value of 8 cations per 12 oxygen atoms.

4.3.2 X-ray absorption near-edge spectroscopy

The element-specific technique of XANES provides information on valency, coordination, and site symmetry (Henderson *et al.*, 1993); however, current interpretation of XANES spectra is qualitative in nature (Brown and Parks, 1989). The similarity of XANES spectra for an unknown and a structurally well-characterized standard indicates that the absorber has the same coordination in both compounds (Brown and Parks, 1989).

The Ti XANES spectra shown in Figure 4.2 demonstrate the resemblance of the schorlomite spectrum to those of rutile and titanite. Analysis of the spectral features of these minerals (Table 4.5) shows them to be very similar to those reported previously for the same mineral species (Waychunas, 1987; Henderson *et al.*, 1993); these analogous spectra were interpreted as indicating the presence of octahedrally coordinated tetravalent titanium only. Consequently, the titanium in this specimen of schorlomite is considered to be present as octahedral Ti^{4+}. The fine structure observed in the titanium spectra at about 4999 eV (Figure 4.2) is due to a monochromator crystal artifact.

The energies of the absorption features of $^{[6]}Ti^{4+}$ in Ba_2TiO_4 and a natural diopside are presented in Table 4.5 along with the spectral features of

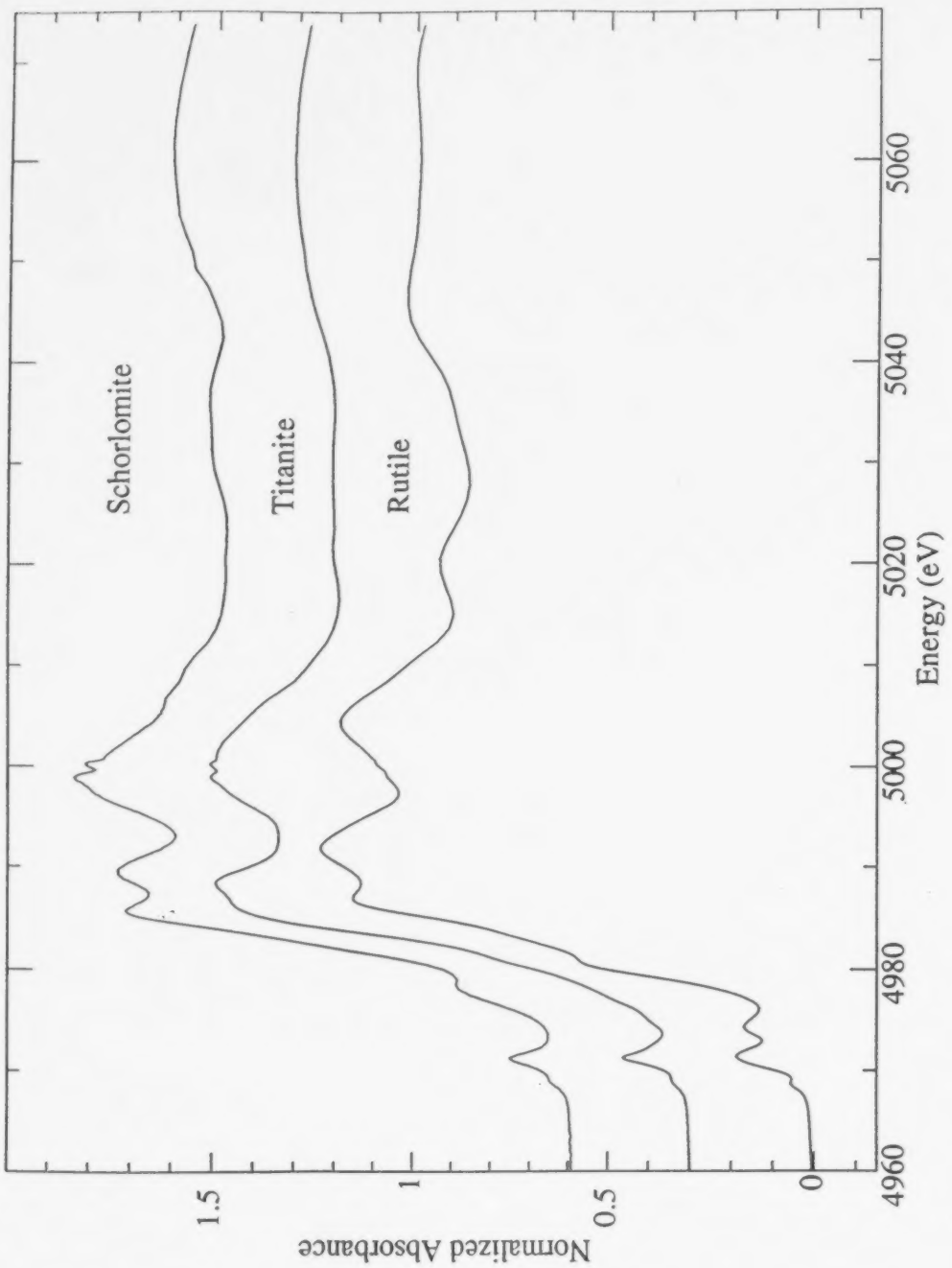

Figure 4.2 Background-subtracted Ti K-edge spectra for schorlomite, and the model compounds titanite ($^{[6]}Ti^{4+}$), and rutile ($^{[6]}Ti^{4+}$). Fine structure at about 4999 eV is a monochromator crystal artifact.

Table 4.5 Energies (eV) of Ti and V X-ray absorption features

Sample	Pre-edge features			Main-edge features		
	1	2	3	4	5	6
<u>Ti spectra</u>						
Titanite	4968.7	4971.2	*	4980.8	4984.5	4988.8
Rutile	4968.6	4971.4	4974.2	4980.3	4986.4	4991.9
Schorlomite	4968.6	4971.1	*	4978.0	4985.3	4989.5
Ba_2TiO_4**	*	4967.8	*	4974.0	4979.5	4983.8
Diopside†	*	4967.8	*	4976.8	4981.1	4989.8
αTi_2O_3**	*	4967.7	*	4976.0	*	4985.5
$NaTi^{3+}Si_2O_6$**	4966.1	4967.3	4969.1	4976.5	4981.9	4987.3
<u>V spectra</u>						
Vanadinite	5469.7			*	5490.0	
Descloizite	5469.7			5483.2	5491.1	
Cavansite	5469.3			5476.8	5485.6	
Roscoelite§	5467.6			5475.6	5486.5	
V_2O_3§	5468.4			5475.7	5488.5	
Schorlomite	*			5476.0	5485.7	

* feature too weak or ill-defined to be fitted
** from Waychunas (1987), values reported relative to the first inflection point of Fe foil (7111.2 eV)
† specimen D13 from Quartieri *et al.*, (1993)
§ from Wong *et al.*, (1984)

$NaTi^{3+}Si_2O_6$ and αTi_2O_3. Comparison of these spectral features to those of schorlomite indicates that neither $^{[4]}Ti^{4+}$ nor $^{[6]}Ti^{3+}$ are present in this schorlomite specimen.

The vanadium XANES spectra are shown in Figure 4.3, and their peak parameters listed in Table 4.5. The spectrum of schorlomite was obtained by fluorescence methods because of its low V concentration, and despite the relatively high noise level the signal was of sufficient quality to determine the coordination and oxidation state of the vanadium. The spectra of vanadinite and descloizite, which contain tetrahedral V^{5+} (Hawthorne and Faggiani, 1979; Dai and Hughes, 1989), are quite similar to each other (Wong *et al.*, 1984). The spectrum of cavansite, with V^{4+} in square-pyramidal coordination (Evans, 1973), corresponds well to spectra of other compounds containing V^{4+} in the same coordination (Wong *et al.*, 1984).

The schorlomite vanadium spectrum differs significantly from the above mentioned vanadium minerals, especially in the lack of a significant pre-edge peak. Instead, the schorlomite spectrum has similar peak energies (Table 4.5) to the spectra of roscoelite (V^{3+} mica) and V_2O_3 (corundum structure), both of which contain octahedrally coordinated V^{3+} (Wong *et al.*, 1984). The vanadium in this specimen of schorlomite is therefore considered to be present as V^{3+} in octahedral coordination.

4.3.3 Infrared spectroscopy

The infrared spectrum of the unheated doubly-polished wafer of schorlomite shows an intense, broad (FWHM about 1850 cm^{-1}) asymmetric absorption estimated to be composed of two overlapping peaks centered around 1900 nm and 2300 nm respectively (Figure 4.4). The heated wafer does not show any peaks in the same region. This band has been reported previously in schorlomite and titanian andradite specimens (Manning and Harris, 1970; Moore and White, 1971; Dowty, 1971; Huggins *et al.*, 1977b). The position and width of this band are similar to bands observed in the gamma polarized absorption spectrum of staurolite (Burns, 1970) and in the Apollo 17 spinel 70002,7 (Mao and Bell, 1975). The interpretation of these bands will be addressed below in the Discussion.

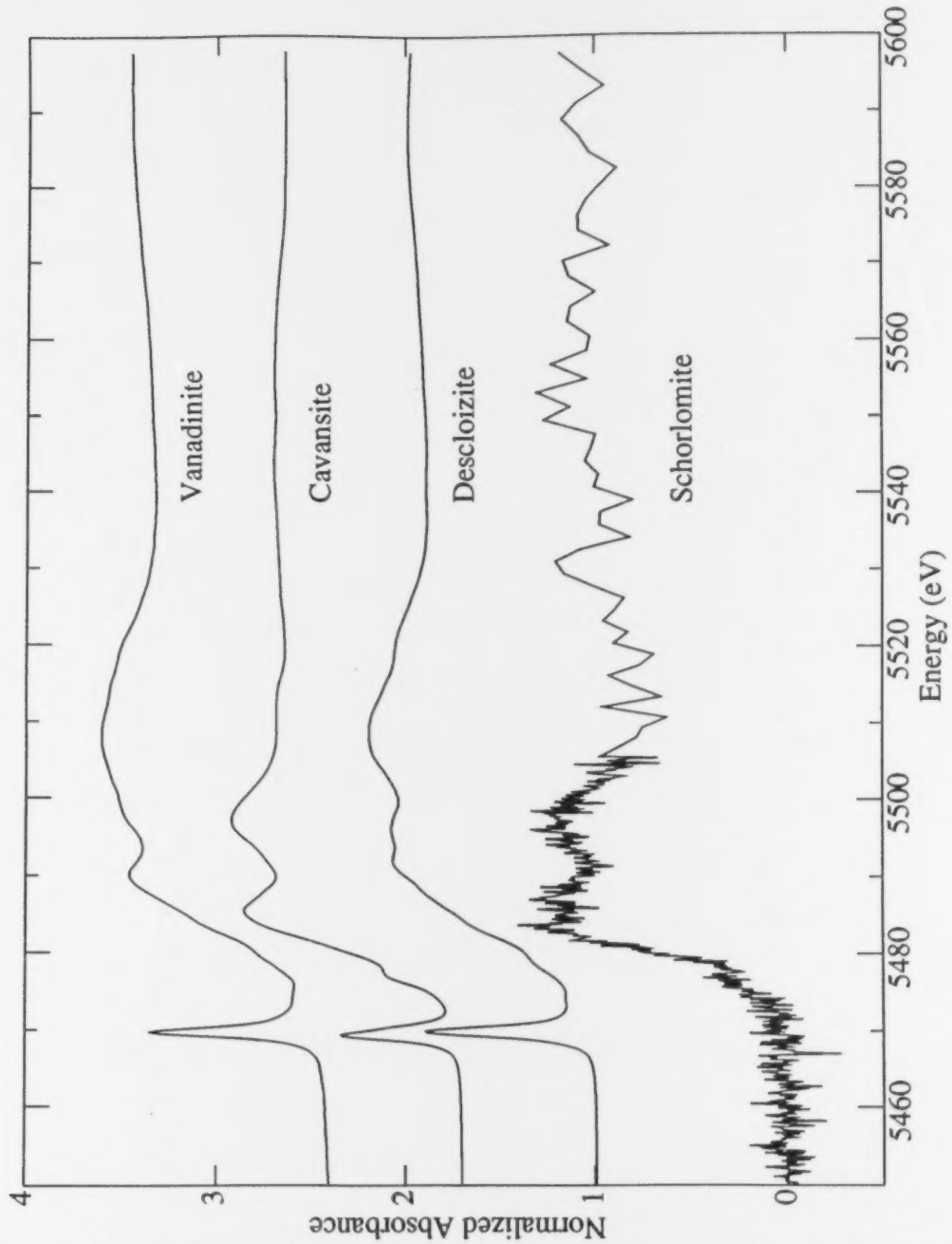

Figure 4.3 Background-subtracted V K-edge spectra for schorlomite, and the model compounds vanadinite ($^{[4]}V^{5+}$), descloizite ($^{[4]}V^{5+}$), and cavansite ($^{[5]}V^{4+}$). Only the schorlomite spectrum was obtained by fluorescence techniques.

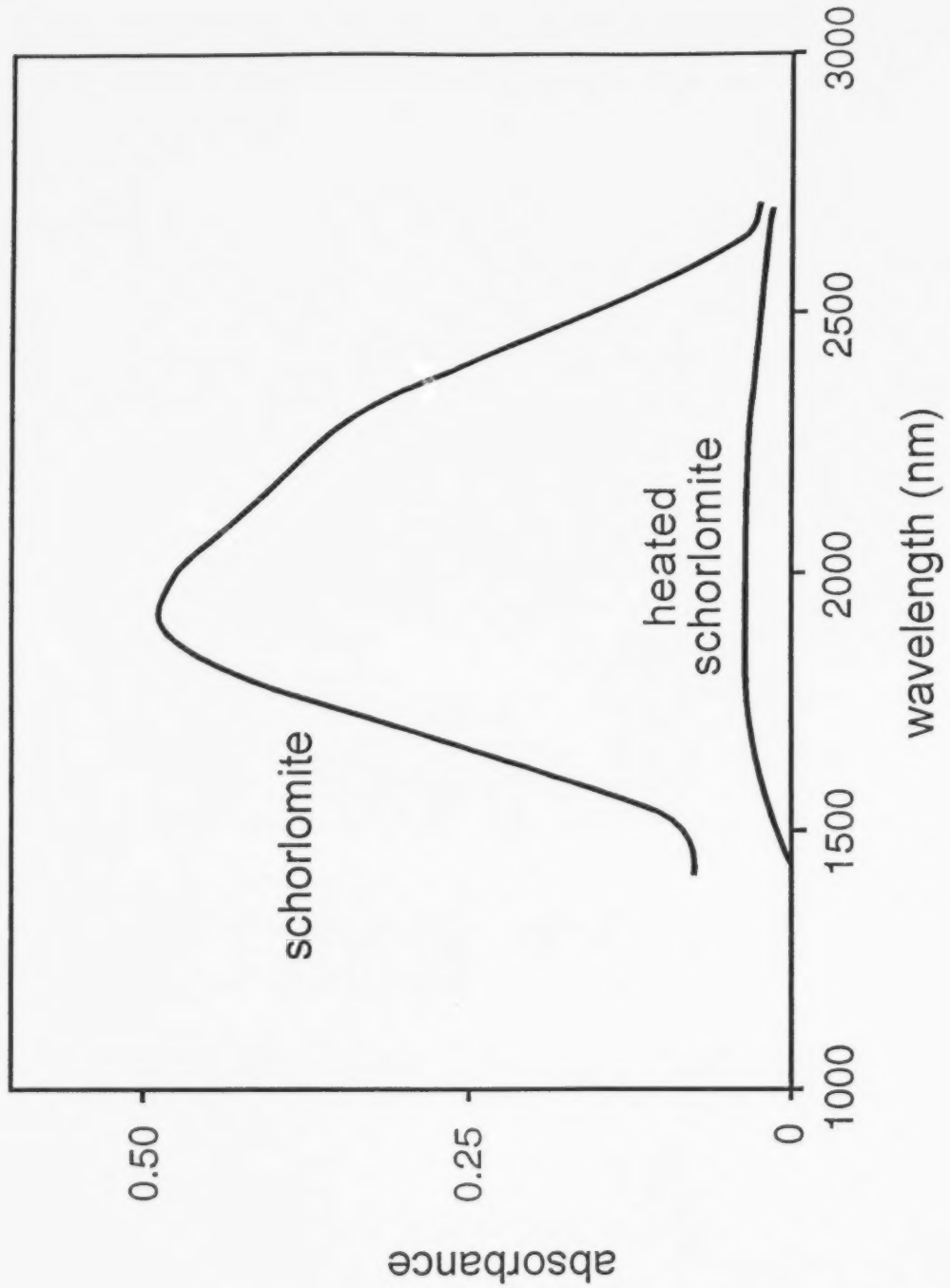

Figure 4.4 Unpolarized near-infrared absorption spectra of schorlomite, 30 μm thick, and heated schorlomite, 50 μm thick.

4.3.4 Mössbauer spectroscopy

Mössbauer spectroscopy was used to constrain the distribution of iron and thereby indirectly place limits on the positions of the other cations. Room temperature spectra were acquired for an unheated powder sample ground in air, an unheated powder sample ground in the presence of solid CO_2, and an unheated doubly polished single-crystal wafer. The three spectra were identical (a representative spectrum is shown in Figure 4.5). Ferrous iron doublets were poorly resolved on the room-temperature spectra. Therefore a spectrum was acquired at 80 K of the unheated powder. Low temperature spectra should be more accurate than 295 K spectra because the differences between the recoil-free fractions at the three non-equivalent sites in garnet decrease at lower temperatures, although the magnitude of the recoil-free fraction increases (Hawthorne, 1988; Kühberger *et al.*, 1989). Figure 4.6 shows the 80 K spectrum with valence and coordination assignments for the various peaks. A room temperature spectrum of the heated schorlomite powder was also acquired and is shown in Figure 4.7 with valence and coordination assignments (note that an undetermined proportion of the octahedral ferric iron should be assigned to ferric oxide resulting from the partial thermal decomposition of the schorlomite). The Mössbauer parameters for both spectra and for the 80 K spectrum of a titanian andradite from Oberrotweil, Germany (from Kühberger *et al.*, 1989) are listed in Table 4.6. The hyperfine parameters for the unheated Ice River schorlomite at low temperature are similar to those of the Oberrotweil titanian andradite. Note that the octahedral ferrous iron doublet is a minor contributor to the absorption envelope and therefore the position of the low-velocity peak is very poorly constrained. Of particular interest for the subsequent Discussion section is the interpretation of tetrahedral ferrous iron based upon the doublet with an isomer shift of 1.03 mm/s.

4.3.5 Optical spectroscopy

Figure 4.8 shows unpolarized optical absorption spectra for both the

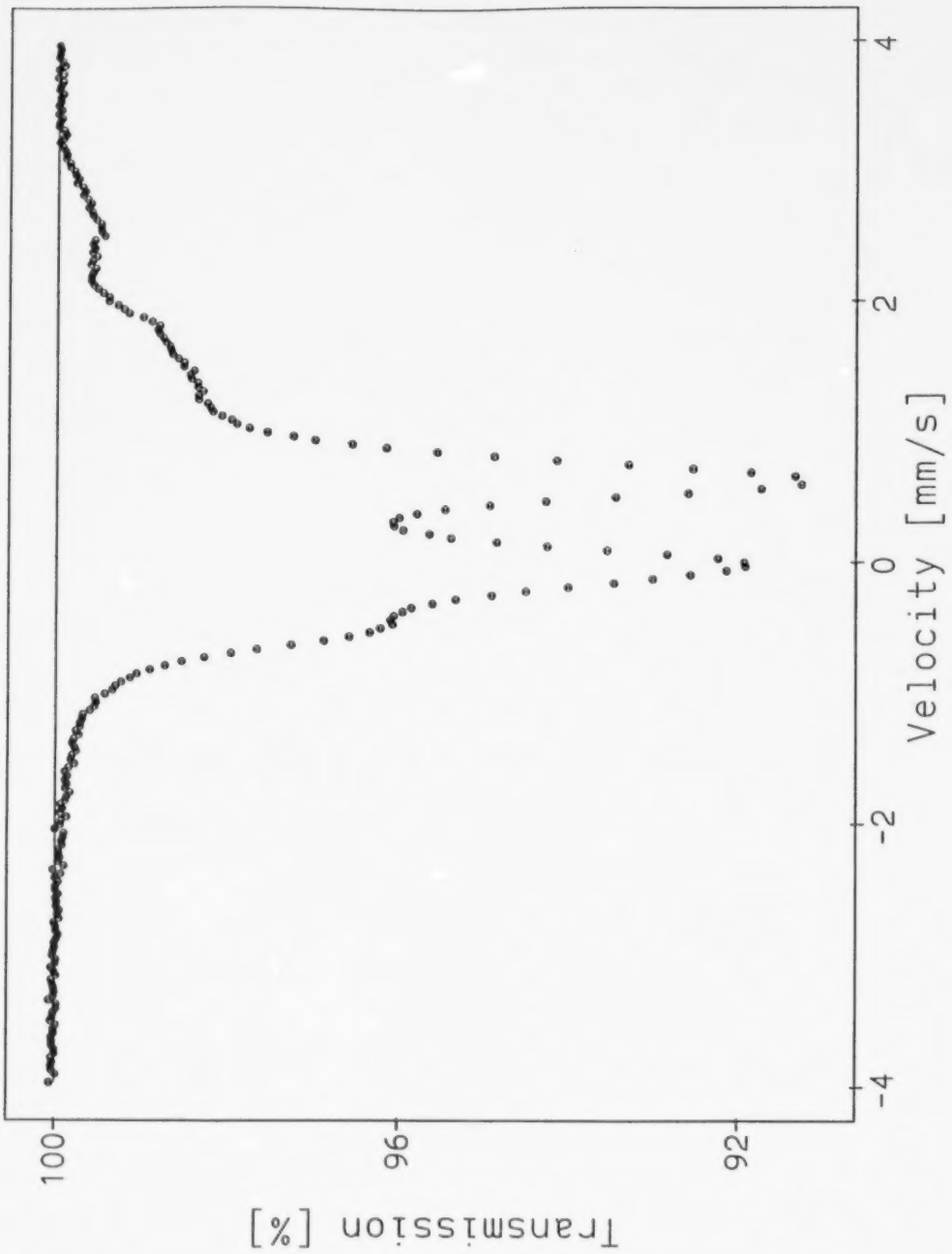

Figure 4.5 Mössbauer spectrum of ^{57}Fe in schorlomite, acquired at 295 K. The baseline is 1.35 x 10^7 counts. The size of the circles expresses the statistical uncertainty associated with each point. The velocity is referenced to the Fe in Rh source; add 0.11 mm/s to correct to velocity relative to Fe metal.

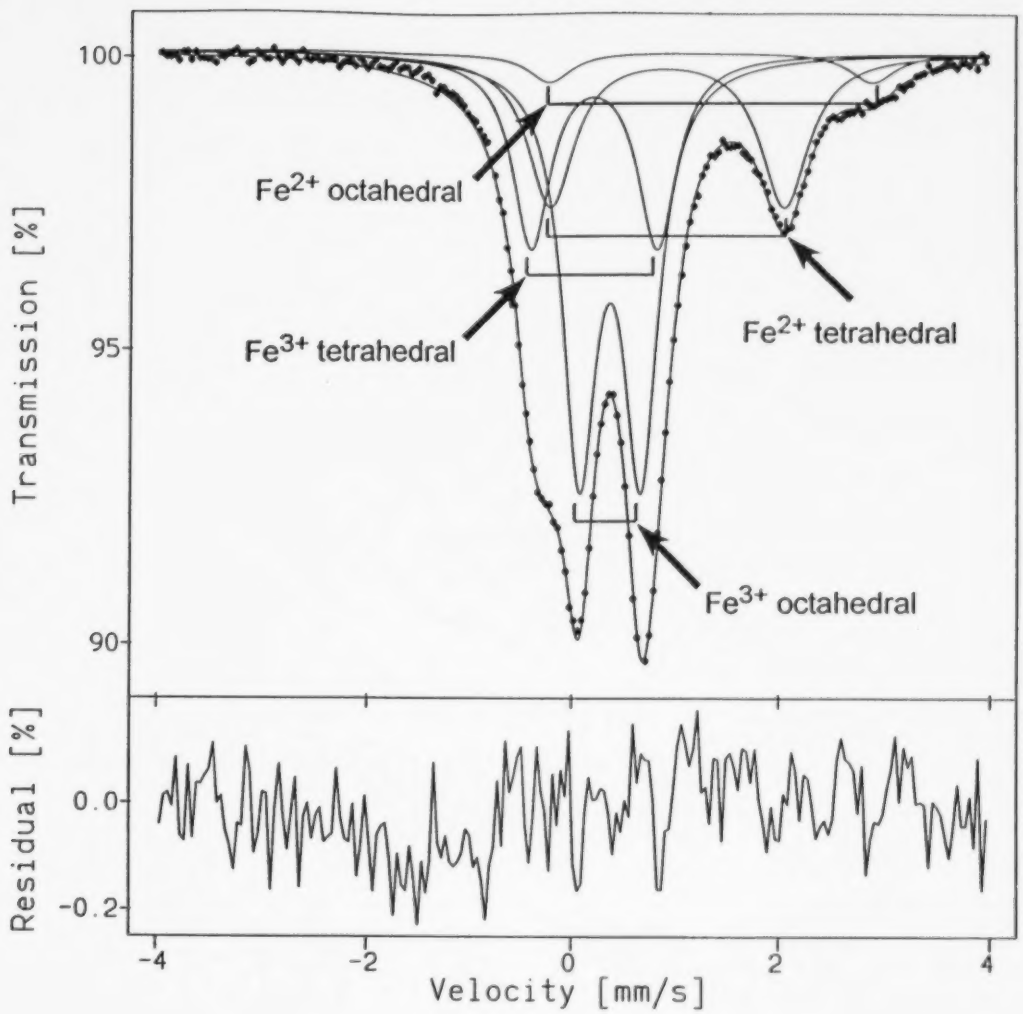

Figure 4.6 Mössbauer spectrum of ^{57}Fe in schorlomite, taken at 80 K. The baseline is 2.68 x 10^6 counts. The spectrum has been evaluated by four doublets. The velocity is referenced to the Fe in Rh source; add 0.11 mm/s to correct to velocity relative to Fe metal.

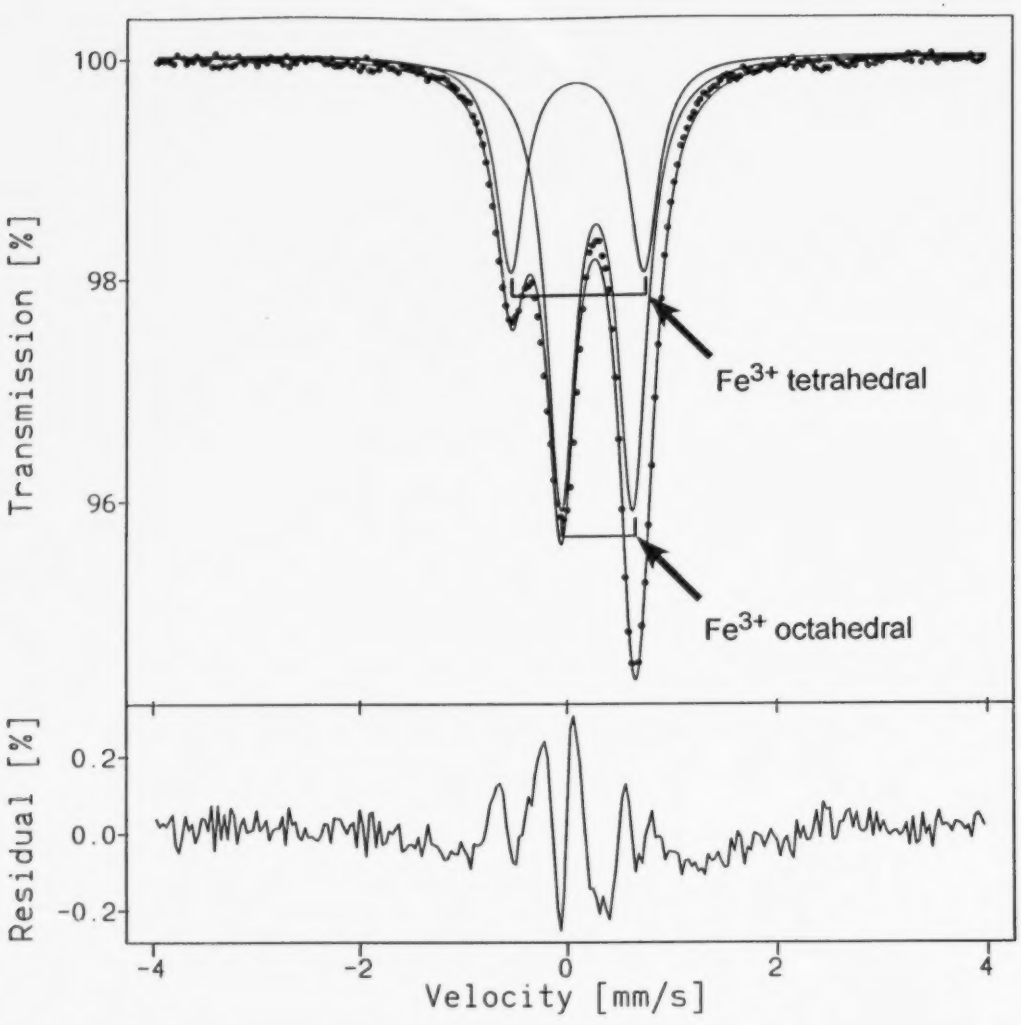

Figure 4.7 Mössbauer spectrum of ^{57}Fe in heated schorlomite, acquired at 295 K. The baseline is 1.52×10^7 counts. The spectrum has been evaluated by two doublets. The velocity is referenced to the Fe in Rh source; add 0.11 mm/s to correct to velocity relative to Fe metal.

Table 4.6 Mössbauer parameters of ^{57}Fe in schorlomite

Sample	T (K)	χ^2	Valence & Site	QS (mm/s)	IS (mm/s)	Width (mm/s)	Area (%)
BY1374M	80	1.78	Fe^{3+}tet	1.24	0.32	0.43	24.8
			Fe^{3+}oct	0.60	0.49	0.41	46.1
			Fe^{2+}tet	2.27	1.03	0.57	24.5
			Fe^{2+}oct	3.12	1.44	0.53	4.5
Oberrotweil	80	0.57	Fe^{3+}tet	1.28	0.37	0.43	21.9
			Fe^{3+}oct	0.64	0.51	0.38	61.3
			Fe^{2+}tet	2.11	1.03	0.48	8.6
			Fe^{2+}oct	3.26	1.22	0.33	4.7
			Fe^{2+}dod	3.64	1.39	0.24	3.4
UA066	295	8.17	Fe^{3+}tet	1.28	0.21	0.34	33.2
			Fe^{3+}oct	0.69	0.40	0.34	66.8

χ^2 per channel; QS = quadropole splitting; IS = isomer shift relative to Fe metal at 298 K; Width = full width at half maximum peak height; Area = fractional area beneath resonant envelope; BY1374M = unheated schorlomite powder; Oberrotweil = data from Kühberger *et al.* (1989); UA066 = schorlomite powder after heating at 1050°C for 600 h; tet = tetrahedral coordination; oct = octahedral coordination; dod = dodecahedral coordination.

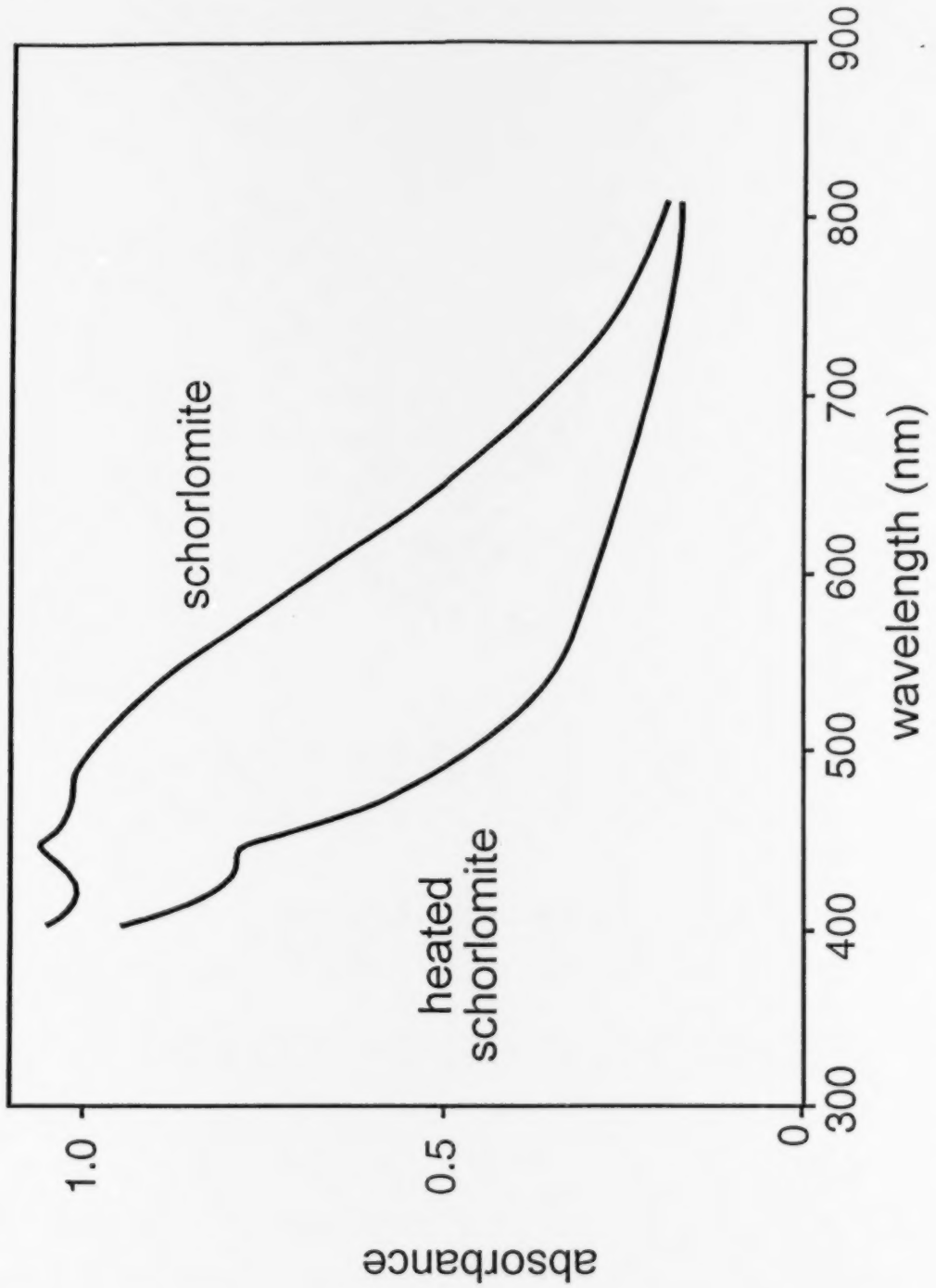

Figure 4.8 Unpolarized optical absorption spectra of schorlomite, 10 μm thick, and heated schorlomite, 50 μm thick.

unheated and heated schorlomite specimens. Both spectra show a narrow, strong peak at about 440 nm, interpreted to be the most intense of the spin-forbidden transitions of octahedral ferric iron, similar to that observed in the spectrum of andradite (Rossman, 1988). The unheated spectrum also has a very broad intense band (FWHM approximately 8000 cm^{-1}) centered at about 500 nm. Similar features have been described previously in titanian andradite and schorlomite (Manning and Harris, 1970; Moore and White, 1971; Dowty, 1971; Huggins *et al.*, 1977b). The width and position of this band resemble the Fe^{2+}-Ti^{4+} optically-activated intervalence charge transfer (IVCT) bands observed in neptunite, taramellite and traskite (Mattson and Rossman, 1988).

4.4 DISCUSSION

4.4.1 Tetrahedral ferrous iron

Tetrahedrally coordinated Fe^{2+}, although uncommon in minerals, is known to occur in members of the spinel group, and silicates such as staurolite and melilite (Kühberger *et al.*, 1989; Hawthorne *et al.*, 1993). In this study results from both infrared and Mössbauer spectroscopies are consistent with Fe^{2+} partially occupying the tetrahedral site in schorlomite.

The absence of the near-infrared band in the heated specimen of schorlomite (Figure 4.4), implies that the band is related to the presence of a reduced species that was oxidised during the heat treatment. The width of the band (~1850 cm^{-1}) is within the typical range of crystal-field transitions (Smith, 1978; Langer, 1988). It closely resembles, in position and width, the near-infrared bands interpreted to represent tetrahedral Fe^{2+} transitions, observed in staurolite and lunar spinel (Burns, 1970; Mao and Bell, 1975). Assignment of the band in schorlomite to dodecahedral Fe^{2+} - tetrahedral Fe^{3+} electron delocalization or charge transfer (Schwartz *et al.*, 1980; Platonov *et al.*, 1991) is inconsistent with its narrow width. Charge transfer transitions are characterized by their large halfwidths, generally > 4000 cm^{-1} (Mattson and Rossman, 1987a). The low-temperature behaviour of the band precludes its

interpretation as a regular crystal-field transition (Moore and White, 1971). The band increases in intensity and wavelength with decreasing temperature (Figure 4.3 of Moore and White, 1971), and has therefore been interpreted as a spin-allowed crystal-field transition of tetrahedral Fe^{2+}, intensified by coupling with adjacent Fe^{3+} (Smith, 1978). Similar intensified spin-allowed transitions of octahedrally coordinated Fe^{2+} have been recognized in Fe-Mg tourmalines, biotite, and partially oxidised vivianite (Smith, 1978; Mattson and Rossman, 1987b; Rossman, 1988). The theory behind the intensification of the Fe^{2+} transitions by coupling with Fe^{3+} is still being developed (Sherman, 1987a; Rossman, 1988). The asymmetry (splitting) of the infrared Fe^{2+} band in schorlomite is a result of the distorted nature of the four-ligand-coordinated site in the garnet structure, a tetragonal disphenoid, point group $\overline{4}$ (S_4 in Schoenflies notation), in comparison to the regular tetrahedron of spinel, point group $\overline{4}3m$ (T_d in Schoenflies notation) (Meagher, 1982; Jaffe, 1988; Rossman, 1988).

The Mössbauer spectra of Ti-rich andradite and schorlomite are more complex than most of the chemically simpler garnets (Hawthorne, 1988). In the Ti-rich garnets, the presence of ferric iron in both tetrahedral and octahedral coordination as well as octahedral ferrous iron, are well established. Dodecahedral ferrous iron may be absent depending on the chemistry of the particular specimen examined. However, the assignment of tetrahedral ferrous iron based on Mössbauer spectroscopy has caused considerable controversy. In accordance with the Mössbauer parameters determined (using constrained doublets) for titanian andradite by Kühberger *et al.* (1989), the peak with the quadropole splitting of 2.27 mm/s and isomer shift of 1.03 mm/s is assigned to tetrahedral ferrous iron (Table 4.6). This isomer shift is similar to the average value of 0.98 mm/s for ferrous iron observed in the three tetrahedral subsites of staurolite (Dyar *et al.*, 1991). The large temperature dependence of the quadropole splitting of this peak in schorlomite (-0.0024 mm/(sK) in this study, -0.0017 mm/(sK) Amthauer *et al.*, 1977; Kühberger *et al.*, 1989), has been

interpreted as evidence for electron delocalization (thermally activated charge transfer), instead of tetrahedral ferrous iron (Schwartz *et al.*, 1980; Yupu and Ruiying, 1985; Wu and Mu, 1986). The lack of anomalous Mössbauer parameters indicates that no electron delocalization is taking place (Amthauer *et al.*, 1977; Hawthorne, 1988; Kühberger *et al.*, 1989). For Fe^{2+}-Fe^{3+} electron delocalization to occur, the iron sites would have to form punctuated chains, sheets, or networks (Sherman, 1987a). This requirement is not met by the garnet structure. In addition, high-spin Fe^{2+} is expected to show temperature-dependent quadropole splitting, due to its electronic state in the distorted tetrahedral site of the garnet structure (Amthauer *et al.*, 1977; Hawthorne, 1988).

4.4.2 Site occupancies

With the constraints provided by XANES, Mössbauer and near-infrared spectroscopies, the distribution of cation species (assuming no vacancies) between the three sites in schorlomite may be calculated (Table 4.7). In accordance with the usual crystal chemistry of the garnet structure, all of the Ca and Na are allocated to the dodecahedral site. No dodecahedral ferrous iron was observed with low temperature Mössbauer spectroscopy, therefore the remainder of the dodecahedral site is filled with Mg and Mn. However, more Mn and Mg are present than are required to fill the dodecahedral site. The excess should occur in octahedral coordination by analogy with the isostructural berzeliite-manganberzeliite series: $\{Ca,Na\}_3[Mg,Mn]_2(As)_3O_{12}$ - $\{Ca,Na\}_3[Mn,Mg]_2(As)_3O_{12}$. The ratio of Mn to Mg is assumed to be the same in the dodecahedral and octahedral sites in Ice River schorlomite because the partitioning behaviour of either element between the two sites is uncertain. The evidence from XANES indicates that all of the titanium is tetravalent, the vanadium trivalent, and that both are in octahedral coordination. Zirconium is assigned to the octahedral site as in the kimzeyite species of garnet $\{Ca\}_3[Zr,Ti]_2(Si,Al,Fe^{3+})_3O_{12}$. The ferrous iron (from the corrected mean

Table 4.7 Cation distribution of Ice River schorlomite

cation	atoms/12 O	crystallographic site		
		dodecahedral	octahedral	tetrahedral
Si	2.348			2.348
Ti	1.058		1.058	
Zr	0.039		0.039	
Al	0.137		0.137	
Fe^{3+}	0.970		0.631	0.339
Fe^{2+}	0.368		0.057	0.311
V^{3+}	0.014		0.014	
Mn	0.032	0.019	0.013	
Mg	0.135	0.080	0.055	
Ca	2.866	2.866		
Na	0.038	0.038		
H_4	0.005			0.005
Total	8.010	3.003	2.004	3.003

volumetric analysis) and the ferric iron are distributed between the octahedral and tetrahedral sites on the basis of the 80 K Mössbauer results. All of the aluminum must be assigned to the octahedral site in order to fill it. The tetrahedral site is occupied by silicon, the ferric and ferrous iron allocated on the basis of Mössbauer spectroscopy, and hydrogen (assumed to occur as hydroxyl in the hydrogarnet substitution). Neither aluminum nor titanium are required to fill the tetrahedral site. The presence of substantial tetrahedrally coordinated iron (both Fe^{3+} and Fe^{2+}) may give rise to an additional distinct tetrahedral site in the garnet structure, an iron-oxygen tetrahedron as well as the silicon-oxygen tetrahedron (unpublished single-crystal structure refinement, Peterson, 1994). The order of occupancy for the tetrahedral site (after Si, and ignoring hydroxyl) based on the above data is $Fe^{3+} > Fe^{2+} >> (Al,Ti)$ in

contrast to the assignments made by Huggins *et al.*, (1977a): Al $\geq$ Fe > Ti, and Schwartz *et al.*, (1980): Fe^{3+} > (Al,Ti^{4+}). This sequence may be influenced by the bulk chemical composition of the individual specimens examined.

Unlike other chemical variations within natural garnets, no single substitution can account for the presence of tetravalent cations (Ti,Zr) in the octahedral site of schorlomite because of their high concentrations. Given the cation distribution from Table 4.7 and assuming that the andradite-schorlomite series contains the cation components Na^{+},Ca^{2+},Fe^{2+},Fe^{3+},Ti^{4+},Si^{4+} (homovalent cations can be treated as one of the above, i.e. Al^{3+} instead of Fe^{3+}) the following coupled substitutions may be written: $^{[8]}Na+{}^{[6]}Ti \rightleftharpoons {}^{[8]}Ca+{}^{[6]}Fe^{3+}$; $^{[6]}Ti+{}^{[6]}Fe^{2+} \rightleftharpoons {}^{[6]}Fe^{3+}{}_{2}$; $^{[6]}Ti+{}^{[4]}Fe^{3+} \rightleftharpoons {}^{[6]}Fe^{3+}+{}^{[4]}Si$; $^{[6]}Ti_{2}+{}^{[4]}Fe^{2+} \rightleftharpoons {}^{[6]}Fe^{3+}{}_{2}+{}^{[4]}Si$.

Schorlomite has often been thought to contain Ti^{3+}. Previous workers have used two methods to calculate the amount of trivalent titanium present. One method was to normalize the cation sum to exactly 8 cations per 12 oxygen atoms by adjusting the $Ti^{3+}/\Sigma Ti$ ratio (after the $Fe^{3+}/\Sigma Fe$ ratio had been determined). The other technique was to compare the $Fe^{3+}/\Sigma Fe$ ratio determined by titration with that measured by Mössbauer spectroscopy; the difference between these was taken to indicate the reducing presence of Ti^{3+} in the wet-chemical determination. Trivalent titanium is not required in the calculated cation distribution listed in Table 4.7. The cation sum agrees within 1 σ analytical uncertainty with the stoichiometric value of 8 cations per 12 oxygen atoms (Table 4.4). Consequently no Ti^{3+} can be calculated on the basis of charge balance considerations. The $Fe^{3+}/\Sigma Fe$ ratio from the mean corrected volumetric determination (0.725 $\pm$ 0.031) agrees within 1 σ error with that measured by 80 K Mössbauer spectroscopy (0.710 $\pm$ 0.008). This implies that the only reduced cations present are Fe^{2+} (and V^{3+}, as shown by XANES).

4.4.3 Intervalence charge transfer

Intervalence charge transfer (IVCT) transitions result from the movement of electron density from one metal cation to another that is in a

different oxidation state (Rossman, 1988). The cations interact with each other either by direct orbital-overlap across shared edges or faces of coordination polyhedra, or by metal-ligand-metal super-exchange across a shared corner (Sherman, 1987a; Rossman, 1988; Hawthorne *et al.*, 1993). IVCT transitions are usually optically induced and give absorption bands in the visible and near-infrared regions (Sherman, 1987a). In some minerals with infinite octahedral chains containing Fe^{2+} and Fe^{3+}, Fe^{2+}-Fe^{3+} IVCT is thermally induced, and can be observed using Mössbauer spectroscopy (Sherman, 1987a; Hawthorne, 1988).

The wide (~8000 cm^{-1}) band centered at 500 nm in the optical absorption spectrum of schorlomite (Figure 4.8) can be assigned to Fe^{2+}-Ti^{4+} IVCT. This band has a sufficiently large width (Mattson and Rossman, 1987a) and is within the normal energy range of Fe^{2+}-Ti^{4+} charge transfer transitions (Sherman, 1987b; Mattson and Rossman, 1988; Platonov *et al.*, 1991).

In Ice River schorlomite, titanium is in octahedral coordination, the majority of the ferrous iron is assigned to the tetrahedral site and the remainder to the octahedral site; no dodecahedral ferrous iron is present (Table 4.7). Therefore, Fe^{2+}-Ti^{4+} charge transfer must take place by metal-ligand-metal super-exchange across the shared corner between tetrahedral Fe^{2+} and octahedral Ti^{4+}. The octahedra in the garnet structure do not share any common ligands, obviating any possibility of charge transfer between them.

Most Fe^{2+}-Ti^{4+} charge transfer transitions in silicate minerals take place across shared polyhedral edges or faces. The mineral traskite, however, has been described as exhibiting Fe^{2+}-Ti^{4+} IVCT, and the Fe and Ti in its structure share only corners in 3/4 of its octahedra (Mattson and Rossman, 1988).

Fe^{2+}-Ti^{4+} charge transfer has been described in pyrope-grossular-almandine garnets from mantle eclogites (Platonov *et al.*, 1991; Langer *et al.*, 1993). Unlike the schorlomite discussed in this paper, the mantle garnets show a broad band (~7000 cm^{-1}) centered between 425 and 465 nm. The ferrous iron in these garnets is entirely in dodecahedral coordination (based on

Mössbauer spectroscopy), and the titanium assumed to be in octahedral coordination as there is sufficient silicon to fill the tetrahedral site. Therefore, the Fe^{2+}-Ti^{4+} charge transfer takes place across the shared edge between dodecahedral ferrous iron and octahedral titanium. The difference in energy (wavelength) between the transition in schorlomite and the transitions in the mantle garnets can be attributed to the different crystallographic sites occupied by the Fe^{2+}. According to Sherman (1987a), when cations occupy crystallographically dissimilar sites they experience different electrostatic potentials and these potential energies affect the energy of the IVCT.

Despite the presence of substantial ferric and ferrous iron in both the octahedral and tetrahedral sites of schorlomite, no evidence of Fe^{2+}-Fe^{3+} IVCT was observed by optical absorption spectroscopy (Table 4.7, Figure 4.8). It is probable that the Fe^{2+}-Fe^{3+} IVCT is buried in the optical spectrum beneath the more intense Fe^{2+}-Ti^{4+} IVCT.

4.5 CONCLUSIONS

1. Titanium in schorlomite occurs only in the octahedral site and is exclusively tetravalent.
2. There is substantial tetrahedrally coordinated ferrous iron in schorlomite (more than 10% of the tetrahedral site in the Ice River specimen).
3. The order of the preference for the tetrahedral site is:

   $Si > Fe^{3+} > Fe^{2+} >> (Al,Ti)$.
4. A general formula for schorlomite may be written as:

   $\{Ca\}_3[Ti^{4+},Fe^{3+}]_2(Si,Fe^{3+},Fe^{2+})_3O_{12}$.
5. The red-brown color of schorlomite is a result of an intense optically-activated Fe^{2+}-Ti^{4+} intervalence charge transfer between tetrahedrally coordinated ferrous iron and octahedrally coordinated titanium.

4.6 REFERENCES CITED

Amthauer, G., Annersten, H., and Hafner, S.S. (1977) The Mössbauer spectrum of ^{57}Fe in titanium-bearing andradites. Physics and Chemistry of Minerals, 1, 399-413.

Appleman, D.E., and Evans, H.T., Jr., (1973) Job 9214: Indexing and least-squares refinement of powder diffraction data. U.S. Geological Survey, Computer Contribution 20, U.S. National Technical Information Service, Document PB2-16188.

Bancroft, G.M. (1973) Mössbauer Spectroscopy: An introduction for inorganic chemistry and geochemists, 252 p. Wiley, New York.

Basso, R., Giusta A.D., and Zefiro, L. (1981) A crystal chemical study of a Ti-containing hydrogarnet. Neues Jahrbuch für Mineralogie Monatshefte, 5, 230-236.

Benoit, P.H. (1987) Adaptation to microcomputer of the Appleman-Evans program for indexing and least-squares refinement of powder-diffraction data for unit-cell dimensions. American Mineralogist, 72, 1018-1019.

Bergerioux, C., Kennedy, G., and Zikovsky, L. (1979) Use of the semi-absolute method in neutron activation analysis. Journal of Radioanalytical Chemistry, 50, 229.

Brown, G.E., Jr., and Parks, G.A. (1989) Synchrotron-based X-ray absorption studies of cation environments in earth materials. Reviews of Geophysics, 27, 519-533.

Burns, R.G. (1970) Mineralogical applications of crystal field theory, 224 p. Cambridge University Press, Cambridge.

Dai, Y., and Hughes, J.M. (1989) Crystal-structure refinements of vanadinite and pyromorphite. Canadian Mineralogist, 27, 189-192.

Deer, W.A., Howie, R.A., and Zussman, J. (1982) Andradite. In Rock-forming minerals, volume 1A: Orthosilicates (2nd edition), p. 617-641. Longman, London and New York.

de Groot, F.M.F., Figueiredo, M.O., Basto, M.J., Abbate, M., Petersen, H., and Fuggle, J.C. (1992) $2p$ X-ray absorption of titanium in minerals. Physics and Chemistry of Minerals, 19, 140-147.

Dingwell, D.B., and Brearley, M. (1985) Mineral chemistry of igneous melanite garnets from analcite-bearing volcanic rocks, Alberta, Canada. Contributions to Mineralogy and Petrology, 90, 29-35.

Dowty, E. (1971) Crystal chemistry of titanian and zirconian garnet: I. Review and spectral studies. American Mineralogist, 56, 1983-2009.

Dyar, M.D., Perry, C.L., Rebbert, C.R., Dutrow, B.L., Holdaway, M.J., and Lang, H.M. (1991) Mössbauer spectroscopy of synthetic and naturally occurring staurolite. American Mineralogist, 76, 27-41.

Evans, H.T., Jr., (1973) The crystal structures of cavansite and pentagonite. American Mineralogist, 58, 412-424.

Geiger, C.A., Langer, K., Bell, D.R., Rossman, G.R., and Winkler, B. (1991) The hydroxide component in synthetic pyrope. American Mineralogist, 76, 49-59.

Giaramita, M.J., and Day, H.W. (1990) Error propagation in calculations of structural formulas. American Mineralogist, 75, 170-182.

Groves, A.W. (1937) Silicate Analysis, 230 p. Nordemann Publishing Company, Inc., New York, N.Y.

Hawthorne, F.C. (1981) Some systematics of the garnet structure. Journal of Solid State Chemistry 37, 157-164.

———— (1988) Mössbauer Spectroscopy. In Mineralogical Society of America Reviews in Mineralogy, 18, 255-340.

Hawthorne, F.C., and Faggiani, R. (1979) Refinement of the structure of descloizite. Acta Crystallographica, B35, 717-720.

Hawthorne, F.C., Ungaretti, L., Oberti, R., Caucia, F., and Callegari, A. (1993) The crystal chemistry of staurolite. 1. Crystal structure and site populations. Canadian Mineralogist, 31, 551-582.

Henderson, C.M.B., Charnock, J.M., Smith, J.V., and Greaves, G.N. (1993) X-ray absorption spectroscopy of Fe, Mn, Zn, and Ti structural environments in staurolite. American Mineralogist, 78, 477-485.

Hoffmann, G.C. (1902) Report of the Section of Chemistry and Mineralogy. Geological Survey of Canada Annual Report, Volume 12, 12R-13R.

Howie, R.A., and Woolley, A.R. (1968) The role of titanium and the effect of TiO_2 on the cell-size, refractive index, and specific gravity in the andradite-melanite-schorlomite series. Mineralogical Magazine, 36, 775-790.

Huggins, F.E., Virgo, D., and Huckenholz, H.G. (1977a) Titanium-containing silicate garnets. I. The distribution of Al, Fe^{3+}, and Ti^{4+} between octahedral and tetrahedral sites. American Mineralogist, 62, 475-490.

———— (1977b) Titanium-containing silicate garnets. II. The crystal chemistry of melanites and schorlomites. American Mineralogist, 62, 646-665.

Jaffe, H.W. (1988) Crystal Chemistry and Refractivity, 335 p. Cambridge University Press, Cambridge.

Koenig, G.A. (1886) On schorlomite as a variety of melanite. Proceedings of the Academy of Natural Sciences of Philadelphia, 355-357.

Koritnig, S., Rösch, H., Schneider, A., and Seifert, F. (1978) Der Titan-Zirkon-Granat aus den Kalksilikatfels-Einschlüssen des Gabbro im Radautal, Harz, Bundesrepublik Deutschland. Tschermaks Mineralogische und Petrographische Mitteilungen, 25, 305-313.

Kühberger, A., Fehr, T., Huckenholz, H.G., and Amthauer, G. (1989) Crystal chemistry of a natural schorlomite and Ti-andradites synthesized at different oxygen fugacities. Physics and Chemistry of Minerals, 16, 734-740.

Lager, G.A., Armbruster, T., Rotella, F.J., and Rossman, G.R. (1989) OH substitution in garnets: X-ray and neutron diffraction, infrared, and geometric-modeling studies. American Mineralogist, 74, 840-851.

Langer, K. (1988) UV to NIR spectra of silicate minerals obtained by microscope spectrometry and their use in mineral thermodynamics and kinetics. In E.K.H. Salje, Ed., Physical Properties and Thermodynamic Behaviour of Minerals, 639-650. D. Reidel Publishing Company, Boston.

Langer, K., Robarick, E., Sobolev, N.V., Shatsky, V.S., and Wang, W. (1993) Single-crystal spectra of garnets from diamondiferous high-pressure metamorphic rocks from Kazakhstan: indications for OH^-, H_2O, and $Fe^{2+}Ti^{4+}$ charge transfer. European Journal of Mineralogy, 5, 1091-1100.

Leigh, G. J., editor (1990) Nomenclature of Inorganic Chemistry, 289 p. International Union of Pure and Applied Chemistry, Blackwell Scientific Publications, London.

Lueck, B.A., and Russell, J.K. (1994) Phenocrystic and cumulate melanite garnet: substitution mechanisms and petrogenesis. Geological Association of Canada and Mineralogical Association of Canada Program with Abstracts, A67.

Lytle, F., Sandstrom, D.R., Marques, E.C., Wong, J., Spiro, C.L., Huffman, G.P., and Huggins, F.E. (1984) Measurement of soft X-ray absorption spectra with a fluorescent ion chamber detector. Nuclear Instrumental Methods, 226, 542-548.

Manning, P.G., and Harris, D.C. (1970) Optical-absorption and electron-microprobe studies of some high-Ti andradites. Canadian Mineralogist, 10, 260-271.

Mao, H.K., and Bell, P.M. (1975) Crystal-field effects in spinel: oxidation states of iron and chromium. Geochimica et Cosmochimica Acta, 39, 865-874.

Mattson, S.M., and Rossman, G.R. (1987a) Identifying characteristics of charge transfer transitions in minerals. Physics and Chemistry of Minerals, 14, 94-99.

———— (1987b) Fe^{2+}-Fe^{3+} Interactions in tourmaline. Physics and Chemistry of Minerals, 14, 163-171.

———————— (1988) Fe^{2+}-Ti^{4+} Charge transfer in stoichiometric Fe^{2+}, Ti^{4+}-minerals. Physics and Chemistry of Minerals, 16, 78-82.

Meagher, E.P. (1982) Silicate Garnets. In Mineralogical Society of America Reviews in Mineralogy, 5, (second edition), 25-66.

Moore, R.K., and White, W.B. (1971) Intervalence electron transfer effects in the spectra of the melanite garnets. American Mineralogist, 56, 826-840.

Onuki, H., Yoshida, T., and Nedachi, M. (1981) Electron probe study of Ti-rich hydroandradites in the Sanbagawa metamorphic rocks. Journal of the Japanese Association of Mineralogists, Petrologists and Economic Geologists, 76, 239-247.

Onuki, H., Akasaka, M., Yoshida, T., and Nedachi, M. (1982) Ti-rich hydroandradites from the Sanbagawa metamorphic rocks of the Shibukawa Area, Central Japan. Contributions to Mineralogy and Petrology, 80, 183-188.

Platonov, A.N., Langer, K., Matsuk, S.S., Taran, M.N., and Hu, X. (1991) Fe^{2+}-Ti^{4+} charge-transfer in garnets from mantle eclogites. European Journal of Mineralogy, 3, 19-26.

Quartieri, S., Antonioli, G., Artioli, G., and Lottici, P.P. (1993) XANES study of titanium coordination in natural diopsidic pyroxenes. European Journal of Mineralogy, 5, 1101-1109.

Rossman, G.R. (1988) Optical Spectroscopy. In Mineralogical Society of America Reviews in Mineralogy, 18, 207-254.

Rossman, G.R., and Aines, R.D. (1991) The hydrous components in garnets: Grossular-hydrogrossular. American Mineralogist, 76, 1153-1164.

Sawaki, T. (1988) Melanite and fassaite from the contact aureole around the Nogo-Hakusan granodiorite body, central Japan. Journal of Mineralogy, Petrology and Economic Geology, 83, 357-373.

Schwartz, K.B., Nolet, D.A., and Burns, R.G. (1980) Mössbauer spectroscopy and crystal chemistry of natural Fe-Ti garnets. American Mineralogist, 65, 142-153.

Sherman, D.M. (1987a) Molecular orbital (SCF-Xα-SW) theory of metal-metal charge transfer processes in minerals. I. Application to $Fe^{2+} \rightarrow Fe^{3+}$ charge transfer and "electron delocalization" in mixed-valence iron oxides and silicates. Physics and Chemistry of Minerals, 14, 355-363.

———————— (1987b) Molecular orbital (SCF-Xα-SW) theory of metal-metal charge transfer processes in minerals. II. Application to $Fe^{2+} \rightarrow Ti^{4+}$ charge transfer transitions in oxides and silicates. Physics and Chemistry of Minerals, 14, 364-367.

Smith, G. (1978) Evidence for absorption by exchange-coupled Fe^{2+}-Fe^{3+} pairs in the near infra-red spectra of minerals. Physics and Chemistry of Minerals, 3, 375-383.

Stevens, I.G., and Stevens, V.E. (1972) Mössbauer effect data index, covering the 1970 literature, 369 p. IFI/Plenum Data Corporation, New York.

Waychunas, G.A. (1987) Synchrotron radiation XANES spectroscopy of Ti in minerals: Effects of Ti bonding distances, Ti valence, and site geometry on absorption edge structure. American Mineralogist, 72, 89-101.

Wong, J., Lytle, R.W., Messmer, R.P., and Maylotte, D.H. (1984) *K*-edge absorption spectra of selected vanadium compounds. Physical Review B, 30, 5596-5610.

Wu, G., and Mu, B. (1986) The crystal chemistry and Mössbauer study of schorlomite. Physics and Chemistry of Minerals, 13, 198-205.

Yupu, T., and Ruiying, C. (1985) An anomalous Mössbauer spectrum of schorlomite. Scientia Sinica, 28, 202-209.

MANUSCRIPT RELEASE

Permission is hereby granted to Andrew John Locock to reproduce the manuscript *Spectroscopy of the cation distribution in the schorlomite species of garnet*, a version of which has been submitted for publication to *American Mineralogist*, the journal of the Mineralogical Society of America, in his thesis *Aspects of the geochemistry and mineralogy of the Ice River Alkaline Intrusive Complex, Yoho National Park, British Columbia.* This permission is subject to the conditions of the general University of Alberta Release Form for the entire thesis.

Co-authors:

Robert W. Luth _____ Date 18 Apr 94

Department of Geology, University of Alberta, Edmonton, Alberta, T6G 2E3

Ronald G. Cavell _____ Date 18/04/94

Department of Chemistry, University of Alberta, Edmonton, Alberta, T6G 2G2

Dorian G.W. Smith _____ Date 18/04/94

Department of Geology, University of Alberta, Edmonton, Alberta, T6G 2E3

M. John M. Duke _____ Date 18-APR-94

SLOWPOKE Reactor Facility, University of Alberta, Edmonton, Alberta, T6G 2N8

5. SUMMARY

The age of the Ice River complex has been determined using U-Pb isotopic methods to be 356 $\pm$ 6 Ma (constrained mainly by the concordant schorlomite). All of the rock-units are considered to be of the same age because minerals from different rock-units lie on the same discordia line.

The Rb-Sr, Sm-Nd, and Pb-Pb isotopic systems all gave scatterchrons (369 $\pm$ 17, 359 $\pm$ 197, 346 $\pm$ 52 respectively, uncertainties are $\pm 2\sigma$ * $MSWD^{1/2}$) whose slope ages overlap within error that determined using the U-Pb system. All of these systems are interpreted to be somewhat disturbed (cf. Parrish *et al.*, 1987). The Rb-Sr system is suspected to have been disturbed during the regional prehnite-pumpellyite facies metamorphism that occurred during Laramide orogenesis. Thermal effects (diffusion) and fluid alteration of the feldspars (Creaser, 1989) and feldspathoids could have partially remobilized Rb and Sr, resetting the Rb-Sr decay system. The Sm-Nd and Pb-Pb systems may have been disturbed by crustal contamination during the ascent of the magma from the mantle to the upper crust, and during the crystallization of the complex (Bell and Blenkinsop, 1989; Kwon *et al.*, 1989). Despite the scatter of the data, the initial Nd and Sr ratios, and the least radiogenic Pb data are consistent with the interpretation that the magma that formed the complex was derived from a mantle source (Bell and Blenkinsop, 1989; Kwon *et al.*, 1989). This mantle source had been depleted in large-ion lithophile elements (and U) for a long time prior to the extraction of the parental magma of the complex (Fitton and Upton, 1987).

The Ice River complex is temporally associated with a suite of Devonian-Mississippian alkaline complexes, carbonatites, and ultramafic diatremes dispersed along the length of the Rocky Mountain thrust and fold belt and the Omineca crystalline belt (Pell, 1987; Pell and Höy, 1989). This suite is interpreted as having originated as a result of relaxation, extension and crustal rifting following the cessation of the compressive regime induced by a mid-late Devonian orogeny to the west (Pell and Höy, 1989; Pell and Hora, 1993).

It is postulated, on the basis of the broad similarity of the rare-earth element patterns of the different rock-units, that the Ice River complex evolved from a single miaskitic parental magma (derived from the mantle, see above). The feldspar-free cumulates were the first to crystallize (they are cross-cut by both carbonatite and nepheline syenite dykes) from the carbonate-bearing magma, forming layered sequences of clinopyroxenite, melteigite, ijolite, pargasite ijolite, melanite ijolite, urtite and wollastonite urtite (Currie, 1975). Primary calcite is a characteristic accessory in these cumulates, and its presence is consistent with the close association of the cumulates and the later carbonatite that cross-cuts them. It is suggested that the remaining magma (relatively richer in alkalis, silica, and carbonate as a result of the removal of the ultramafic-mafic cumulates) split into two immiscible portions, a carbonatite magma, and a syenitic magma. This is consistent with the observation that rocks intermediate between the carbonatite, the cumulates and the feldspathoid syenites appear to be absent from the complex (Allan, 1914; Currie, 1975). The syenitic and carbonatite magmas evolved penecontemporaneously. The syenitic magma gave rise to a zoned syenite complex of miaskitic nepheline and sodalite syenites, with late peralkaline pegmatites. The fluid associated with the syenitic magma autometasomatically altered the syenites, producing late-stage seams and pockets and the zeolite syenite (Currie, 1975; Grice and Gault, 1981).

The crystal chemistry of schorlomite was examined early in the history of investigations into the Ice River complex (Hoffmann, 1902). The concordant schorlomite used in the U-Pb dating was investigated to determine the valence state(s) of iron and titanium and the crystallographic sites occupied by these elements. The results from X-ray absorption near-edge spectroscopy (XANES) are consistent with exclusively tetravalent titanium occupying the octahedral site only. The tetrahedral site is deficient in silicon and the results of low-temperature ^{57}Fe Mössbauer spectroscopy indicate that the remainder of the site is occupied by ferric iron and substantial ferrous iron. A spin-allowed

intensified crystal-field transition of tetrahedral ferrous iron is present in the near-infrared spectrum. The optical absorption spectrum is dominated by an intense band centered at 500 nm with a full width of 8000 cm^{-1} at half maximum peak height; this band is assigned to an Fe^{2+}-Ti^{4+} intervalence charge transfer transition between tetrahedral ferrous iron and octahedral titanium. The cation site occupancies in this specimen of schorlomite can be expressed by the following formula: $\{Ca_{2.866}Mg_{0.080}Na_{0.038}Mn_{0.019}\}_{\Sigma 3.003}$ $[Ti^{4+}_{1.058}Fe^{3+}_{0.631}Al_{0.137}Fe^{2+}_{0.057}Mg_{0.055}Zr_{0.039}V^{3+}_{0.014}Mn_{0.013}]_{\Sigma 2.004}$ $(Si_{2.348}Fe^{3+}_{0.339}Fe^{2+}_{0.311}[4H]_{0.005})_{\Sigma 3.003}O_{12}$

On the basis of these results for the Ice River schorlomite, the spectres of octahedrally-coordinated trivalent Ti or tetrahedrally-coordinated tetravalent Ti (e.g. Kühberger *et al.*, 1989) in garnet may be laid to rest.

5.1 REFERENCES CITED

Allan, J.A. (1914) Geology of Field Map-area, B.C. and Alberta. Memoir 55, 312 p. Geological Survey of Canada, Ottawa.

Bell, K., and Blenkinsop, J. (1989) Neodymium and strontium isotope geochemistry of carbonatites. In K. Bell, Ed., Carbonatites, Genesis and Evolution, p.278-300. Unwin Hyman, London.

Creaser, R.A. (1989) The geology and petrology of middle Proterozoic felsic magmatism of the Stuart Shelf, South Australia, 434 p. Ph.D. thesis, LaTrobe University, Bundoora, Victoria.

Currie, K.L. (1975) The Geology and Petrology of the Ice River Alkaline Complex, British Columbia. Bulletin 245, 68 p. Geological Survey of Canada, Ottawa.

Fitton, J.G., and Upton, B.G.J. (1987) Introduction. In J.G. Fitton & B.G.J. Upton, Eds., Alkaline Igneous Rocks. Blackwell Scientific Publications, London.

Grice, J.D., and Gault, R.A. (1981) Edingtonite and natrolite from Ice River, British Columbia. Mineralogical Record, July-August, 221-226.

Hoffmann, G.C. (1902) Report of the Section of Chemistry and Mineralogy. Geological Survey of Canada Annual Report, Volume 12, 12R-13R.

Kühberger, A., Fehr, T., Huckenholz, H.G., and Amthauer, G. (1989) Crystal chemistry of a natural schorlomite and Ti-andradites synthesized at different oxygen fugacities. Physics and Chemistry of Minerals, 16, 734-740.

Kwon, S.-T., Tilton, G.R., and Grünenfelder, M.H. (1989) Lead isotope relationships in carbonatites and alkalic complexes: an overview. In K. Bell, Ed., Carbonatites, Genesis and Evolution, p. 360-387. Unwin Hyman, London.

Parrish, R.R., Heinrich, S., and Archibald, D. (1987) Age of the Ice River complex, southeastern British Columbia. In Radiogenic Age and Isotopic Studies: Report 1, Geological Survey of Canada, Paper 87-2, 33-37.

Pell, J.A. (1987) Open File 1987-17 Alkaline ultrabasic rocks in British Columbia. Province of British Columbia, Ministry of Energy, Mines and Petroleum Resources, Mineral Resources Division, Geological Survey Branch.

Pell, J.A., and Hora, Z.D. (1993) Devonian carbonatites and related rocks in the Canadian Cordillera. Joint Annual Meeting of the Geological Association of Canada and Mineralogical Association of Canada Program and Abstracts, A82.

Pell, J.A., and Höy, T. (1989) Carbonatites in a continental margin environment - the Canadian Cordillera. In K. Bell, Ed., Carbonatites, Genesis and Evolution, p.200-220. Unwin Hyman, London.

APPENDIX 1: FERROUS IRON DETERMINATION

General Discussion

The finely powdered sample is decomposed in a mixture of sulfuric and hydrofluoric acids. Most iron-bearing minerals are decomposed by this process, forming soluble ferrous and ferric iron compounds. The resulting solution is eventually titrated with standardized potassium permanganate solution, which oxidizes the ferrous iron to ferric iron, but has no effect upon the ferric iron already present. The amount of ferrous iron is measured by the volume of standard potassium permanganate solution required to oxidize it. Any pyrite present will be unattacked in the decomposition. Pyrrhotite, however, will dissolve and its iron content will be included with the ferrous iron.

Preliminary Procedure

Prepare a litre of boiled distilled water, (the boiling removes dissolved oxygen). Rinse and fill a clean, calibrated, burette with standardized potassium permanganate solution.

Weigh out to the nearest 0.1 mg, 0.5 g of sample into a 35 mL platinum crucible which has a well-fitting cover. Moisten the powder with a little water. In another platinum crucible prepare a mixture of 5 mL concentrated sulfuric acid, 5 mL concentrated hydrofluoric acid, and 5 mL boiled water. Add the acid mixture to the sample and immediately replace the cover. Transfer the crucible to a hot plate and heat with a Bunsen burner flame until fuming. Continue to heat the mixture on a hot plate for 10 minutes keeping the contents simmering but not boiling violently.

Titration of Sample

While the crucible is heating, add 50 mL of saturated boric acid solution (a stock solution should be made up), 200 mL of boiled water, and 5 mL concentrated sulfuric acid to a special 600 mL beaker used only for this determination (the hydrofluoric acid etches the beaker). In the presence of

hydrofluoric acid, ferrous iron is extremely susceptible to oxidation by air. The boric acid neutralizes the hydrofluoric acid, stabilizing the ferrous iron.

When the time of heating is up, grasp the crucible around its center, using platinum tongs. Do not remove the cover, but hold it in place with the end of a glass stirring rod. Gently drop the crucible and cover into the beaker containing the boric acid. Titrate at once with standardized potassium permanganate solution from the burette (do not forget to take the initial reading of the burette), with thorough stirring, until a faint pink blush persists for several seconds in spite of stirring. Take the final burette reading. Given the volume of permanganate and its concentration, the amount of ferrous iron can be calculated.

Notes

Examine any residue in the beaker after the titration. A black residue may be undecomposed minerals containing ferrous iron. If the amount is appreciable, it is advisable to repeat the determination with a more finely-ground sample, and a longer period of heating. A white residue of undissolved quartz is common. Pyrite will remain as a brassy yellow residue. If the sample contained carbon or graphite, this will remain as a light black residue. Calcium fluoride may be precipitated by minerals rich in calcium; use more sulfuric acid in this case.

Potassium permanganate is a strong oxidizing agent and will oxidize not only ferrous iron but also other reduced cations. This effect can be corrected for if the amount of the other reduced cation(s) is (are) known independently. Trivalent vanadium may be taken as an example of this effect. If present the trivalent vanadium (as well as the ferrous iron) will consume permanganate ion following the reaction:

$$5\ V^{3+} + 2\ Mn^{7+}O_4^- + 2\ H_2O = 5\ V^{5+}O_2^+ + 2\ Mn^{2+} + 4\ H^+$$

and for ferrous iron:

$$5\ Fe^{2+} + Mn^{7+}O_4^- + 8\ H^+ = 5\ Fe^{3+} + Mn^{2+} + 4\ H_2O$$

Therefore, per mole present, trivalent vanadium consumes twice as much permanganate as ferrous iron. This leads to a correction (in terms of weight percent oxide) of the form:

$$FeO_{true} = FeO_{measured} - 1.9174 * V_2O_3$$

where the measured ferrous oxide is the uncorrected result from the titration, and the weight percent vanadium sesquioxide has been determined independently (by electron microprobe, neutron activation analysis, or some other method).

This technique of ferrous iron determination has been modified from the in-house procedures at the Department of Geology, University of Alberta, and pages 82-85 of:

Groves, A.W. (1937) Silicate Analysis, 230 p. Nordemann Publishing Company, New York, N.Y.

APPENDIX 2: SAMPLE ROCK-TYPES AND LOCATIONS

The identification code and rock-type of each rock sample analyzed in this thesis are tabulated below. The sample locations are plotted on a geological map (Figure A2.1) of the complex following this list. Specimens with the sample code "Ice xx" are designated by a solid square followed by their number. Similarly, specimens with the sample code "I90.xx" are indicated by an unfilled circle, and those with the modifier "I92.xx" are denoted by solid triangles. The sodalite syenite was not assigned an alphanumeric code and is indicated by an unfilled square.

Sample code	Rock-type
Ice 8	clinopyroxenite (titanite-rich)
Ice 22	pargasite ijolite
Ice 23	pegmatitic nepheline-sodalite syenite
Ice 35	nepheline syenite
Ice 38	wollastonite urtite
Ice 40	calcareous shale (Ottertail Formation)
I90.3	perovskite melteigite
I90.4	schorlomite megacryst from melteigite
I90.6	olivine hornblendite (phlogopite-rich)
I90.7	ijolite
I90.9	melanite ijolite
I90.13	calcite-carbonatite
I90.19	nephe'ine syenite
I92.8	clinopyroxenite (kaersutite-bearing)
I92.34	pegmatitic nepheline-sodalite syenite (andradite and fluorite-bearing)
I92.35*	nepheline syenite
I92.37*	eudialyte syenite
--	sodalite syenite

The two samples in this list marked with * were collected from sedimentary deposits in the floor of the valley outside of Yoho National Park. They are considered to have been derived from the Ice River complex on the basis of their physical proximity and mineralogic composition.

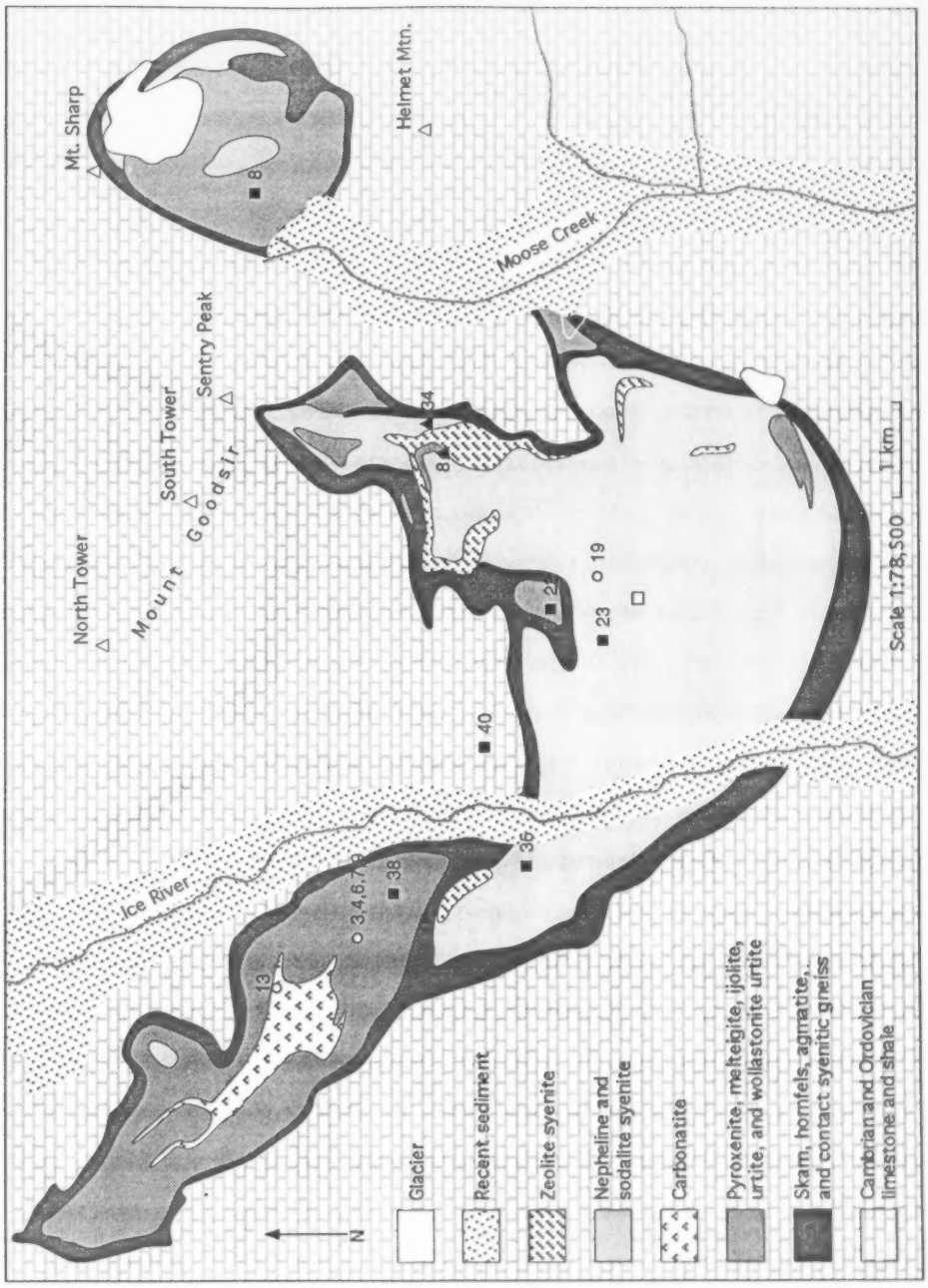

Figure A2.1 Geological map of the Ice River complex (after Currie, 1975). Symbols described in text above.

APPENDIX 3: INFORMATION FOR PARKS SERVICES

My mandate in this study, in addition to the imperatives to describe the age, origin, and mineralogy of the Ice River complex, included the condition that I advise the Parks Service as to the accessibility and preservation of the complex.

The Ice River complex, at the time of its discovery and first description, was one of the few (less than 100) known occurrences of alkaline rocks in the world (Woolley, 1987). The novelty and rarity of the rock-types exposed in the Ice River complex prompted the monumental study of Allan (1914). Presently, alkaline rocks have been described from over 2000 localities worldwide, including more than 300 carbonatites (Woolley, 1987). However, only two carbonatite-bearing alkaline complexes have been recognized in the Canadian Rocky Mountains, of which the Ice River complex is the largest, best described, and easiest to visit (Pell and Höy, 1989).

The rarity of the rocks that make up the Ice River complex will attract the occasional geologically-oriented visitor. However, a stronger motivation for some visitors is the range of unusual mineral species that may be found in the complex. The attractive cornflower-blue mineral sodalite is found in veins and talus throughout the complex. The Ice River complex is also the only accessible locality in Canada, and one of few in the world, for the rare barium-zeolite mineral edingtonite (Grice and Gault, 1981; Grice *et al.*, 1984). Large gem-quality natrolite crystals have been known from the complex since the early part of the century (Phillips, 1916), and the complex is well known to the lapidary community as a source of these crystals (Sinkankas, 1962). The edingtonite and natrolite crystals occur in the zeolite syenite. As can be seen on Figure A3.1, the majority (but not all) of the zeolite syenite is exposed outside of the boundaries of the national parks, and thus determining the provenance (and legality) of a given specimen is not possible. Unless the exposures of the Ice River complex currently outside of the park boundaries

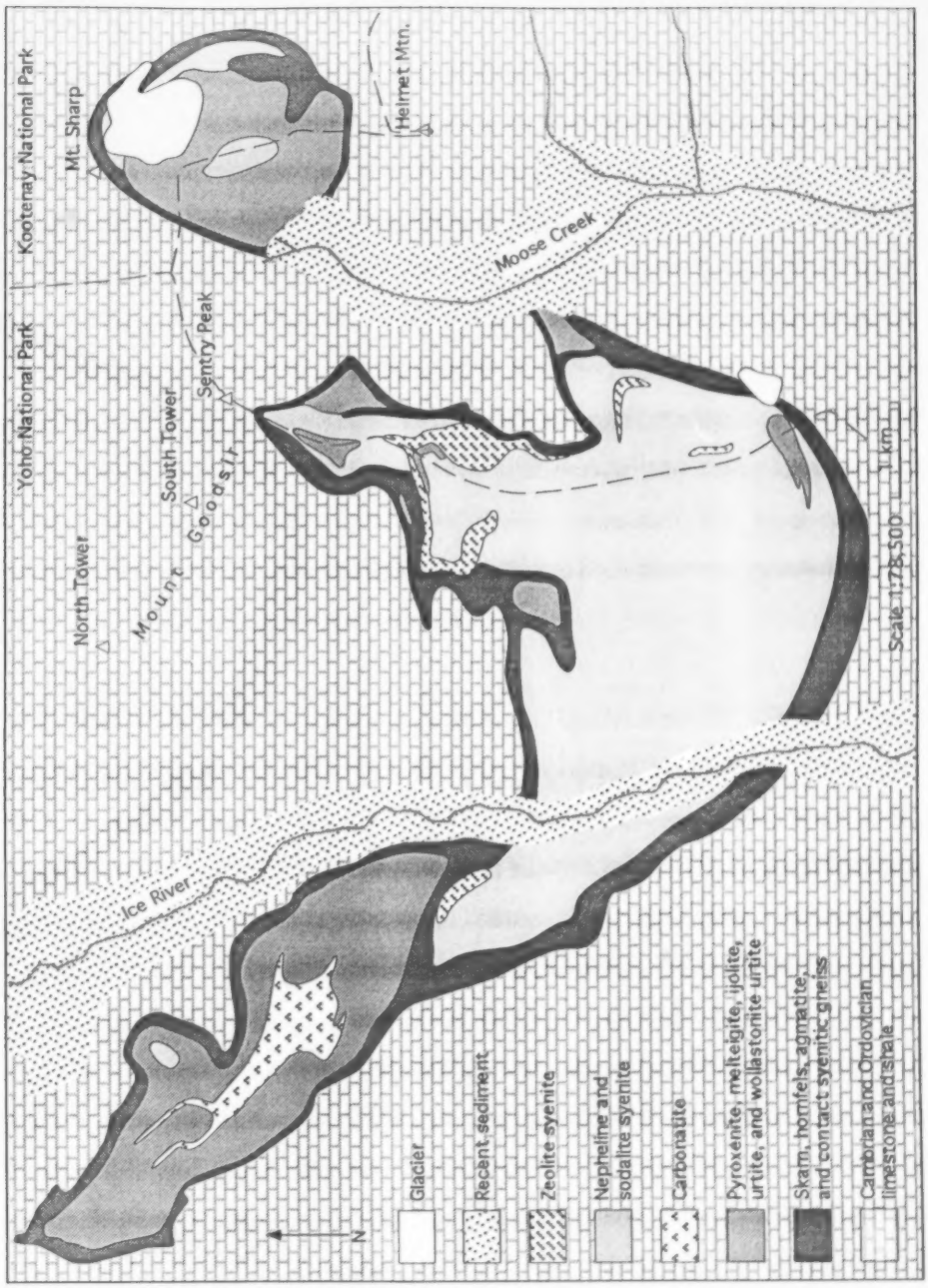

Figure A3.1 Geological map of the Ice River complex (after Currie, 1975), showing the boundaries of the national parks.

are incorporated into the parks, collection of material of dubious origin will always be a problem.

The Parks Service regulations require a permit for any rock-collecting in the national parks. The depredations of unscrupulous collectors are thought to be minute, however, in comparison to the major agent of destruction of the Ice River complex - erosion. Estimates of erosion rates in mountainous areas range from 10 mm/1000 years to 1000 mm/1000 years (Saunders and Young, 1983). Taking an intermediate erosion rate of 100 mm/1000 years, it may be calculated that the Ice River complex (29 km^2 in area, average density of 2.6 tonnes/m^3) loses **7500 tonnes every year**. Other sources of material loss from the area are therefore considered to be insignificant.

The Parks Service have been very helpful in the course of this research and I would like to thank them for their assistance, and for my free and easy access to the complex.

REFERENCES CITED

Allan, J.A. (1914) Geology of Field Map-area, B.C. and Alberta. Memoir 55, 312 p. Geological Survey of Canada, Ottawa.

Grice, J.D., and Gault, R.A. (1981) Edingtonite and natrolite from Ice River, British Columbia. Mineralogical Record, July-August, 221-226.

Grice, J.D., Gault, R.A., and Ansell, H.G. (1984) Edingtonite: the first two Canadian occurrences. Canadian Mineralogist, 22, 253-258.

Pell, J.A., and Höy, T. (1989) Carbonatites in a continental margin environment - the Canadian Cordillera. In K. Bell, Ed., Carbonatites, Genesis and Evolution, p. 200-220.

Phillips, A.H. (1916) Some new forms of natrolite. American Journal of Science, 42 (whole-number 192), 472-474.

Saunders, I., and Young, A. (1983) Rates of surface processes on slopes, slope retreat and denudation. Earth Surface Processes and Landforms, 8, 473-501.

Sinkankas, J. (1962) Gem Cutting, A Lapidary's Manual (2nd edition), p.269. Van Nostrand Reinhold, New York.

Woolley, A.R. (1987) Alkaline Rocks and Carbonatites of the World, Part I: North and South America, 216 p. British Museum of Natural History, London.

APPENDIX 4: PETROGRAPHIC DESCRIPTIONS

Ice 8 clinopyroxenite (titanite-rich)

80-90 diopside

3-7 hastingsite

3-5 titanite

3-5 nepheline

2-3 magnetite

Accessory perovskite, phlogopite, calcite, pyrrhotite, apatite, chlorite (alteration of diopside) and magnetite. This coarse-grained rock shows strong cumulus textures with nepheline and calcite as intercumulus phases.

Ice 22 pargasite ijolite

40-50 nepheline

20-30 pargasite

15-25 diopside

2-5 titanite

Accessories include apatite, zoisite (as microlites confined to the nepheline), calcite and cancrinite. This rock shows strong cumulus textures, with coarse pargasite, finer-grained diopside, and intercumulus nepheline.

Ice 23 pegmatitic nepheline-sodalite syenite

35-45 orthoclase microperthite

15-20 aegirine

10-15 nepheline

10-15 sodalite

10-15 cancrinite

3-4 magnetite

Accessory zircon, biotite, ilmenite, hematite and fluorite.

This coarse-grained rock has been deuterically altered.

Ice 35 nepheline syenite

40-50 orthoclase microperthite

20-30 nepheline

15-20 hastingsite

8-12 hedenbergite

2-5 sodalite

Accessory minerals include titanite, magnetite, melanite (titanian andradite) and cancrinite. This medium-grained rock has a poikilitic texture.

Ice 38 wollastonite urtite

68 nepheline

15 hedenbergite

10 wollastonite-1*A*

2.5 titanite

2 calcite

Accessory sodalite, cancrinite, biotite, pyrite, apatite, and pectolite (as 5 x 50 micron crystals with wollastonite).

Ice 40 calcareous shale (Ottertail Formation)

Extremely fine-grained mixture of quartz, calcite, feldspar.

190.3 perovskite melteigite

38 diopside

31 nepheline

6.5 perovskite

6 apatite

5 biotite

3.5 cancrinite

3 magnetite

3 pyrrhotite

Accessory calcite, titanite and schorlomite. This very coarse-grained rock shows cumulate textures with primary calcite, but cancrinite alteration of nepheline.

I90.4 schorlomite megacryst from melteigite

Opaque (at 30 microns thickness), 98% schorlomite, accessories include apatite, biotite, calcite, diopside, nepheline and pyrite.

I90.6 olivine hornblendite (phlogopite-rich)

40-50 hastingsite

20-30 olivine (chrysolite)

20-30 phlogopite

Accessories include apatite, magnetite, calcite, ilmenite, and diopside. The olivine occurs as highly rounded aggregates enclosed in anhedral hastingsite and phlogopite.

I90.7 ijolite

40-50 nepheline

35-45 diopside

3-5 biotite

2-3 titanite

Accessory minerals include calcite, apatite, pyrrhotite, magnetite, and cancrinite. This very coarse-grained rock shows cumulate textures with primary calcite, but cancrinite alteration of nepheline.

I90.9 melanite ijolite

35-45 diopside

35-45 nepheline

10-15 melanite (titanian andradite)

Accessories include calcite, apatite and cancrinite (from the alteration of the nepheline; the calcite is primary). The melanite occurs as euhedral crystals that are extremely heavily included with nepheline and diopside.

I90.13 calcite-carbonatite

88.5 calcite

7 aegirine-augite

3 biotite

Accessory minerals include apatite, pyrochlore, hematite, ilmenite and strontianite. The non-calcite minerals tend to occur in polymineralic clumps in the coarse-grained calcite.

I90.19 nepheline syenite

40-50 orthoclase microperthite

20-30 nepheline

15-20 hedenbergite

8-12 hastingsite

3-6 sodalite

Accessory titanite, melanite (titanian andradite) and cancrinite.

The melanite occurs in 2 generations, the first as anhedral fragments in the nepheline-feldspar groundmass, and the second as anhedral sections associated with sodalite veining.

I92.8 clinopyroxenite (kaersutite-bearing)

80-90 diopside

10-15 kaersutite

2-7 apatite

2-5 magnetite

This rather dense rock exhibits good cumulate textures and is noteworthy for its absence of "light" minerals.

I92.34 pegmatitic nepheline-sodalite syenite

35-45 orthoclase microperthite

15-20 aegirine

10-15 nepheline

10-15 sodalite

10-15 cancrinite

10-15 fluorite

3-4 magnetite

3-4 andradite

This coarse-grained rock has been heavily deuterically altered.

I92.35* nepheline syenite

48 orthoclase microperthite

30 nepheline

9.5 hastingsite

4 hedenbergite

3.5 sodalite

Accessories include titanite, cancrinite, apatite, and very minor zircon and barite.

I92.37* eudialyte syenite

30-40 eudialyte

20-30 nepheline

20-30 aegirine

10-15 albite

5-10 amphibole

2-7 cancrinite

The eudialyte has been heavily altered in this rock.

-- sodalite syenite

No thin section was cut for this sample but its mineralogy, estimated from hand specimen, consists of orthoclase microperthite, sodalite, nepheline, aegirine-augite, and ilmenite.